Dark Matter and Neutrinos:

A Love-Hate Relationship

A tale of weak interactions

Andrés Olivares-Del Campo

A Thesis presented for the degree of
Doctor of Philosophy

Institute for Particle Physics Phenomenology
Department of Physics
Durham University
United Kingdom

May 2019

Dark Matter and Neutrinos:

A Love-Hate Relationship

A tale of weak interactions

Andrés Olivares-Del Campo

Submitted for the degree of Doctor of Philosophy

May 2019

Abstract: Dark matter (DM) and neutrinos provide the two most compelling pieces of evidence for new physics beyond the Standard Model (SM) but they are often treated as two different sectors. A tantalising avenue of investigation is the possibility that a stronger connection between these two particles exists. In this thesis, we explore the phenomenological implications of a neutrino-DM coupling and show that the complementarity between cosmological observables and indirect detection searches can be used to exclude large regions of the parameter space for different DM models. After conducting a complete study of all the possible renormalizable scenarios with such a coupling, we discuss two gauge-invariant realisations of models where the DM phenomenology is dominated by its interactions with neutrinos. While in these models, neutrinos set the strongest constraints, they can also be an obstacle in our quest to understand DM. Indeed, they will soon become a source of an important background for direct detection experiments. Here, we also compute the changes in this background in the presence of new physics within the neutrino sector. We find that it can increase significantly for light DM masses. This means that future discovery claims by direct detection experiments must be carefully examined if a signal is found well above the expected SM neutrino background.

Contents

List of Figures

List of Tables

Declaration

The work in this thesis is based on research carried out in the Department of Physics at Durham University. No part of this thesis has been submitted elsewhere for any degree or qualification.

The following chapters have been published in the form of papers:

- Chapter 2 is based on [1] and [2]

  C. A. Argüelles, A. Kheirandish, A. Olivares-Del Campo, I. Safa, and A. C. Vincent. *'Constraining dark matter annihilation into neutrinos: The most invisible channel'*, to appear, and

  A. Olivares-Del Campo, S. Palomares-Ruiz, and S. Pascoli. *'Implications of a dark matter-neutrino coupling at Hyper-Kamiokande'*, Proceedings in 53rd Rencontres de Moriond on Electroweak Interactions and Unified Theories (Moriond EW 2018), arXiv:1805.09830

- Chapter 3 is based on [3]

  C. Bœhm, A. Olivares-Del Campo, S. Palomares-Ruiz, and S. Pascoli. *'Dark matter-neutrino interactions through the lens of their cosmological implications'*, Phys. Rev. D97 (2018) no.7, 075039, arXiv:1711.05283

- Chapter 4 is based on [4]

  M. Blennow, E. Fernandez-Martinez, A. Olivares-Del Campo, S. Pascoli, S. Rosauro-Alcaraz, and A. V. Titov. *'Neutrino portals to dark matter'*, arXiv:1903.00006, submitted to European Physical Journal C

- Chapter 5 is based on [5]

  C. Bœhm, D. G. Cerdeño, P. A. N. Machado, A. Olivares-Del Campo, and E. Reid. *'How high is the neutrino floor?'*, JCAP 1901 (2019) 043, arXiv:1809.06385

Acknowledgements

I would like to start by thanking my supervisors, Prof. Celine Bœhm and Prof. Silvia Pascoli, for all your support throughout my PhD. I have learned a lot from you and I am very grateful for the many opportunities you have given me.

All this work would not have been possible without the amazing collaborators I have had: Carlos Argüelles, Mattias Blennow, David Cerdeño, Ahmet Coskuner, Enrique Fernandez-Martinez, Ali Kheirandish, Pedro Machado, Maura Ramirez-Quezada, Elliott Reid, Salva Rosauro-Alcaraz, Ibrahim Safa, Arsenii Titov, Aaron Vincent, Ye-Ling Zhou, and Kathryn Zurek. Special thanks go to Sergio Palomares-Ruiz for his patient help during my first project. I would also like to thank Patrick Tunney for suggesting a fitting subtitle for this thesis.

I have been very lucky to start my PhD with a great cohort of PhD students: Andrew Cheek, Matheus Hostert, Kristian Moffat, Alexis Plascencia, Jack Richings, Julia Stadler, and Philip Waite. Thanks a lot for the excellent physics discussions and great times together.

Most importantly, I thank my family: My parents Tomás and Pepa, my grandmother Josefina, my aunt Maite, and my brother Martín. Without your unconditional support I would not be here. I would also like to thank Jorge Arrieta-Aldea for the many years of friendship. My high-school friends, Miika Korja, Maite Sandoval, Deeya Jhummon, and my Tier 1 pals for all the laughs together. Last but not least, thanks to Macarena Teja-Ubach. You have been a very important part of my life during these last four years.

I gratefully acknowledge financial support from the European Research Council under ERC Grant “NuMass” (FP7-IDEAS-ERC ERC-CG 617143).

This thesis is dedicated to

my grandfather and my grandmother

Chapter 1

Introduction

> *Why do humans do Sciences, why do they do Arts? The things that are least important for our survival are the very things that make us humans.*
>
> — Savas Dimopoulos

Throughout the twentieth century, there has been growing evidence for the existence of an invisible matter component which accounts for around 85% of the total matter in our Universe. This has been called *dark matter* (DM) [6, 7]. Dark matter is traditionally thought to be a neutral, non-relativistic heavy particle. However, there are many things about its nature that remain unknown. Does it interact with any other particles in the Standard Model (SM) and if so, how much? What is its mass and spin? Is DM a single fundamental particle or does it form a composite sector? How was the amount of DM that has been observed today created? Throughout this thesis we will try to answer some of these questions using neutrinos as a tool.

In this introductory chapter, we start by summarizing the different observational evidence that suggests DM exists in Sec. 1.1. We then explain the standard dark matter thermal generation mechanism in Sec. 1.2 and review the status of different DM searches in Sec. 1.3. In Sec. 1.4 we shortly discuss the significance of neutrino

masses and their mixing while we dedicate Sec. 1.5 to the phenomenological implications of a neutrino-DM coupling. This chapter ends with an outline of the thesis in Sec. 1.6.

1.1 Evidence for dark matter

All the observational evidence that we have about DM so far is purely based on its gravitational effects. Alternative theories of gravity such as modified Newtonian dynamics (MOND) [8–10] can also explain some of the physical phenomena currently associated to DM. However, what is fascinating and compelling about DM is that observations at both small and large scales seem to consistently point towards a particle interpretation of DM. MOND theories however, present large tensions when trying to describe observables at different scales [11]. There are several in-depth reviews that explain the observational evidence for DM [12–16]. In this section we will discuss certain observables that motivate the existence of DM.

1.1.1 Galactic scales

A strong evidence for the existence of DM is the observed velocity distribution of rotating galaxies at galactic scales [17, 18]. A more striking observation is that DM can also account for the matter distribution of the Bullet Cluster, which is a galaxy merger thought to be produced after the collision of two galaxy clusters [19]. The spatial distribution of the luminous matter within this galaxy merger has been mapped out from the emission of X-ray radiation recorded by the Chandra observatory (see left panel of Fig. 1.1). At the same time, the DM distribution within the galaxy merger can be found by comparing numerical general relativity simulations to the lensing effects observed in the Bullet Cluster (see right panel of Fig. 1.1). By comparing these two images, one can see how the concentration of the luminous mass falls behind the centre of the gravitational mass. This agrees

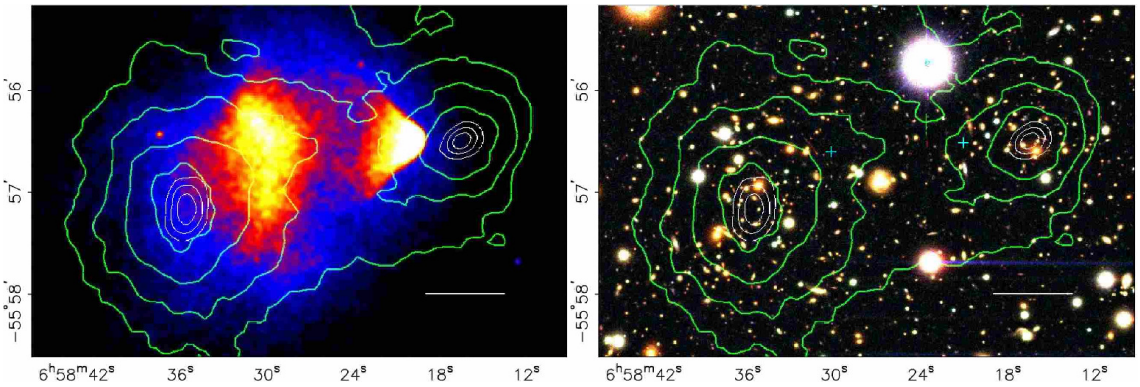

Figure 1.1: Color images of the Bullet Cluster in the X-ray (left panel) and optical (right panel) range taken by the Chandra observatory and the Magellan telescope respectively. The white bars correspond to a distance of 200 kpc. The green contours show the mass distribution as inferred from lensing measurements. These figures are taken from [20].

very well with what one would expect to occur when two objects with a component that does not interact very strongly (the DM) and a more interacting component (the luminous matter) collide: the weakly interacting particles go through each other while the particles that interact more, drag behind. In fact, Ref. [20] showed that the offset between the position of the centre of their distributions corresponds to an 8σ effect.

1.1.2 The cosmic microwave background and large scale structure formation

Beyond astrophysical observations, DM played a very important role in shaping the Universe as it is observed today. At early times, the electrostatic forces between the charged particles that constituted the ionizing plasma competed against the gravitational attraction among themselves. Consequently, baryonic matter could not clump together to form structures until it became neutral at recombination [21]. Before this time, the baryonic density behaved as a driven harmonic oscillator with the photon pressure and gravity acting as driving and restoring forces respectively. At recombination, protons and electrons formed neutral elements which meant that photons no longer scattered off the plasma. Thus, photons were able to decouple from

the thermal bath and travelled through the Universe to produce what we observe today as the cosmic microwave background (CMB). Nevertheless, these photons carry information about the baryonic density since they were strongly coupled to it until recombination happened.

The CMB was first detected by Penzias and Wilson in the 1960s [22] and gives information about the temperature of the photons emitted during recombination from different parts of the Universe. Although the temperature distribution looks largely homogeneous, it shows small anisotropies associated to baryonic matter perturbations in the early Universe. Moreover, the angular distribution of these temperature anisotropies can be expressed in terms of spherical harmonics $Y_{lm}(\theta, \phi)$ with a particular multipole moment l associated to the angular position θ. Nevertheless, these fluctuations are not large enough to account for the seeds of structure formation [23]. This demands the existence of an additional neutral matter component able to form gravitational wells earlier in time, which also contributed to the gravitational potential driving the baryonic matter oscillations. Consequently, the shape of the oscillatory pattern in the CMB spectrum (see Fig. 1.2) gives us information about the baryonic and DM relic densities. By measuring these anisotropies, Planck has been able to determine the relic baryonic (Ω_b) and non-baryonic ($\Omega_{\rm DM}$) matter densities of our Universe. They are [7]

$$\Omega_b h^2 = 0.0224 \pm 0.0001\,, \qquad \Omega_{\rm DM} h^2 = 0.120 \pm 0.001\,. \tag{1.1.1}$$

where the parameter h is related to the measurement of the expansion rate of the universe today.

One can also describe the distribution of matter in the Universe using the so-called matter power spectrum $P(k)$, which is related to the Fourier transform of the matter density inhomogeneities $\delta(x) \equiv [n(x) - n_{\rm Avg}]\,/n_{\rm Avg}$ for different wave numbers $k = 2\pi/\lambda$, where λ is the spatial scale. Therefore, $P(k)$ represents the variance in the matter distribution and consequently, a small value corresponds to a smooth distribution while a large value implies the presence of significant underdense and overdense regions. In this way, when $P(k)$ is suppressed, small structures are erased

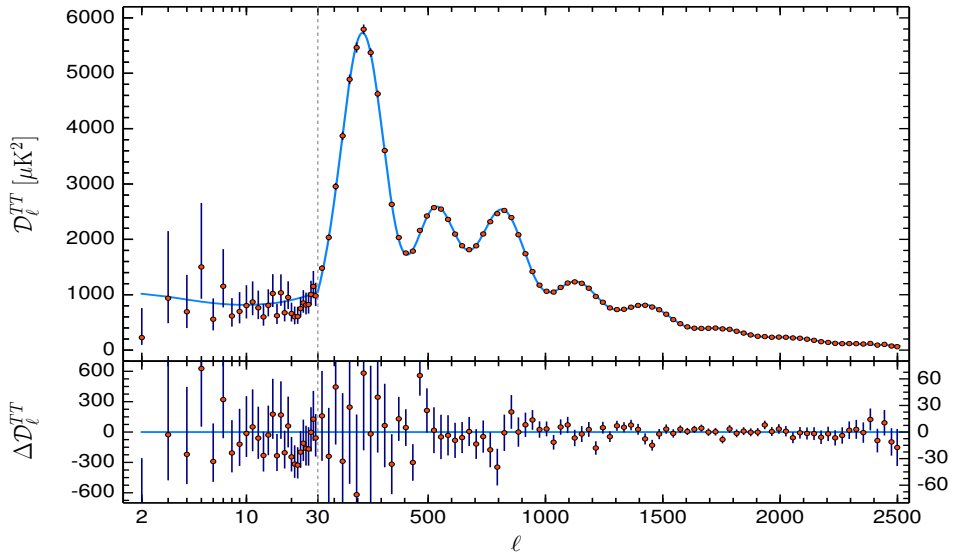

Figure 1.2: Spectrum of the temperature fluctuations of the CMB, where $\mathcal{D}_l^{TT} \equiv \left\langle \left(\frac{\Delta T}{T_{\rm Avg}}\right)^2 \right\rangle$. Figure taken from [7].

and galaxies form large structures. Furthermore, the shape of this spectrum strongly depends on the dark matter velocity and its interactions (see Fig. 1.3). For this reason, $P(k)$ can be used to infer certain DM properties by comparing the expected spectrum from $N-$body simulations (e.g. [24, 25]) with the measurements from large galaxy surveys such as the Sloan Digital Sky Survey [26]. In Sec. 1.5.2 we will discuss how the matter power spectrum also changes in the presence of sizable DM-neutrino interactions and can therefore be used to constrain the strength of such interactions.

1.2 Thermal dark matter

As we have discussed, the effects of DM have only been observed via its gravitational interactions. Consequently, collisionless DM has been the main paradigm for the last four decades [13, 28]. However, at the very least, DM generated thermally needs to have other type of interactions to be produced in the early Universe. A plausible hypothesis is that, if DM is a fundamental particle with a given mass, these interactions are *weak*. This is the so-called weakly interacting massive particle (WIMP) hypothesis (see Refs. [29, 30] for recent reviews).

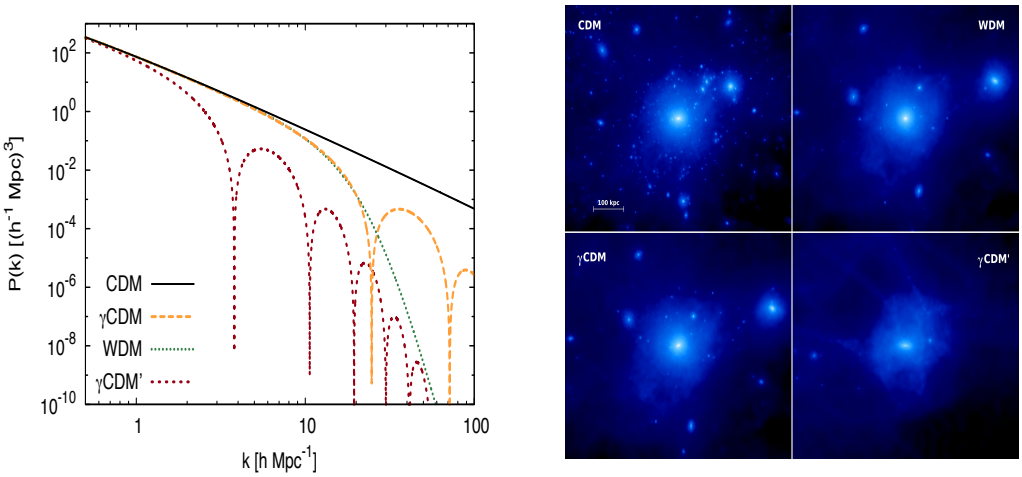

Figure 1.3: Matter power spectrum (left panel) and simulated distribution of a Milky Way-like halo (right panel) for different DM models with low and high DM velocities (CDM and WDM respectively), and models where non-relativistc dark matter interacts with photons with different strengths. Figure taken from [27].

Throughout this thesis we consider a WIMP DM candidate interacting mostly with neutrinos. Therefore, we now review how the observed DM relic abundance today could have been generated within the WIMP hypothesis. An interesting possibility is that it was produced in the same way as the SM particles. That is, via a thermal mechanism. This implies that DM would have been in thermal equilibrium with SM particles in the early Universe, meaning that the probability that a DM particle χ and its antiparticle $\overline{\chi}$ annihilate to a SM particle-antiparticle pair y, $\overline{y}$ was the same as the probability of the reverse process, so that there was no change in the number of DM particles at early times. As the universe cools down, the DM becomes non-relativistic and the forward reaction is favoured so that DM particles annihilate and their number density is decreased. Furthermore, when the universe expands, the density of DM particles was further diluted and consequently, it became increasingly difficult for DM particles to annihilate in order to maintain thermal equilibrium. This occurred when the rate of the reaction $\Gamma \equiv n_\chi \langle \sigma v_{\rm r} \rangle$ dropped below the Hubble

parameter $H \equiv \frac{\dot{a}}{a}$, which describes the expansion of the Universe.[1] At this point in time, DM chemically decoupled from the thermal bath (i.e., it was no longer in thermal equilibrium) and the density of DM particles approached a constant relic density which, as we have already mentioned, it has been measured today by Planck. This mechanism is generally referred to as thermal 'freeze-out'.

The DM relic density can be computed by solving the Boltzmann equation, which describes the change in the number density of DM particles, n_χ, when they are created or destroyed via their interaction with other particles as the Universe expands:

$$\frac{1}{a^3}\frac{d(n_\chi a^3)}{dt} = \langle \sigma v_{\rm r} \rangle (n_\chi^2 - (n_\chi^0)^2) \tag{1.2.1}$$

where n_χ^0 is the equilibrium DM density. We have assumed that $n_\chi = n_{\bar{\chi}}$ and that for large rates $n_{y,\bar{y}} = n_{y,\bar{y}}^0$. At high temperatures (i.e., early times), $n_\chi \sim n_\chi^0$ but, as the Universe cools down, DM particles become non-relativistic (when the temperature drops below the DM mass) and the DM equilibrium abundance is exponentially suppressed since $n_\chi^0 \sim e^{-m_\chi/T}$. Therefore, at some point in the evolution of the Universe, the number density of DM particles will be so small that they are no longer able to maintain their equilibrium abundance so that the density approaches a constant value as explained above. This is called the freeze-out point. The larger $\langle \sigma v_{\rm r} \rangle$ is, the longer DM remains in equilibrium with SM particles (i.e., the later the freeze-out point occurs) and consequently, the smaller the relic density is (see Fig. 1.4).

Even though Eq. 1.2.1 needs to be solved numerically to find the number density n_χ at every moment in time, we can consider the solutions for the number density well before and after freeze out and impose that both solutions are equal at the time of freeze out (up to a matching constant of order one, which we call c). In this way, we can compute the temperature at which freeze out happens by iterative solving

[1] In the previous definitions, n_χ refers to the DM number density, $\langle \sigma v_{\rm r} \rangle$ represents the thermally averaged cross section σ multiplied by the relative velocity $v_{\rm r}$ between DM particles, and the scale factor $a(t)$ describes the physical distance between two points as the Universe evolves.

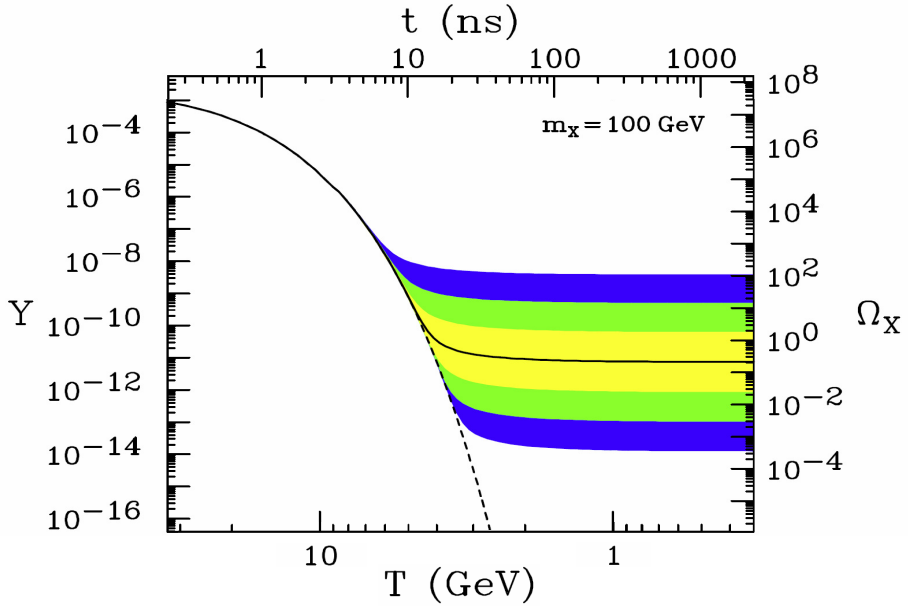

Figure 1.4: Evolution of the thermal DM relic abundance with temperature and time for a DM mass of 100 GeV. Y is the yield, defined as $Y \equiv \frac{n_\chi}{s}$, where s is the entropy density. The top and bottom of the coloured lines correspond to different values of $\langle \sigma v_{\rm r} \rangle$, differing from the black line by $10, 10^2$ and 10^3. Lines over the black line represent smaller values of $\langle \sigma v_{\rm r} \rangle$ while the ones below show larger values. Figure from [31].

the following equation [32]

$$x_f = \ln\left[\sqrt{\frac{45}{8}}\frac{c\,(2+c)\,g\,m_\chi M_{pl}\langle\sigma v_{\rm r}\rangle|_{x_f}}{2\pi^3\sqrt{g_\star x_f}}\right], \tag{1.2.2}$$

where $x_f = m_\chi/T_f$, $M_{pl} = 1.22 \times 10^{19}$ GeV is the Planck mass, g are the degrees of freedom of the DM candidate and $g_\star$ is the number of relativistic degrees of freedom during freeze out. By expanding the thermally averaged cross section in terms of its constant and velocity-dependent terms in the non-relativistic limit, with $v_{\rm CM}$ representing the DM velocity in the centre of mass frame, we get

$$\langle \sigma v_{\rm r} \rangle = \langle a + b v_{\rm CM}^2 + c v_{\rm CM}^4 \rangle \simeq a + 6b(m_\chi/T)^{-1} + 30c(m_\chi/T)^{-2} \tag{1.2.3}$$

we can find an analytical expression for the number density after freeze out so that a relation between the DM relic density today and the annihilation cross section is found to be [33]

$$\Omega_{\rm DM}h^2 = 8.55 \times 10^{-11}\frac{1}{\sqrt{g_\star}}\frac{x_f}{(a + \frac{3b}{x_f} + \frac{10c}{x_f^2})}\ {\rm GeV}^{-2}\,. \tag{1.2.4}$$

where $\Omega_{\rm DM} \propto m_\chi n_\chi$.

In order to obtain the value of the relic density $\Omega_{\rm DM}h^2 = 0.120 \pm 0.001$ measured by Planck, the thermally averaged velocity independent annihilation cross section[2] must be roughly $\langle \sigma v_{\rm r} \rangle \sim 3 \times 10^{-26}\,{\rm cm}^3/{\rm s}$, which is of a similar order of magnitude as the characteristic cross section of the weak interaction. Since in this thesis we are considering a thermal DM production mechanism, we will use this value of $\langle \sigma v_{\rm r} \rangle$ as a benchmark to which we compare our results.

1.3 Dark matter searches

A thermal mechanism of DM production is very appealing since it is based on the paradigm of thermal decoupling, which has made very accurate predictions for observables in the early Universe such as the CMB or the abundances of light elements [29]. For this reason, most of the DM searches carried out during the last 30 years have looked for a WIMP particle. While nowadays there are many other experiments searching for particles beyond the WIMP hypothesis such as axion-like particles [35], light DM [36] or composite DM [37], in this section we will focus on the experiments relevant to WIMP DM candidates. Most search strategies can be divided into three categories: Direct detection, indirect detection and collider searches, depending on the interaction considered (see Fig. 1.5). We will see in Chapters 2, 3 and 4 that, if DM interacts mostly with neutrinos, indirect detection will be the most powerful way of constraining different DM models.

1.3.1 Direct detection

Direct detection aims at determining the nature of DM particles through their scattering off a target in underground detectors. A worldwide experimental effort has lead to the design and construction of extremely sensitive experiments, based on a variety of targets and techniques, which are exploring DM-nuclei interactions

[2] If the cross section is v^2- or v^4-dependent, a value of $\langle \sigma v_{\rm r} \rangle \simeq 6 \times 10^{-26}\,{\rm cm}^3/{\rm s}$ or $\langle \sigma v_{\rm r} \rangle \simeq 9 \times 10^{-26}\,{\rm cm}^3/{\rm s}$ respectively is then required at freeze-out [34].

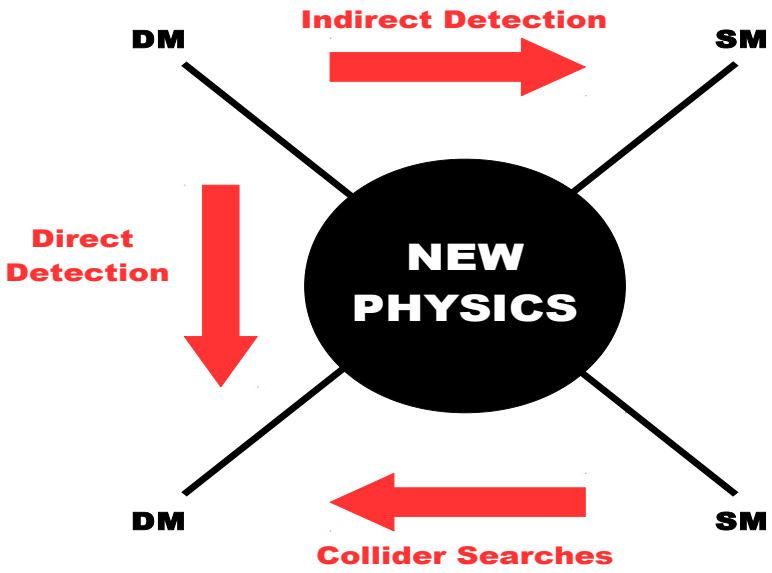

Figure 1.5: Summary of different DM search strategies depending on the interaction considered.

with unprecedented precision. A fundamental aspect in direct DM searches is the reduction of the SM events in order to isolate DM ones. Modern experiments employ various techniques, such as the construction of extremely radiopure detectors, the use of a shielding, and the measurement of various channels (e.g., ionisation and scintillation) to discriminate DM signals against the background. The lack of a DM signal above the background can be used to set strong bounds on the WIMP-nucleon elastic scattering cross section for different DM masses. Results in the literature are often expressed in terms of the spin-independent and spin-dependent elastic scattering cross sections. The former is related to the WIMP interaction with all nucleons while the latter refers to the interaction of the WIMP with nucleons with an intrinsic angular momentum, which depends on the target nuclei.

Currently, the strongest limits for DM masses larger than ~ 10 GeV are given by the large liquid xenon detector based at Gran Sasso (Italy), XENON1T [38], which is able to constrain spin-independent WIMP-nucleon cross sections down to $\sim 10^{-46}\,\mathrm{cm}^2$ (see Fig. 1.6). In Chapter 4, we show how these bounds are so stringent that, for large DM masses, they are able to constrain the parameter space of models where the DM-quark interactions are loop-suppressed. Finally, direct detection of sub-GeV DM

via scattering off electrons has gained significant attention recently [39–42]. However, these bounds are not strong enough yet to be relevant for the phenomenology we discuss in this thesis and we do not consider them further.

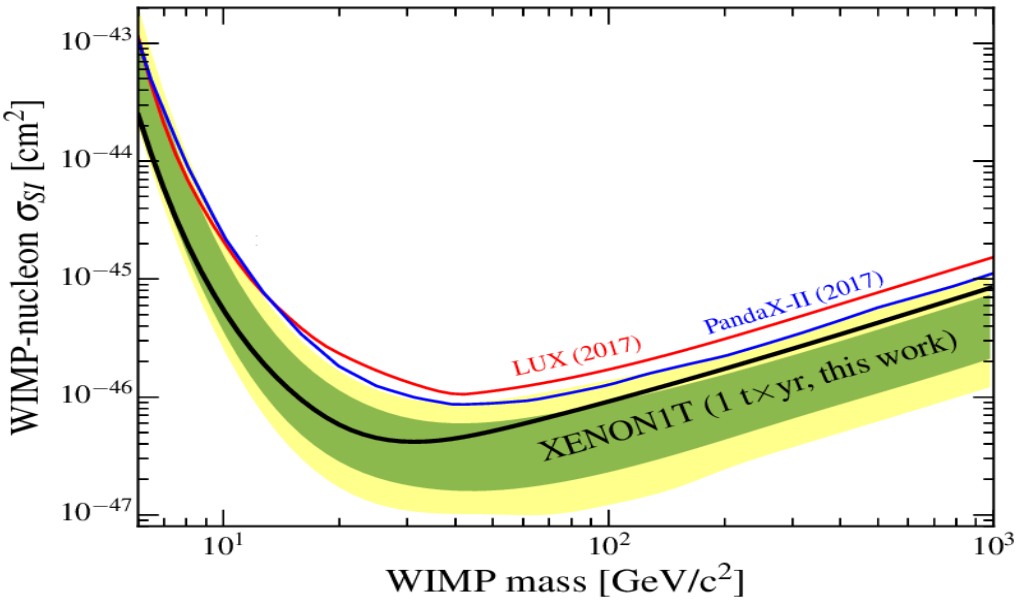

Figure 1.6: 90% limits on the spin-independent elastic scattering WIMP-DM cross section from XENON1T (black) with 1σ (green) and 2σ (yellow) sensitivity bands. The plot includes previous results from the LUX collaboration [43] and PandaX-II [44] for comparison. Figure adapted from [45].

1.3.2 Indirect detection

Indirect detection experiments look for the final states in the DM annihilation or decay to SM particles. Self-annihilation of DM particles is expected to be sizable today in regions with a high DM density if there is no large matter-antimatter asymmetry in the dark sector, although indirect detection signatures might still be present if DM is asymmetric (see Ref. [46] for a comprehensive review).

The flux of SM particles produced by DM depends on the particular annihilation or decay channel and on the density profile used. A popular choice is the Navarro-Frenk-White (NFW) profile which has the following form [24]

$$\rho(r) = \frac{\rho_0}{(r/r_s)(1 + r/r_s)^2}\,, \tag{1.3.1}$$

where the scale radius r_s dictates the shape of the profile and ρ_0 is the DM density at the galactic centre.

The most studied final states are charged leptons and photons since they are easy to detect. However, the main challenge that indirect detection faces is the presence of large uncertainties in the halo parameters such as r_s or ρ_0. This is particularly relevant when attributing a DM origin to certain observed excesses since large uncertainties can challenge such interpretations [47–50]. This is the case for several potential DM signals that have appeared in DM searches over the last few years. In particular, there has been a lot of discussion about the galactic centre gamma ray excess of photons with GeV energies as measured by the Fermi satellite [51, 52]. Nevertheless, whether a DM interpretation of this excess is correct or not is still inconclusive [53].

Furthermore, DM annihilation into photons or charged particles in the early Universe can leave an imprint in the power spectrum of the CMB due to the ionizing energy injection in the thermal bath. This is particularly relevant for light DM masses ($m_\chi < 10$ GeV) since for such masses, the number density of DM is large (i.e., $n_\chi \propto \frac{1}{m_\chi}$), which in turn leads to a high annihilation rate. Therefore, a measurement of the CMB multipole spectrum can be used to set constraints on the annihilation cross section times the ionizing efficiency $f(z)$, which depends on the particular annihilation channel. The models we study in Chapter 4 lead to DM-charged lepton interactions and consequently, we will constrain their parameter space using the ionizing efficiencies computed in Ref. [54] and the bounds derived from the CMB measurement by Planck [7], as well as the indirect detection constraints on the DM annihilation to charged leptons from the Fermi satellite [55].

Nevertheless, in this thesis, we are mostly interested in DM-neutrino interactions and we dedicate Chapter 2 to indirect detection constraints from DM annihilation to neutrinos. Furthermore since we study stable DM candidates, we do not discuss the constraints that can be placed by studying DM decay signals but refer the interested reader to Refs. [56, 57] for further discussion on this topic.

Finally, it is interesting to point out that a powerful aspect of indirect detection is that, for velocity-independent annihilation cross sections, constraints set by such searches can be compared to the $\langle \sigma v_{\rm r} \rangle$ required to generate the right relic abundance. Therefore, these constraints can be used to rule out certain regions of the parameter space for thermal DM models as we will discuss in Chapters 3 and 4.

1.3.3 Collider searches

In models where the DM candidate couples strongly to quarks, an interesting avenue to explore is the direct creation of DM at, for example, proton-proton colliders such as the LHC.[3] There have been several model-dependent analyses that focus on traditional super-symmetric WIMP candidates, such as the neutralino [58, 59]. Recently, model-independent searches using an effective field theory or a simplified model approach have become increasingly popular [60]. However, the former is only valid if the energy scale of new physics is larger than the energy of the particles involved in the collision [61]. The latter approach relies on certain assumptions about the nature of the mediator that need to be taken into account carefully, especially when comparing collider results with other experimental constraints such as the ones derived from direct detection experiments [62].

DM particles, being weakly interacting, do not leave signatures in the detector. Consequently, most collider searches focus on reconstructing the "missing" transverse energy accompanied by the emission of a physical object such as a jet, a photon, a Z or a Higgs boson, which is used to compute the missing energy of the collision (see Refs. [16, 29] for detailed reviews about such analyses). In other words, if after looking at the final states of a proton-proton collision momentum conservation seems to be violated, it is possible that a DM particle has been created.

The leptophilic models that we will discuss in Chapters 3 and 4 will generally not

[3] Lepton colliders can also provide with a complementary search strategy if DM couples to the charged leptons, but we will not discuss them here as the derived constraints are often less stringent for large DM masses.

have any tree-level interactions with quarks and, when loop-induced, they will be too weak to produce any interesting collider phenomenology.

1.4 Neutrino masses and mixing

Neutrinos are the least understood particles within the SM. The discovery of neutrino oscillations at neutrino detectors such as Super-Kamiokande (SK) in Japan [63] during the late 1990's, has confirmed the light, but massive nature of neutrinos. Indeed, in order to explain neutrino mixing, we are motivated to introduce neutrino mass terms in the SM, which lead to a non-trivial relationship between the neutrino flavour and mass bases:

$$\nu_{\alpha L} = U^*_{\rm PMNS}\nu_{iL}\,, \tag{1.4.1}$$

where $\alpha = e, \mu, \tau$ and $i = 1, 2, 3$ for the flavour and mass basis respectively. The unitary mixing matrix $U_{\rm PMNS}$ is called the Pontecorvo-Maki-Nagawaka-Sakata (PMNS) matrix [64–66]. A priori, the SM model does not tell us anything about the particular form of the PMNS matrix since neutrinos are massless in the SM. Nevertheless, a non-diagonal matrix implies that flavour neutrinos do not have a definite mass but rather, they are a superposition of neutrinos with different masses.

1.4.1 Neutrino oscillations

The PMNS matrix can be described by six parameters[4]: Three angles and three complex phases (a Dirac phase δ and two Majorana phases α_1, α_2 depending on whether neutrinos are Dirac or Majorana fermions). The usual convention followed to parametrize the PMNS matrix is [67]

$$U_{\rm PMNS} = \begin{pmatrix} 1 & 0 & 0 \\ 0 & c_{23} & s_{23} \\ 0 & -s_{23} & c_{23} \end{pmatrix} \begin{pmatrix} c_{13} & 0 & s_{13}e^{-i\delta} \\ 0 & 1 & 0 \\ -s_{13}e^{i\delta} & 0 & c_{13} \end{pmatrix} \begin{pmatrix} c_{12} & s_{12} & 0 \\ -s_{12} & c_{12} & 0 \\ 0 & 0 & 1 \end{pmatrix} \begin{pmatrix} e^{i\alpha_1} & 0 & 0 \\ 0 & e^{i\alpha_2} & 0 \\ 0 & 0 & 1 \end{pmatrix}. \tag{1.4.2}$$

[4]Since the PMNS matrix is a 3×3 unitary matrix, it can be parametrised by three angles and six complex phases. However, three of these complex phases can be absorbed by field redefinitions.

where $c_{ij} \equiv \cos(\theta_{ij})$ and $s_{ij} \equiv \sin(\theta_{ij})$ parametrize the rotations by an angle θ_{ij} in the $i-j$ plane. All the mixing angles have been measured at neutrino oscillation experiments and, while these experiments are not sensitive to the Majorana phases $\alpha_{1,2}$ [68, 69], there are hints for $\delta \neq 0$ with low significance [70]. The central values of the oscillation parameters for normal ordering ($m_{\nu_1} < m_{\nu_2} < m_{\nu_3}$) from the latest global fit combining results from solar, atmospheric, reactor and accelerator neutrino experiments are [71]

$$\theta_{12} = 33.82^\circ\,,\ \theta_{23} = 49.7^\circ\,,\ \theta_{13} = 8.61^\circ\,,\ \delta = 217^\circ\,. \tag{1.4.3}$$

In this way, the PMNS matrix introduces a misalignment between the flavour and mass bases which in turn, can generate transitions between different neutrino flavours. We can calculate the probability for this transition to occur by considering the free particle neutrino states in a free theory. This means that Eq. 1.4.1 (dropping for simplicity the subscript L for the neutrinos and PMNS for U) becomes

$$|\nu_\alpha\rangle = U_{\alpha i}|\nu_i\rangle\,, \tag{1.4.4}$$

where U is the PMNS matrix and we have explicitly written the matrix indices for clarity. As neutrinos travel a particular distance L, the time evolution of a mass eigenstate with energy E_i is given by

$$|\nu_\alpha, L\rangle = U_{\alpha i}e^{-iE_iL}|\nu_i\rangle, \tag{1.4.5}$$

where for nearly massless neutrinos, we can assume $t \approx L$. Consequently, the probability that a neutrino with flavour α becomes a neutrino with flavour β after a distance L is travelled is given by

$$P_{\alpha\beta} \equiv P(\nu_\alpha \to \nu_\beta) = |\langle\nu_\beta|\nu_\alpha, L\rangle|^2 = |\sum_{i=1}^{3} U_{\alpha i}U^*_{\beta i}e^{-iE_iL}|^2\,. \tag{1.4.6}$$

In the context of indirect detection searches, neutrinos produced from DM annihilation travel long distances before they reach the detectors on Earth. For these large propagation distances, we can ignore the exponential term and consider an incoherent mixture of mass eigenstates arriving at the detector. Therefore, the oscillation

probability simply becomes

$$P_{\alpha\beta} = \sum_{i=1}^{3} |U_{\beta i}|^2 |U_{\alpha i}|^2 \tag{1.4.7}$$

so that, by substituting the best fit values for the oscillation parameters from Eq. 1.4.1 we get

$$P_{\alpha\beta} = \begin{pmatrix} 0.55 & 0.20 & 0.25 \\ 0.20 & 0.42 & 0.38 \\ 0.25 & 0.38 & 0.37 \end{pmatrix} . \tag{1.4.8}$$

This mixing effect is taken into account in the following chapter when we discuss the indirect detection constraints on the annihilation cross section of DM to neutrinos.

1.4.2 Generating neutrino masses

The need for neutrino mass terms presents a problem for the SM since only left-handed neutrinos have been observed and consequently, we cannot write down a renormalizable mass term consistent with gauge invariance. A simple extension of the SM that explains neutrino masses is the addition of extra degrees of freedom that correspond to a right-handed neutrino N_{R}. Adding the following term to the SM Lagrangian

$$\mathcal{L}_{\mathrm{SM}} \supset -y_\nu \overline{L_L} \tilde{H} N_R + \text{h.c.} \xrightarrow{\text{EWSB}} \frac{y_\nu v}{\sqrt{2}} \overline{\nu_L} N_R + \text{h.c.}\,, \tag{1.4.9}$$

leads to a neutrino mass term $m_\nu = y_\nu v/\sqrt{2}$ after electroweak symmetry breaking (EWSB), where L_L is the SM leptonic doublet, $\tilde{H} = i\sigma_2 H^*$, y_ν is the neutrino Yukawa coupling and the Higgs vacuum expectation value (vev) is $v = \langle H^0 \rangle = 246$ GeV. In this way, neutrinos acquire a mass of ~ 0.1 eV compatible with the current data if $y_\nu \sim 10^{-12}$, which is several orders of magnitude smaller than the Yukawa couplings for other SM fermions. While this option is viable, the large hierarchy between Yukawa couplings is often seen as rather "unnatural" (even though we still do not understand the hierarchy between, for example, the top and the electron mass). Furthermore, when considering the additional field N_R, there is no SM symmetry forbidding the Majorana mass term

$$\mathcal{L}_{\mathrm{SM}} \supset -\frac{M}{2} \overline{N_R} N_L^c + \text{h.c.}\,, \tag{1.4.10}$$

where $N_L^c = C\overline{N_R}^T$ with the charge conjugation matrix $C = i\gamma^0\gamma^2$. This term violates the accidental lepton number symmetry of the SM, which leads to lepton number violating processes. While this is not necessarily a problem, the presence of an additional symmetry such as $B - L$ would directly forbid the addition of a neutrino Majorana mass term, implying that neutrinos are purely Dirac.

At low energies, one may also be tempted to write a Majorana mass term for the left-handed neutrino

$$\mathcal{L}_{\text{SM}} \supset -\frac{m_M}{2}\overline{\nu_L}\nu_R^c + \text{h.c.}\,, \tag{1.4.11}$$

which also violates lepton number. Since neutrinos belong to an $SU(2)$ doublet, this term does not respect gauge invariance and consequently, requires the addition of an extra particle to the SM which allows us to construct such an operator. The most popular ways of doing this are the well-known Type I [72–74], Type II [75–77] and Type III [78] see-saw mechanisms.

Combining all the gauge-invariant mass terms together, we can construct the following neutrino mass matrix in the flavour basis

$$\mathcal{L}_{\text{SM}} \supset -\frac{1}{2}\begin{pmatrix}\overline{\nu_L} & \overline{N_L^c}\end{pmatrix}\begin{pmatrix}0 & y_\nu v/\sqrt{2} \\ y_\nu^T v/\sqrt{2} & M\end{pmatrix}\begin{pmatrix}\nu_R^c \\ N_R\end{pmatrix} + \text{h.c.}\,, \tag{1.4.12}$$

so that, by rotating the flavour to the mass basis using the appropriate unitary matrix, we get the physical masses of the neutrino states:

$$m_{1,2} = \frac{M}{2} \mp \sqrt{\left(\frac{M}{2}\right)^2 + \left(\frac{y_\nu v}{\sqrt{2}}\right)^2} \tag{1.4.13}$$

where $m_{1,2}$ are the masses of the active and heavy neutrinos respectively[5]. In this way, a mixing between the active and the heavy neutrinos, which is proportional to y_ν, is also induced. Consequently, the smallness of the active neutrino masses often requires this mixing to be small. Nevertheless, there are other alternatives that allow for neutrino mass generation in a minimal way with sizable active-heavy mixing. For example, radiative neutrino mass models [79, 80] (see also Ref. [81] for a comprehensive review) suggest that light neutrino masses are generated via loop

[5]By active we mean the SM neutrinos in the flavour basis while by heavy we refer to the additional mass eigenstate ν_4.

processes, which also explains why they are so small. Furthermore, the linear [82,83] and the inverse see-saw models [84] are two different mechanisms that allow for $y_\nu \sim \mathcal{O}(1)$, implying large active-heavy neutrino mixing. While throughout this thesis we do not invoke a specific neutrino mass mechanism, in Chapter 4 we exploit a large mixing between the SM and the heavy neutrinos in order to construct models with large neutrino-DM interactions.

1.5 Constraints on dark matter-neutrino interactions

As we have seen, the generation of neutrino masses requires the existence of at least two additional particle to the SM since the measurement of two non-zero mass differences implies the existence of two massive neutrinos at least. An interesting possibility is to consider this particle to also be a DM candidate, or the mediator to a dark sector [85]. In the words of neutrino physicist Jose W. F. Valle "*neutrinos might explain dark matter through an emergent theory*" [86]. Furthermore, an interaction between DM and neutrinos can have phenomenological consequences via the annihilation of DM to neutrinos or via the DM$-\nu$ elastic scattering. In this section we will review the dominant physical effects produced by DM-neutrino interactions.

1.5.1 Dark matter annihilation to neutrinos

We have already seen in Sec. 1.2 that in a thermal scenario, the annihilation cross section that is needed to explain the observed abundance is about $\langle \sigma v_{\rm r} \rangle \simeq 3 \times 10^{-26}\,{\rm cm}^3/{\rm s}$ for a constant cross section. Consequently, if $\chi + \overline{\chi} \to \nu + \overline{\nu}$ is the dominant annihilation channel, we can constrain the parameter space of our models by requiring $\langle \sigma v_{\rm r} \rangle_{\nu\overline{\nu}}$ to be large enough to produce the right DM relic abundance. Similarly, when DM annihilations to neutrinos are sizable, indirect detection constraints from DM and neutrino experiments are particularly relevant, as we discuss

in the following chapter.

Big bang nucleosynthesis and neutrino reheating

The epoch of the Universe when light nuclei such as deuterium (D), helium (^3He ,^4He) and lithium (^7Li) were created is known as big bang nucleosynthesis (BBN). The relic abundance of these elements can be inferred from the emission spectrum of different astrophysical objects [87], which agrees very well with the theoretical predictions of a thermal mechanism [88]. However, DM annihilation into neutrinos after the time neutrinos decouple from electrons (i.e., at $T \lesssim T_{\rm dec} \sim 2.3$ MeV [89]), can reheat the neutrino sector, which would increase the expansion rate of the Universe during BBN. Therefore, neutron freeze-out occurs earlier and the relic abundances of deuterium and helium increase [90–96].

The raise in the neutrino energy density ρ_ν is equivalent to increasing the number of relativistic degrees of freedom ($N_{\rm eff}$) in the early Universe, according to

$$\rho_\nu \equiv \rho_\gamma \left[1 + \frac{7}{8}\left(\frac{T_\nu}{T_\gamma}\right)^{4/3} N_{\rm eff}\right] \ , \tag{1.5.1}$$

where ρ_γ is the energy density of photons. As can be seen from Fig. 1.7, the specific value of $N_{\rm eff}$ depends on the nature and mass of the DM candidate. However $N_{\rm eff}$ cannot be arbitrarily large as this would impact the CMB angular power spectrum at decoupling [97–109]. By comparing the predicted value of $N_{\rm eff}$ for different DM models with the measured value by Planck, one can eventually rule out DM candidates much lighter than a few MeVs (see Table 1.1).

The derivation of the precise value of the DM mass bound assumes that DM was in thermal equilibrium with neutrinos. Nevertheless, even in the case of non-thermal DM, a limit on $N_{\rm eff}$ could be set, if DM annihilates (or decays) into neutrinos after BBN and before decoupling.

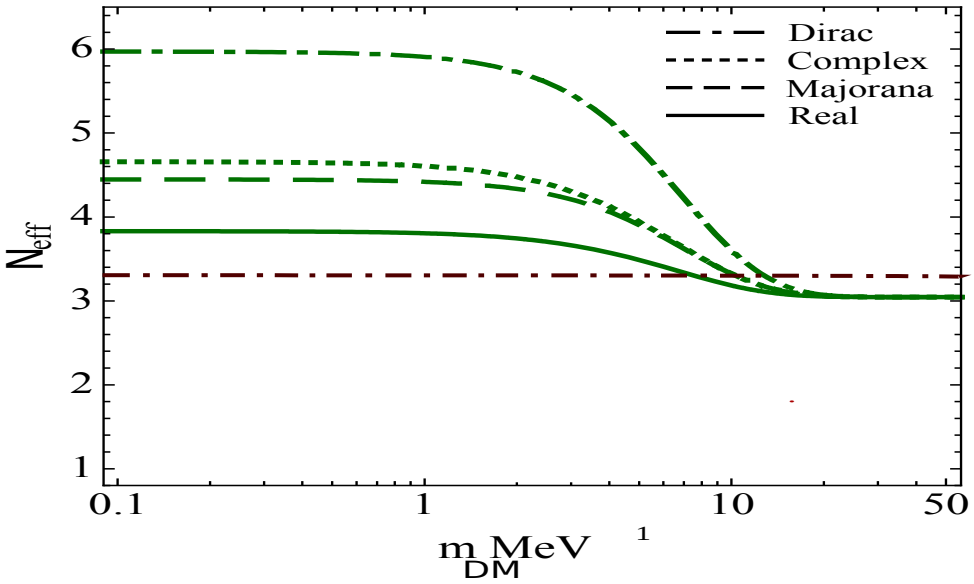

Figure 1.7: Change in N_{eff} as a function of the DM mass for different DM candidates. The brown dashed line corresponds to a value of $N_{\text{eff}} = 3.27 \pm 0.30$ as measured by Planck [7]. Figfure modified from [105].

1.5.2 Structure formation

We have already mentioned that the matter power spectrum $P(k)$ gives us an indication of the matter distribution in the early Universe. An interaction between DM and neutrinos can also alter the physics of the CMB and Large Scale Structures (LSS) [110–112].

DM-neutrino interactions imply that DM is no longer collisionless and consequently, as the DM particles scatter off neutrinos, they diffuse out and wash out the smallest primordial fluctuations. This *collisional damping* effect translates into a suppressed (oscillating) matter power spectrum (see Fig. 1.8), which can mimic a warm DM spectrum [113].

By confronting the CMB and LSS predictions to observations, one can get an upper bound on the strength of DM-ν interactions. Using Planck's angular matter power spectrum, one obtains that the DM-ν elastic scattering cross section cannot exceed $\sigma_{\text{el}} < 6 \times 10^{-34} \left(\frac{m_\chi}{\text{MeV}}\right)$ cm^2 [114, 115]. This limit is based on physical processes that took place in the linear regime and is therefore fairly robust. Nevertheless, it would be a bit stronger with extremely precise polarised data. An alternative is to

	[105]	[108]	[109]
Real scalar DM	No constraint	$m_\chi < 4.0$ MeV	$m_\chi < 3.8$ MeV
Complex scalar DM	$m_\chi < 3.9$ MeV	No constraint	$m_\chi < 7.8$ MeV
Dirac DM	$m_\chi < 7.3$ MeV	$m_\chi < 10.0$ MeV	$m_\chi < 11.4$ MeV
Majorana DM	$m_\chi < 3.5$ MeV	No constraint	$m_\chi < 7.7$ MeV
Vector DM	No constraint	No constraint	$m_\chi < 10.0$ MeV

Table 1.1: 95% conservative lower bounds on the DM mass for different DM candidates based on the Planck measurements of $N_{\rm eff}$. Different constraints correspond to analyses using different combinations of Planck observables and numerical codes. The particular analyses can be found in the references cited in the table.

require the matter distribution in the early Universe to be compatible with Lyman-α observations. This means that the damping can only happen at small scales, which translates into a constraint on the elastic scattering cross section of [116]

$$\sigma_{\rm el} < 10^{-36} \left(\frac{m_\chi}{\rm MeV}\right) \ {\rm cm}^2 \ , \tag{1.5.2}$$

for a constant elastic cross section, and

$$\sigma_{\rm el} < 10^{-48} \left(\frac{m_\chi}{\rm MeV}\right) \left(\frac{T_\nu}{T_0}\right)^2 \ {\rm cm}^2 \ , \tag{1.5.3}$$

for a temperature-dependent cross section, where $T_0 = 2.35 \times 10^{-4}$ eV is the photon temperature today. While there are uncertainties regarding the use of Lyman-α emitters to constrain the matter power spectrum, similar limits have been derived using the number of satellite companions of the Milky Way [27, 117–119]. Such limits are conservative and could become much stronger with a better understanding of the role of baryons in galaxy formation, since astrophysical feedback processes may also reduce the number of satellites (see, e.g., Ref. [120]).

Finally, in the presence of neutrino-DM interactions, the propagation of neutrinos through DM halos could be modified as well, leading to dips in supernova neutrino spectra due to resonant interactions with DM [122, 123], or changes in the spectrum or isotropy of the high energy cosmic neutrinos observed by IceCube [124–126]. Nevertheless, these physical processes yield sub-leading effects for the models we discuss in this thesis.

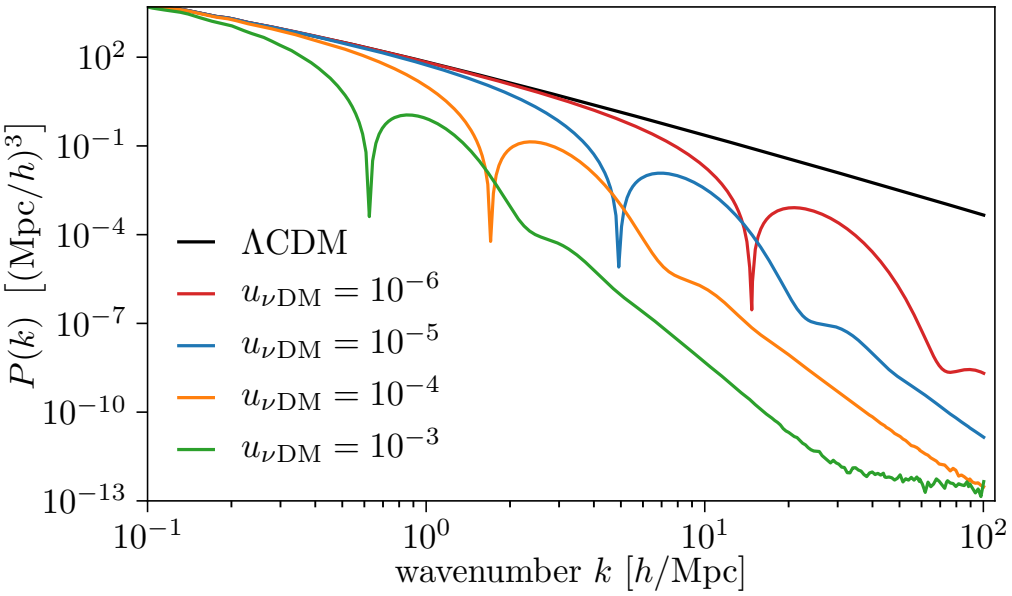

Figure 1.8: Matter power spectrum $P(k)$ as a function of the wavenumber k for different values of the elastic scattering cross section, where $u_{\nu\chi} \equiv \frac{\sigma_{\mathrm{el}}}{\sigma_{\mathrm{Th}}} \left(\frac{m_\chi}{100\,\mathrm{GeV}}\right)^{-1}$ and σ_{Th} is the Thomson cross section. Figure taken from [121].

1.6 Thesis outline

This thesis aims to understand the role that neutrinos play in our understanding of DM. Specifically, we study the phenomenology of neutrino-DM interactions and determine the possible changes in the neutrino background for DM direct detection experiments in the presence of new physics.

In Chapter 2, we begin by describing the necessary ingredients to conduct indirect detection searches using neutrinos and provide with an overview of the current status of such searches. We then describe in detail an analysis carried out using SK data for low energy neutrinos. This analysis allows us to constraint the annihilation cross section of DM to neutrinos for light DM masses. Furthermore, we make projections for the use of gadolinium in the detector and for the future project Hyper-Kamiokande (HK).

In Chapter 3, we highlight the complementarity between cosmological observables and indirect detection searches when studying DM properties. In particular, following a simplified model approach, we perform a phenomenological study and consider all

the different possibilities in which DM can couple to neutrinos in a minimal way. We then examine the allowed parameter space of the DM and the mediator masses for each possible model. In this way, we determine that the models with the richest DM phenomenology are those with Dirac DM candidates and scalar or vector mediators.

Building upon what we learned from the study described in Chapter 3, we explore the possibility of constructing gauge-invariant scenarios where the DM phenomenology is dominated by its interactions with neutrinos in Chapter 4. With this goal in mind, we study the DM phenomenology of two different implementations of the neutrino portal in which neutrinos mix with a SM singlet fermion that interacts directly with dark matter through either a scalar or vector mediator. For both of these scenarios, we show that future neutrino detectors will be able to rule out certain regions of the parameter space.

In Chapter 5, we compute the contribution to the coherent elastic neutrino-nucleus scattering cross section from new physics models in the neutrino sector. We then use this information to calculate the maximum value of the so-called neutrino floor for direct dark matter detection experiments, which determines when these detectors are sensitive to the neutrino background. We find that the increase in the neutrino floor can be significant. This implies that future claims by direct detection experiments must be carefully examined if a signal is found well above the expected SM neutrino floor.

Finally, we summarise our conclusions and discuss avenues for future work in Chapter 6.

Chapter 2

Galactic searches for dark matter using neutrinos

> *No matter how complex our instruments may be, no matter how sophisticated and subtle our theories and calculations are, it's still our consciousness that finally interprets our observations. And it does so according to its knowledge and conception of the event under consideration.*
>
> — David Bohm

We have explained in the introduction (Sec. 1.3.2) that indirect detection is a popular strategy to try to understand DM properties. In the context of indirect detection, studying neutrinos as a final state particle is particularly interesting. Neutrinos are the weakest interacting particles in the SM and consequently, the hardest particles to detect. Therefore, the limits derived on the DM annihilation to neutrinos can be interpreted as an upper bound on the *total* DM annihilation cross section [127, 128].

In this chapter, we will discuss the current status of galactic searches for DM annihilation to neutrinos in the Milky Way. Furthermore, an analysis done with MeV neutrinos detected at Super-Kamiokande (SK) will be presented in detail.

2.1 Galactic searches

DM annihilations in high density regions like the Milky Way may lead to a detectable monochromatic flux[1] of neutrinos (and antineutrinos) in neutrino detectors [128–130]. For a velocity-independent cross section, the differential neutrino flux per flavour at Earth by DM annihilations in the Milky Way halo is given by [129]

$$\frac{d\phi}{dE_\nu} = \underbrace{\frac{\kappa\langle\sigma v_{\rm r}\rangle}{4\pi m_\chi^2}}_{\text{Particle physics}} \frac{1}{3} \underbrace{F}_{\text{Oscillations}} \delta(E_\nu - m_\chi) \underbrace{J}_{\text{Astrophysics}} \equiv \Gamma(\langle\sigma v_{\rm r}\rangle, m_\chi)\,\delta(E_\nu - m_\chi)\ , \tag{2.1.1}$$

where m_χ is the mass of the DM candidate and the delta function accounts for the monochromatic nature of the flux. Note that the same equation applies for the differential antineutrino flux per flavour. Let us discuss the different terms that contribute to the neutrino-antineutrino flux separately:

- **Particle physics term:** The annihilation cross section $\langle\sigma v_{\rm r}\rangle$ depends on the underlying particle physics model. Furthermore, the factor κ changes according to the nature of the DM candidate since the number of combinations in which DM particles pair up in order to annihilate depends on whether the DM particle is self-conjugate or not. In this way $\kappa = \frac{1}{2}$ for self-conjugate DM while for a Dirac/complex DM candidate, a DM antiparticle can only annihilate with half of the total number of DM particles and $\kappa = \frac{1}{4}$.

- **Neutrino oscillations term:** F is a numerical factor which depends on the particular neutrino flavour an experiment can measure. As we discussed in Sec. 1.4, the neutrino flavour that arrives at Earth depends on the neutrino flavour produced at the source. For the results presented throughout this thesis, we use the appropriate F-factor depending on the neutrino flavour the experimental analysis is based on. For example, the dominant detection channel at low energies for an experiment like SK is via electron antineutrinos.

[1] Since the direct annihilation of non-relativistic DM particles to a neutrino-antineutrino pair is a two to two process, each neutrino produced in this annihilation will carry away an energy equal to the DM mass.

Consequently, if an equal mixture of neutrino flavours is produced at the source, $F = P_{ee} + P_{\mu e} + P_{\tau e}$, where the probability that a neutrino with flavour α becomes a neutrino with flavour β ($P_{\alpha\beta}$) was given in Eq. 1.4.8.

- **Astrophysical term:** The so-called J-factor contains information about the DM density distribution in our galaxy and it is defined as the integral of the square of the DM density along the line of sight (l), i.e., $J = \int d\Omega \int_{l.o.s} \rho^2 \left(r\left(l,\psi\right)\right) dl$. In this definition, $\rho(r)$ is the DM density profile within the halo, $r = \sqrt{R_0^2 - 2\,l\,R_0\,\cos\psi + l^2}$, with ψ being the angle between the Galactic Centre (GC) and the line of sight and R_0 is the distance between the Sun and the GC. Furthermore, the upper limit of integration $l_{\rm max} = \sqrt{R_{\rm halo}^2 - \sin\psi^2 R_0^2} + R_0\cos\psi$ is a function of the radius of the halo $R_{\rm halo}$. This quantity can be estimated numerically using different DM halo profiles. As mentioned in Sec. 1.3.2, there are uncertainties in the value of J associated with the specific halo profile and halo parameters used [49]. Nevertheless, if we consider all sky searches by integrating over the whole angular region[2], different halo profiles only change the value of J by a factor of 3 at most [128]. In what follows we choose an NFW profile [24] where the Sun's distance to the GC is given by $R_0 = 8.5$ kpc, the DM density at that position is $\rho_0 = 0.6\,\mathrm{GeV/cm^3}$, and we use a halo parameter of $r_s = 25.5$ kpc based on the central values from Ref. [49]. Calculating the J-factor over the whole sky with these parameters yields $J = 3.23 \times 10^{23}\ \mathrm{GeV^2/cm^5}$ for a velocity independent cross section.

In this way, we can use the observed neutrino flux at different neutrino detectors to set constraints on the annihilation cross section of DM to neutrinos.

[2]Note that for analyses that focus on the neutrinos arriving from the Galatic Centre direction, the J-factor would be an integral over the relevant $\Delta\Omega$ region, instead of the whole angular region (see for example, Ref, [131].

2.1.1 Velocity-dependent cross section

In the previous section, we have discussed DM annihilations into neutrinos for velocity-independent cross sections. Nevertheless, depending on the nature of the DM candidate, the leading term in the annihilation cross section to neutrinos can be proportional to $v_{\rm CM}^2$ or $v_{\rm CM}^4$, where $v_{\rm CM}$ is the DM velocity in the centre of mass frame. The DM velocity distribution depends on the kinematical details of the structure in which it is bound, as well as its distance from the centre of that distribution. Assuming a Maxwell-Boltzmann distribution with dispersion $v_0(r)$, the annihilation rate will be proportional to:

$$\langle v^n \rangle = \int d^3v v^n f(v,r), \tag{2.1.2}$$

where $f(v,r)$ is the normalized dark matter phase space distribution. For v^2- and v^4-dependent annihilation cross sections, this respectively yields

$$\langle v^2 \rangle = 3v_0^2(r)\,, \tag{2.1.3}$$
$$\langle v^4 \rangle = 15v_0^4(r)\,. \tag{2.1.4}$$

The velocity dependence of the cross section leads to change in the J-factor. One could derive reasonably accurate limits on the annihilation cross section for the velocity-dependent case by simply rescaling the constant cross section limits by the appropriate power of the DM velocity in the halo ($v_{\rm halo} \sim 2 \times 10^{-3}$ c [132]). Nevertheless, we can follow the procedure done in Ref. [133] and obtain the dispersion velocity v_0 by solving the spherical Jeans equation, assuming isotropy and hydrostatic equilibrium:

$$\frac{d(\rho(r)v_0^2(r))}{dr} = -\rho(r)\frac{d\phi(r)}{dr}\,, \tag{2.1.5}$$

where $\phi(r)$ is the total gravitational potential at radius r. We include not only the contribution of the DM halo to $\phi(r)$, but also follow Ref. [134] and include a parametrisation of the Milky Way bulge and disk potentials to account for their masses:

$$\phi(r)_{\rm bulge} = -\frac{G_N M_b}{r + c_b}\,, \tag{2.1.6}$$

$$\phi(r)_{\rm disk} \;=\; -\frac{G_N M_d}{r}\left(1-e^{-r/c_d}\right)\,, \tag{2.1.7}$$

where G_N is Newton's gravitational constant, $M_b = 1.5\times10^{10}M_\odot$ and $c_b = 0.6$ kpc are the bulge mass and scale radius, while $M_d = 7\times10^{10}M_\odot$ and $c_d = 4$ kpc are the disk mass and scale radius [134], with the solar mass $M_\odot = 1.99\times10^{30}$ kg.

The galactic J-factor can then be re-evaluated via:

$$J_{v^n} = \int d\Omega \int_{\rm l.o.s.} \langle (v/c)^n \rangle(r)\rho^2\left(r\left(l,\psi\right)\right) dl\,. \tag{2.1.8}$$

For the NFW halo profile (see Eq. 1.3.2), using the halo parameters we mentioned before and integrating over the whole angular region, we get $J_{v^2} = 4.35\times10^{17}$ GeV^2/cm^5 and $J_{v^4} = 9.73\times10^{11}$ GeV^2/cm^5. Consequently, the constraints on the annihilation cross section of DM to neutrinos must be rescaled by J/J_{v^2} and J/J_{v^4} for v^2- and v^4- dependent cross sections respectively. As anticipated, this means that such constraints are much weaker since the neutrino flux generated from DM annihilations to neutrinos is suppressed for velocity dependent cross sections.

2.1.2 Summary of current and future experimental searches

As discussed previously, the energy of the neutrino produced in the direct annihilation of two DM particles to a neutrino-antineutrino pair is the same as the mass of the DM particle. Consequently, different neutrino experiments that focus on studying specific neutrino energy regimes allow us to place bounds on the cross section of DM annihilation to neutrinos for different DM masses. From low to high DM masses, the dominant current constraints are given by

- **Borexino:** Borexino is liquid scintillator neutrino experiment located in the Gran Sasso Underground Laboratory, Italy. This experiment was primary built to study solar neutrinos at sub-MeV energies via $\nu - e$ elastic interactions in the liquid scintillator and had a 71.3 tons fiducial mass in its latest run [135].

Nevertheless, it is also a great $\bar{\nu}_e$ detector and has the advantage of a reduced reactor neutrino background due to its large distance from nuclear power stations. The electron antineutrino is detected via the inverse beta decay (IBD) interaction, $\bar{\nu}_e + p \to n + e^+$. Consequently, we can only probe neutrino energies over 1.8 MeV due to its kinematic threshold. From the electron antineutrino flux measured at Borexino during 1218 days [136], we can set a conservative bound on the annihilation cross section of DM to neutrinos for DM masses between $\sim 2 - 16$ MeV.

- **Super-Kamiokande at low energies:** Under Mount Ikeno in Japan, one can find the 22.4 kton water-Cherenkov detector, Super-Kamiokande (SK) [137]. In the same way as Borexino, SK detects electron antineutrinos mainly via IBD at low neutrino energies but, due to its larger size, we can also use this detector to set $\langle \sigma v_{\rm r} \rangle$ bounds for larger DM masses (between $10 - 200$ MeV). The reason why this occurs is that larger statistics make up for the decrease in the IBD cross section as the neutrino energy increases. For this detector, we perform a detailed analysis using 2853 days of data, which is explained later in Sec. 2.2.

- **Yüksel et. al. analysis:** In Ref. [128], a combined analysis of the measured neutrino and antineutrino flux for all flavours at the Fréjus [138], AMANDA [139] and SK detectors leads to a conservative upper bound on the cross section for DM masses between 100 MeV to 300 TeV. The authors acknowledge however, that a dedicated experimental analysis would improve their bounds by 1 or 2 orders of magnitude.

- **Super-Kamiokande at high energies:** In 2015, the SK collaboration published their first results of a dedicated search for a neutrino flux arising from DM annihilations in the GC [130]. The analysis is based on the atmospheric muon neutrino and antineutrino data collected over 5325.8 days. In fact, this analysis improves the bounds derived in Ref. [128] by $2-3$ orders of magnitude

for DM masses between $1 - 10$ GeV as it was expected.

- **ANTARES:** The neutrino telescope ANTARES is located ~ 2.5 km below the Mediterranean Sea. It contains 900 photomultipliers which capture the Cherenkov light of charged particles going through the detector [140]. This detector is most sensitive to muon neutrinos and it is able to reconstruct the direction from which they enter the detector. Its great angular resolution allows the ANTARES collaboration to place very strong limits on the DM self annihilation to neutrinos for DM masses between 53 GeV and 100 TeV. This analysis is based on the muon neutrinos and antineutrinos arriving from the GC direction during 9 years of data taking [141, 142].

- **IceCube:** IceCube is a cubic-kilometer neutrino detector in the South Pole. It is made of ice and it contains 5160 photomultipliers which capture the Cherenkov light emitted by the charged leptons created when a neutrino hits the detector [143]. Due to its large size, IceCube is sensitive to all neutrino flavours as each charged lepton displays a particular topology in the detector. The collaboration has performed an analysis constraining the neutrino flux arriving from DM annihilation in the GC by looking at the particle cascades produced by neutral or charged currents at the detector. They were able to place competitive limits on the DM annihilation cross section for DM masses between 25 GeV and 10 TeV [144]. However, its lowest angular resolution compared to the angular resolution of ANTARES means that IceCube's limits are not as good as ANTARES' for DM masses above 1 TeV.

Future neutrino, DM, and even gamma-ray detectors will also be able to set stringent constraints on the DM annihilation cross section to neutrinos. From lowest to largest DM masses, the most relevant experiments are:

- **DUNE:** This experiment is a 46.4 kton neutrino liquid argon detector to be built in the United States [145]. Consequently, its main advantage in

detecting neutrinos from DM annihilation is its improved energy resolution with respect to water Cherenkov detectors like SK, ANTARES or IceCube. DUNE is most sensitive to electron neutrinos and antineutrinos, which are detected via charged current interactions $\nu_e/\bar{\nu}_e + {}^{40}\mathrm{Ar} \rightarrow \mathrm{e}^-/\mathrm{e}^+ + \mathrm{X}$ (where X is the remaining nuclei after the interaction). An analysis done in Ref. [146] has placed the strongest constraints on the DM annihilation cross sections to neutrinos for DM masses between $20 - 90$ MeV, assuming that DUNE takes data for 3000 days.

- **Hyper-Kamiokande:** Building on SK's technology, a new water Cherenkov detector with a fiducial volume of 187 kton called Hyper-Kamiokande (HK) will be built in Japan [147]. Due to its larger size, this detector will be able to place stronger limits on the DM annihilation cross section to neutrinos [2]. Furthermore, the possibility of doping both the SK and the HK detectors with gadolinium will reduce the dominant background for the low energy SK analysis by a factor of 5 and consequently, improve the constraints on the DM annihilation cross section. We discuss these possibilities in detail in Sec. 2.2.

- **DARWIN:** DARWIN is a proposed liquid xenon direct detection DM experiment, with a fiducial mass which has not been determined yet [148]. DARWIN is able to detect all neutrino flavours via neutrino coherent scattering and consequently, it can also place competitive limits on the neutrino flux created by DM self-annihilation. McKeen and Raj have performed an analysis in Ref. [149] assuming a fiducial volume of 40 ton and a run-time of 3000 days. With these assumptions, they are able to set limits on the DM annihilation cross section for DM masses between $20 - 1000$ MeV

- **CTA**: The Cherenkov Telescope Array (CTA) will be an array of gamma-ray detectors located in the northern and southern hemisphere [150]. The reason why this telescope can be relevant is that, instead of looking for the neutrinos produced in DM annihilation, one could try to observe the gamma

ray- spectrum produced by electroweak bremsstrahlung from such neutrinos [151]. Consequently, future gamma-ray telescopes such as CTA will be able to place strong limits on the DM annihilation cross section to neutrinos, especially for high DM masses due to the $\ln(m_\chi^2/m_W^2)$ enhancement in the cross section arising from the weak corrections. One should also note that the annihilation to a $\nu_\tau, \bar{\nu}_\tau$ pair produces a harder gamma-ray spectrum than the annihilation to $\nu_{e,\mu}, \bar{\nu}_{e,\mu}$ pairs [152]. This explains the different CTA sensitivities to the neutrino flavour in Fig. 2.1.

The main features of the experimental analyses described above and the limits on the annihilation cross section to neutrinos are summarised in Table 2.1 and Fig. 2.1

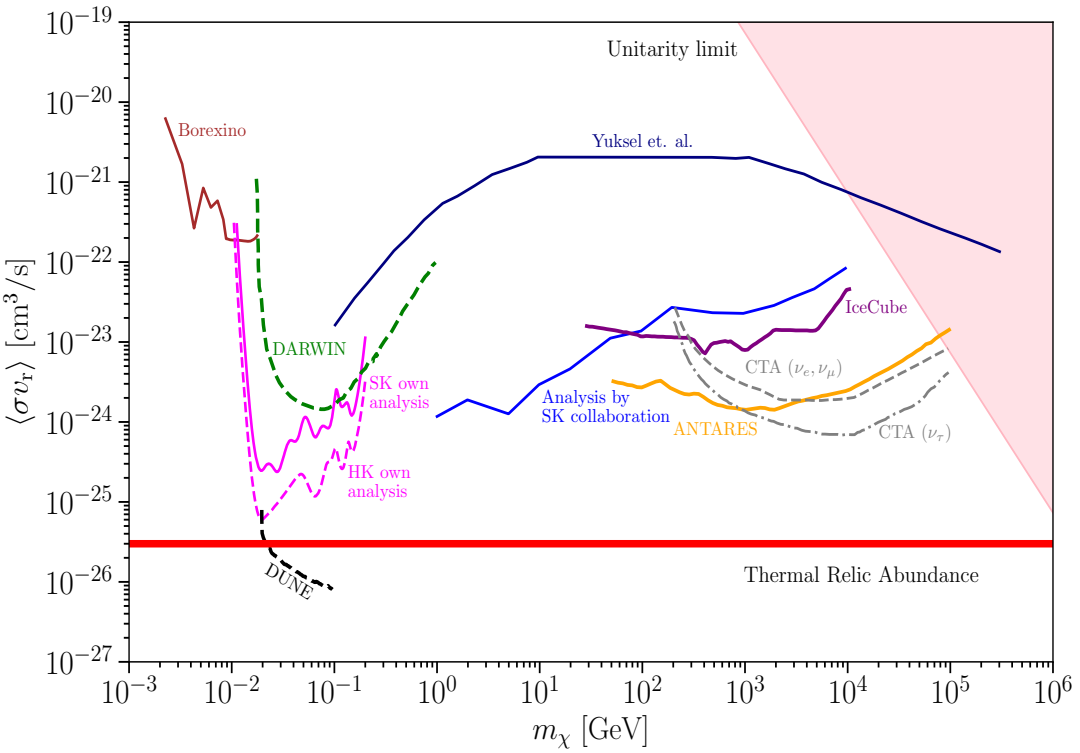

Figure 2.1: 90% current limits (solid lines) and projections (dashed lines) on the thermally averaged DM annihilation cross section to neutrinos as a function of the DM mass from a variety of experiments. Everything above the lines is excluded by the different experiments mention in the labels. The thick red line corresponds to the value that is needed to explain the observed abundance in thermal DM scenarios, i.e., $\langle \sigma v_r \rangle = 3 \times 10^{-26}$ cm^3/s. The pink area represents the region of the parameter space where the cross section is no longer unitary, i.e., $\langle \sigma v_r \rangle > 4\pi c/(m_\chi^2 v_{\rm halo})$ [153] with $v_{\rm halo} \sim 2 \times 10^{-3}$ c [132].

Energy range	Experimental analysis	Directionality	Detected flavour
$2.5 - 15$ MeV	Borexino [136]	×	$\bar{\nu}_e$
$15 - 10^3$ MeV	SK [3], HK [2]	×	$\bar{\nu}_e$
	DUNE [146]	×	ν_e, $\bar{\nu}_e$
	DARWIN [149]	×	All flavours
$1 - 10^4$ GeV	SK [130]	✓	ν_μ, $\bar{\nu}_\mu$
$20 - 10^4$ GeV	IceCube [144]	✓	All flavours
$50 - 10^5$ GeV	ANTARES [142]	✓	ν_μ, $\bar{\nu}_\mu$
$0.2 - 100$ TeV	CTA [151]	×	All flavours

Table 2.1: Summary table of the most relevant analyses (current and future) that set limits on the cross section of DM annihilation to neutrinos at the Galactic Centre for different energy ranges. The table also indicates whether the experimental analysis takes into account the direction neutrinos arrive from and the neutrino flavour the analysis is based on.

2.2 Super-Kamiokande analysis for MeV dark matter masses and Hyper-Kamiokande prospects

The neutrino flux from DM self-annihilation described by Eq. 2.1.1 could leave a signature at neutrino detectors which would look like a peak over the background at a neutrino energy that corresponds to the DM mass. We can calculate the expected number of neutrinos that could be observed at a detector from the annihilation of two DM particles using the following equation

$$\mathcal{N} \simeq \sigma_{\rm det}\left(E_\nu = m_\chi\right) \phi \, N_{\rm target} \, t \, \epsilon \,, \tag{2.2.1}$$

where $\sigma_{\rm det}$ is the detector cross section and is evaluated at $E_\nu = m_\chi$. ϕ is the total flux of neutrinos or antineutrinos, $N_{\rm target}$ is the total number of particles in the detector, t is the exposure time and ϵ is the detector energy efficiency.

Neutrinos interact very weakly with other SM particles and are therefore very difficult to observe directly. However, in their interaction with free and bound nucleons, they produce a charged lepton which interacts via the electromagnetic force and consequently, can be detected using different technologies such as water Cherenkov, liquid scintillator or liquid argon detectors.

As already mentioned, SK uses a water based Cherenkov detector with a fiducial volume of 22.5 kton, which corresponds to $N_{\rm target} = 1.5 \times 10^{33}$ free protons. This type of detector identifies different particles by their emitted Cherenkov radiation, which provides with a good energy resolution but has the limitation of not being able to identify particles with a kinetic energy below the Cherenkov threshold.

Here we improve and update the analysis performed in Refs. [56, 129]. In these references, it was found that neutrino experiments with a low-energy threshold such as SK can be used to place limits on DM-ν interactions for DM candidates with masses in the MeV range. In what follows, we combine SK data from the diffuse supernova neutrino searches, using the energy resolutions, thresholds and efficiencies from SK-I, II, III phases [154–157] for a total data taken period of 2853 days. For neutrino energies between $10 - 200$ MeV, we simulate the expected neutrino signal from DM annihilations and the relevant backgrounds for each phase. Since we only consider the dominant interactions within this energy range, we include the interactions of antineutrinos with free protons (IBD) as well as the interactions of neutrinos and antineutrinos with bound nucleons, as done in Refs. [56, 129].

In order to determine the possibility of obtaining a signal, one needs to take into account the backgrounds at the energy range of interest ($10-200$ MeV). The relevant backgrounds for this energy range are:

- The electrons produced from the decay of "invisible muons" (created by $\nu_\mu, \bar{\nu}_\mu$ atmospheric neutrinos) are the dominant background at low energies. They have energies below the Cherenkov threshold and therefore cannot be detected.

- Atmospheric ν_e and $\bar{\nu}_e$ neutrinos. Which could be reduced by tagging the

associated neutron produced in the IBD interaction.

- Spallation products produced by muon interactions around the detector. This sets the lower energy threshold of the detector.

- Reactor $\bar{\nu}_e$ neutrinos, whose flux is much larger than the expected neutrino flux from DM annihilation below 10 MeV.

Therefore, we will estimate the contribution from the first two backgrounds, consider the spallation cuts applied to each SK phase, and start our analysis from 10 MeV in order to avoid the reactor flux background.

In order to estimate the signal we are interested in, one needs to take into account the finite energy resolution of the detector. This can be done by multiplying the neutrino flux by a Gaussian energy distribution $R(E_e, E_{\rm vis}) = \frac{1}{\sqrt{2\pi}} e^{-\frac{E_{\rm vis}^2}{2\sigma^2}}$, where E_e is the true electron energy, $E_{\rm vis}$ is the observed electron energy, and σ is the corresponding energy resolution of each SK phase. Then, the number of monochromatic neutrinos from DM annihilation per bin l and for each SK phase i is calculated via the following quantity

$$\begin{aligned} A_l^i =& A_s^i \int \Bigg[\Big(\frac{d\sigma_f^{\bar{\nu}_e}}{dE_e}(E_{\bar{\nu}_e}, E_e) + \frac{1}{2} \frac{d\sigma_b^{\bar{\nu}_e}}{dE_e}(E_{\bar{\nu}_e}, E_e) \Big) \frac{d\Phi^{\bar{\nu}_e}}{dE_{\bar{\nu}_e}}(E_{\bar{\nu}_e}) \\ &+ \frac{1}{2} \frac{d\sigma_b^{\nu_e}}{dE_e}(E_{\nu_e}, E_e) \frac{d\Phi^{\nu_e}}{dE_{\nu_e}}(E_{\nu_e}) \Bigg] dE_e dE_{\nu_e} \times \int_{E_l}^{E_{l+1}} \epsilon(E_{\rm vis}) R(E_e, E_{\rm vis}) dE_{\rm vis} \end{aligned} \tag{2.2.2}$$

where the data has been distributed in 18 bins of 4 MeV between 16 MeV and 88 MeV. $\frac{d\sigma_f^{\bar{\nu}_e}}{dE_e}(E_{\bar{\nu}_e}, E_e)$ represents the interaction of antineutrinos with free protons under the inverse beta decay process which is numerically calculated from [158, 159]. $\frac{d\sigma_b^{\nu_e/\bar{\nu}_e}}{dE_e}(E_{\nu_e/\bar{\nu}_e}, E_e)$ represents the interaction of neutrinos/antineutrinos with nuclei (bound nucleons) and the factor of 2 accounts for the fact that in water, there are two free protons per each oxygen nuclei. This interaction was calculated using the Fermi gas model [160] with a Fermi momentum of 225 MeV and a binding energy of 27 MeV. Note that the integral over the flux reduces to evaluating the neutrino energy at the DM mass due to the delta function in the flux expression (see Eq. 2.1.1). Finally, A_s^i is a normalisation constant so that $\sum_l A_l^i = 1$ for each SK phase. In this

way, if we define α as the total number of neutrinos from DM self-annihilation, αA_l^i represents the fraction of neutrinos from DM annihilation at each energy bin for the SK phase i.

Similarly, the atmospheric ν_e and $\bar{\nu}_e$ backgrounds can be estimated by defining a coefficient B_l^i which can be calculated in a similar way as Eq. 2.2.2 but integrating over the atmospheric neutrino and antineutrino flux at SK. The atmospheric fluxes are computed by FLUKA [161, 162] and we used a linear interpolation to estimate the values of the flux at all energies of interest.

The number of invisible muons is estimated by considering the interaction of atmospheric muon neutrinos/antineutrinos with free and bound nucleons which produce muons and antimuons. Then, by integrating E_μ between m_μ and the Cherenkov treshold ($p_\mu = 120$ MeV for muons) the number of such muons/antimuons is determined. These muons/antimuons will be stopped in the rocks surrounding the detector and decay at rest to produce electrons/positrons within the detector, which can be mistaken with the electrons/positrons produced by $\nu_e, \bar{\nu}_e$ from DM annihilation and therefore, contribute to the background. One can define a coefficient C_l^i in order to consider the fraction of such events at each bin. This coefficient is calculated as follows:

$$\begin{aligned} C_l^i =& C_s^i \Big((N_+ + 0.816 N_-) \int \frac{d\Gamma_{\text{michel}}}{dEe}(E_e) + 0.184 N_- \int \frac{d\Gamma_{\text{orbit}}}{dEe}(E_e) \Big) dE_e \\ & \times \int_{E_l}^{E_{l+1}} \epsilon(E_{\text{vis}}) R(E_e, E_{\text{vis}}) dE_{\text{vis}} \end{aligned} \tag{2.2.3}$$

where N_+ is the number of antimuons and N_- is the number of muons below the Cherenkov tresshold. Most of the decayed muons follow a Michel spectrum $\frac{d\Gamma_{\text{michel}}}{dEe}(E_e)$ [163]. Nevertheless, one needs to take into account the fact that 18.4% of the μ^- are trapped in an atomic orbit which slightly modifies the spectrum to $\frac{d\Gamma_{\text{orbit}}}{dEe}(E_e)$ [164]. Again, C_s^i is a normalization constant so that $\sum_l C_l^i = 1$.

Once these coefficients are calculated, one can construct a χ_i^2 for each SK phase assuming that each quantity is normally distributed:

$$\chi_i^2 = \sum_{l=1}^{18} \frac{[(\alpha \cdot A_l^i) + (\beta \cdot B_l^i) + (\gamma \cdot C_l^i) - N_l^i]^2}{\sigma_{\text{stat}}^2 + \sigma_{\text{sys}}^2}\,, \tag{2.2.4}$$

where N_l^i is the number of events at the $l-$th bin taken from each $i-$th SK phase [154–157] and α, β, γ are the χ^2 fitting parameters that represent the total number of neutrinos from DM annihilation, neutrinos from the atmospheric neutrino flux and neutrinos from invisible muons respectively. The statistical error is $\sqrt{N_l^i}$ and dominates over the systematic error which is $\sim 6\%$ for each bin. We then combine these χ_i^2 into a single quantity, $\chi^2 = \chi_{\rm I}^2 + \chi_{\rm II}^2 + \chi_{\rm III}^2$, as done in Ref. [165]. The total χ^2 is minimized with respect to the rate of events of the two background components, resulting in a function of the event rate from DM annihilations, i.e., $\chi^2(\alpha)$. The 90% confidence level (C.L.) limit on the DM event rate, α_{90}, is obtained from

$$\frac{\int_0^{\alpha_{90}} \chi^2(\alpha)\, d\alpha}{\int_0^{\infty} \chi^2(\alpha)\, d\alpha} = 0.9 \ . \tag{2.2.5}$$

We show in Fig. 2.2 the 90% C.L. limit on the annihilation cross section from the SK data (blue solid line), which is obtained by solving [165]

$$\Gamma(\langle \sigma v_{\rm r} \rangle, m_\chi)\, A_{\rm tot} = \alpha_{90} \quad , A_{\rm tot} \equiv \frac{\sum_i A^i\, t_i}{\sum_i t_i} \ , \tag{2.2.6}$$

where A^i ($i = \{\rm I, II, III\}$) is the number of events for a monochromatic neutrino flux, $\delta(E_\nu - m_\chi)$, for each SK phase at the detector, and t_i are the corresponding data-taking times. Note that $\Gamma(\langle \sigma v_{\rm r} \rangle, m_\chi)$ was defined in Eq. 2.1.1.

From this analysis, we can determine the sensitivity of the next generation experiment Hyper-Kamiokande (HK). We start by estimating the number of neutrino events at HK for MeV energies using a scaling in fiducial volume of a factor of ~ 8.3, which corresponds to the ratio of the planned HK fiducial volume (187 kton) to the current SK fiducial volume (22.5 kton). In addition, studies show that adding 0.1% by mass of gadolinium (Gd) to the water detector would allow to tag the neutron produced in the IBD process which in turn, would reduce the background due to invisible muons by a factor of 5 [166]. In this analysis, we use the same energy resolution and efficiency for HK as the ones achieved during the different SK phases. The energy resolution is an important experimental parameter when determining the sensitivity of such monochromatic searches and therefore, our limits will be weaker

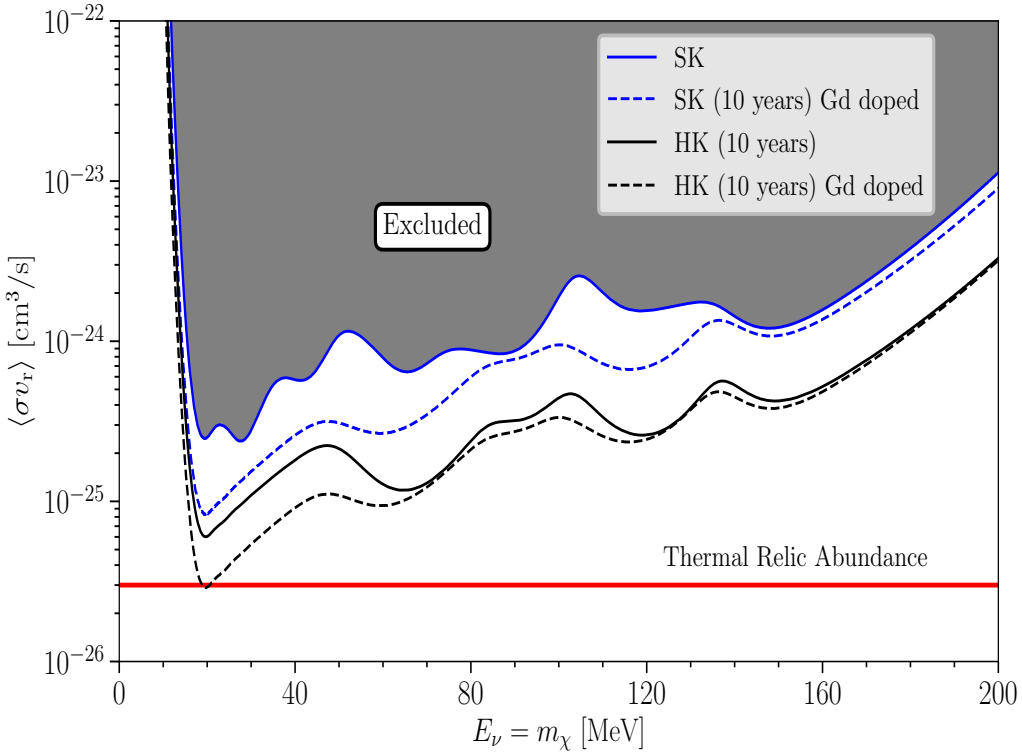

Figure 2.2: 90% confidence level limits on the DM self-annihilation cross section to neutrinos for different DM masses. The blue and black line correspond to the analysis done with SK data and the projections for HK respectively. The dashed lines represent the projections for the a Gd-doped detector for SK and HK and a data taken time of 10 years. The red line corresponds to the approximate value of the self-annihilation cross section of 3×10^{-26} cm^3/s, which is required to yield the observed relic abundance. Although this value will be smaller for MeV DM masses and it is model dependent, here we include this line as a benchmark point to which we compare our sensitivities to. A more precise analysis is done in Chapter 4 using appropiate numerical simulations.

if HK has a lower energy resolution than SK. We show in Fig. 2.2 the constraints on the thermally averaged DM annihilation to neutrinos that HK will be able to reach with 10 years of data-taking time with (solid black line) and without (dashed black line) Gd-doping. For reference we also include the sensitivity of a Gd-doped SK detector (which is actually an approved project [167]) after 10 years of taking data (dashed blue line). This figure shows that HK will be able to probe DM annihilation cross sections one order of magnitude larger than the analysis done using SK data. Moreover, adding Gd to the detector will allow to discover or rule out models where

DM annihilates into neutrinos for DM masses ~ 20 MeV. A more detailed analysis considering more backgrounds and more sophisticated statistics [165] could lead to better results and might allow us to probe a larger range of the parameter space where the thermal relic density could be achieved for different DM masses.

2.3 Conclusions

In this chapter we have reviewed the current status of indirect detection DM searches using neutrinos. For the different analyses presented, we have assumed that 100% of the DM annihilates to neutrinos and we have discussed how this allows to set strong model independent constraints on the DM self annihilation cross section to neutrinos for different DM masses. Furthermore, we have performed an analysis using SK data to constrain DM masses at low energies ($10 - 200$ MeV), and have showed the sensitivity that future large scale water Cherenkov neutrino detectors such as HK will have.

Competitive constraints from DM annihilations in the Sun to neutrinos, or other SM particles that decay to neutrinos, have also been derived by neutrino detectors such as SK [168] and IceCube [169]. These exploit the higher DM concentration expected in the solar interior since it could capture DM particles from the halo via scatterings. In all the realisations we study in this thesis, we explore the connection between the DM and the neutrino sector with very suppressed interactions with the rest of the SM and, in particular, with quarks. Thus, in these scenarios, the Sun does not accrete DM particles effectively and the constraints from these searches do not apply.

Chapter 3

Exhausting all the possibilities

> *Like every elementary particle. You can think of neutrinos as little points, as tiny pieces of reality. Strangely enough, these bizarre little chunks might be the answer to why we are here.*
>
> — Juan José Gómez Cadenas

We have seen the power of indirect detection searches in constraining the thermal DM parameter space for a wide range DM masses. In this chapter, we will explore the different ways in which a DM candidate can interact with neutrinos via renormalizable 4−dimensional operators. We will perform an exhaustive analysis of all the possible spin combinations of the DM candidate and mediator that connects neutrinos to the DM sector. We will also discuss the allowed region of the parameter space for each scenario when the constraints discussed in Sec. 1.5 are taken into account.

3.1 Scenarios considered

In order to determine the viability of models with DM-ν interactions, we can carry out a systematic study assuming that DM only interacts with left-handed active neutrinos. In this way, we can establish the list of all possible dimension 4 scenarios (i.e., the combination of DM and mediator particles) consistent with Lorentz invariance[1]. Here we follow a simplified model approach and consider only the interaction terms that are relevant at low energies. Two possible UV-completions where the DM phenomenology is dominated by neutrinos will be discussed in Chapter 4.

In this chapter, we refer to the DM candidate as χ. The mediator is referred to as Z' if it is a spin-1 particle, ϕ if it is a spin-0 particle and N if it is a spin-1/2 particle. The expressions for the relevant interaction terms in the Lagrangian, and for the approximate elastic scattering and annihilation cross sections are summarized in Table 3.1. When the DM candidate is a spin-1 particle, we consider a real vector candidate, since the only difference with the case of complex vector DM coupled to a Dirac (Majorana) mediator is a factor of $\frac{1}{4}$ ($\frac{5}{12}$) in the annihilation cross section[2]. To perform our calculations, we have assumed that

- There are only left-handed neutrinos in the final and/or initial states. For simplicity, we do not differentiate between neutrino species.
- Neutrino masses can be neglected. Nevertheless, the neutrino mass generation mechanism and the particular nature (Dirac vs Majorana) of neutrinos would impose further constraints on the parameter space.
- The elastic scattering cross section could be safely averaged over the range $\cos\theta \in [-0.95, 0.95]$, to avoid the co-linear divergence [170, Chapter 20.3].
- The DM-ν coupling (g) is equal to 1. This means that we are probing the

[1]Scenarios with DM candidates of any spin interacting with a triplet scalar mediator have a very similar phenomenology to those cases with a spin-1 mediator. Thus, we disregard them for simplicity.

[2]This is due to the fact that a real vector DM with a fermion mediator annihilates via a t- and a u- channel, while a complex vector DM proceeds via a t- channel only.

regime where DM is strongly coupled to neutrinos. Limits can be rescaled accordingly when $g \ll 1$ and will be discussed in the text.

- For the calculations of the elastic scattering we have assumed that neutrinos follow a Fermi-Dirac distribution with temperature T_ν and consequently, $\langle E_\nu^2 \rangle \simeq 12.9\, T_\nu^2$ and $\langle E_\nu^4 \rangle \simeq 396\, T_\nu^4$.
- Indirect detection bounds are computed considering the total observed DM relic abundance and a regeneration mechanism [171] is assumed for the regions of the parameter space where the DM would be under-abundant otherwise.

We have checked that all the scenarios considered in this chapter predict a late kinetic decoupling (in agreement with the way the collisional damping bound was derived in [116]) and that the elastic cross section calculations are valid at low energies (see Appendix B in Ref. [3] for the full expressions and their approximations at low and high energies). The elastic scattering cross section depends on the neutrino temperature T_ν. The latter differs from the photon temperature after the standard neutrino decoupling. Moreover, DM-ν interactions may modify the neutrino temperature by reheating the neutrino sector due to DM annihilations, as discussed in Sec. 1.5.1. However, the difference between the neutrino and photon temperatures is bound to be small, owing to the $N_{\rm eff}$ constraint. Hence we have approximated the neutrino temperature to $T_\nu = T_\gamma$ throughout this work.

Scenario	Lagrangian ($\mathcal{L}_{\rm int}$)	$\sigma \mathbf{v}_{\rm r}$	$\sigma_{\rm el}$
Complex Scalar DM Dirac Mediator	$-g\,\chi\,\overline{N_{\rm R}}\,\nu_{\rm L}\ +\ \text{h.c.}$	$\frac{g^4}{12\,\pi}\frac{m_\chi^2}{(m_\chi^2+m_{\rm N}^2)^2}\,v_{\rm CM}^2$	$\frac{g^4}{32\,\pi}\frac{m_\chi^2\,y^2}{(m_{\rm N}^2-m_\chi^2)^2}$
Real Scalar DM Dirac Mediator		$\frac{4\,g^4}{15\,\pi}\frac{m_\chi^6}{(m_\chi^2+m_{\rm N}^2)^4}\,v_{\rm CM}^4$	$\frac{g^4}{8\,\pi}\frac{m_\chi^6\,y^4}{(m_{\rm N}^2-m_\chi^2)^4}$
Complex Scalar DM Majorana Mediator		$\frac{g^4}{16\,\pi}\frac{m_{\rm N}^2}{(m_\chi^2+m_{\rm N}^2)^2}$	$\frac{g^4}{32\,\pi}\frac{m_\chi^2\,y^2}{(m_{\rm N}^2-m_\chi^2)^2}$
Real Scalar DM Majorana Mediator		$\frac{g^4}{4\,\pi}\frac{m_{\rm N}^2}{(m_\chi^2+m_{\rm N}^2)^2}$	$\frac{g^4}{8\,\pi}\frac{m_\chi^6\,y^4}{(m_{\rm N}^2-m_\chi^2)^4}$
Dirac DM Scalar Mediator	$-g\overline{\chi_{\rm R}}\nu_{\rm L}\phi\ +\ \text{h.c.}$	$\frac{g^4}{32\,\pi}\frac{m_\chi^2}{(m_\chi^2+m_\phi^2)^2}$	$\frac{g^4}{32\,\pi}\frac{m_\chi^2\,y^2}{(m_\chi^2-m_\phi^2)^2}$
Majorana DM Scalar Mediator		$\frac{g^4}{12\,\pi}\frac{m_\chi^2}{(m_\chi^2+m_\phi^2)^2}\,v_{\rm CM}^2$	$\frac{g^4}{16\,\pi}\frac{m_\chi^2\,y^2}{(m_\chi^2-m_\phi^2)^2}$
Vector DM Dirac Mediator	$-g\overline{N_{\rm L}}\gamma^\mu\chi_\mu\nu_{\rm L}\ +\ \text{h.c.}$	$\frac{2\,g^4}{9\,\pi}\frac{m_\chi^2}{(m_\chi^2+m_{\rm N}^2)^2}$	$\frac{g^4}{4\,\pi}\frac{m_\chi^2\,y^2}{(m_\chi^2-m_{\rm N}^2)^2}$
Vector DM Majorana Mediator		$\frac{g^4}{6\,\pi}\frac{m_{\rm N}^2}{(m_\chi^2+m_{\rm N}^2)^2}$	
Complex Scalar DM Vector Mediator	$-g_\chi Z'^\mu((\partial_\mu\chi)\chi^\dagger-(\partial_\mu\chi)^\dagger\chi)$ $-g_\nu\overline{\nu_L}\gamma^\mu Z'_\mu\nu_{\rm L}$	$\frac{g_\chi^2\,g_\nu^2}{3\,\pi}\frac{m_\chi^2}{(4\,m_\chi^2-m_{\rm Z'}^2)^2}\,v_{\rm CM}^2$	$\frac{g_\chi^2\,g_\nu^2}{8\,\pi}\frac{m_\chi^2\,y^2}{m_{\rm Z'}^4}$
Dirac DM Vector Mediator	$-g_{\chi_{\rm L}}\overline{\chi_{\rm L}}\gamma^\mu Z'_\mu\chi_{\rm L}\ -\ g_{\chi_{\rm R}}\overline{\chi_{\rm R}}\gamma^\mu Z'_\mu\chi_{\rm R}$ $-g_\nu\overline{\nu_L}\gamma^\mu Z'_\mu\nu_{\rm L}$	$\frac{g_\chi^2\,g_\nu^2}{2\,\pi}\frac{m_\chi^2}{(4\,m_\chi^2-m_{\rm Z'}^2)^2}$	$\frac{g_\chi^2\,g_\nu^2}{8\,\pi}\frac{m_\chi^2\,y^2}{m_{\rm Z'}^4}$
Majorana DM Vector Mediator	$-\frac{g_\chi}{2}\bar{\chi}\gamma^\mu Z'_\mu\gamma^5\chi$ $-g_\nu\overline{\nu_L}\gamma^\mu Z'_\mu\nu_{\rm L}$	$\frac{g_\chi^2\,g_\nu^2}{12\,\pi}\frac{m_\chi^2}{(4\,m_\chi^2-m_{\rm Z'}^2)^2}\,v_{\rm CM}^2$	$\frac{3\,g_\chi^2\,g_\nu^2}{32\,\pi}\frac{m_\chi^2\,y^2}{m_{\rm Z'}^4}$
Vector DM Vector Mediator	$-g_\chi\frac{1}{2}\chi^\mu\partial_\mu\chi^\nu Z'_\nu\ +\ \text{h.c.}$ $-g_\nu\overline{\nu_L}\gamma^\mu Z'_\mu\nu_{\rm L}$	$\frac{g_\chi^2\,g_\nu^2}{\pi}\frac{m_\chi^2}{(4\,m_\chi^2-m_{\rm Z'}^2)^2}\,v_{\rm CM}^2$	$\frac{g_\chi^2\,g_\nu^2}{8\,\pi}\frac{m_\chi^2\,y^2}{m_{\rm Z'}^4}$

Table 3.1: This table presents the relevant interaction terms in the Lagrangian, the approximate expressions for the annihilation cross section and the low-energy limit of the elastic scattering for all possible scenarios that involve DM-ν interactions (12 in total). Only the leading terms in $v_{\rm CM}$ and $y = (s - m_{\rm DM}^2)/m_\chi^2 \simeq 2\,E_\nu/m_\chi$ (where s is the usual Mandelstam variable) are presented for the annihilation cross section and the elastic scattering cross section, respectively. We refer the reader to Appendix B in Ref. [3] for the full expressions of the elastic scattering cross sections.

3.2 Results for scalar or fermion mediators

Eight out of the twelve scenarios tabulated in Tab. 3.1 involve spin-0 and spin-1/2 mediators. Many share common properties, so we will articulate the discussion accordingly. In all of these eight scenarios, a left-handed neutrino couples directly to the DM candidate and the mediator must be heavier than the DM candidate to prevent DM from decaying. This stability condition excludes half the parameter space of the $(m_\chi - m_{\rm Mediator})$ plane, as shown in Fig. 3.1.

In all these eight configurations, the DM annihilation cross section never involves an s- channel and is therefore never resonantly enhanced[3]. Furthermore, in most cases, we observe that the annihilation cross section is dominated by a velocity-independent term, except for complex scalar or Majorana DM for which it is v^2-suppressed and for real DM candidates, as it is v^4-suppressed. As expected, a velocity-suppressed cross section weakens the indirect detection constraint (since $v_{\rm CM} \sim 2 \times 10^{-3}\ c$ in the halo today [132]), which in turns opens up the parameter space, as shown explicitly in Fig. 3.1 (right panel) (see Sec. 2.1.1 for details).

The elastic scattering cross section associated with these scenarios is proportional to the square of the neutrino energy (E_ν^2). The only exception occurs for real DM candidates in which case the elastic scattering cross section varies as E_ν^4 (see Table 3.1). We note also that, for a very strong mass degeneracy ($m_{\rm Mediator} - m_\chi \ll E_\nu$), the denominator of the propagator depends on the DM mass and the transferred momentum, which is similar to the neutrino energy. Consequently, this factor of E_ν^2 or E_ν^4 in the denominator cancels out with the factor in the numerator. Therefore, the elastic cross section no longer depends on the neutrino energy and it can be considerably enhanced [172]. This is shown as the region along the diagonal in Fig. 3.1.

All (elastic scattering and annihilation) cross sections depend on both the DM

[3]In the case of a triplet scalar mediator, the annihilation cross section proceeds via an s- channel, but we have not considered it in the eight scenarios above.

and mediator masses, as well as the coupling g. One can therefore constrain both the DM and mediator masses using the collisional damping and indirect detection constraints for a fixed value of the coupling g, which we take to be unity in the figures for definiteness.

3.2.1 Fermion DM and scalar mediators

Most of the scenarios listed in this section predict a similar phenomenology. For illustration purposes, we shall focus on fermion DM particles coupled to a scalar mediator. However, the discussion below can be easily extended to other scenarios.

The corresponding Lagrangian is given by

$$\mathcal{L}_{\rm int} \supset - g\,\phi\,\overline{\chi_{\rm R}}\,\nu_{\rm L} \;+\; \text{h.c.}\,, \tag{3.2.1}$$

where χ is the DM candidate and can be either a Dirac or Majorana particle. Since the neutrino is a member of an $SU(2)$ doublet, one can consider two minimal extensions of the SM which include such a coupling. First, $\chi_{\rm R}$ can be promoted to an $SU(2)$ doublet like in supersymmetric models [173, 174] or supersymmetry-inspired models [172]. This would constrain the DM mass to be heavier than few GeVs or even few TeVs in the presence of co-annihilations [175, 176]. Second, we can assume $\chi_{\rm R}$ to be a singlet and the scalar ϕ a $SU(2)$ doublet like in inert doublet models [177]. This would also imply that the DM necessarily interacts with charged leptons, a scenario which is strongly constrained by cosmological observations, astrophysics and particle physics experiments [178]. Therefore, such interactions would need to be suppressed, for instance by a very heavy charged mediator [172, 179].

In order to consider masses below the 100 GeV scale for the DM and the mediator, both fields need to be singlets. The required coupling in Eq. (3.2.1) can then be generated via mixing with extra scalar or fermion doublets. If the mixing occurs via an extra fermion doublet R, the strongest constraints arise from lepton flavour violating processes at one loop and from measurements of the anomalous magnetic moments of the electron and the muon [172, 180, 181]. On the other hand, if one

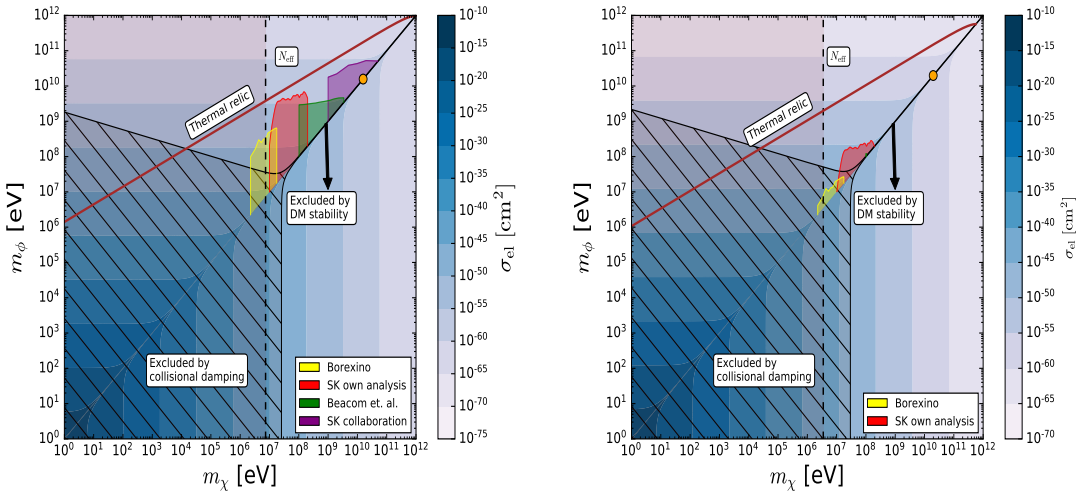

Figure 3.1: Elastic scattering of Dirac DM (left panel) and Majorana DM (right panel) coupled to a scalar mediator in the $m_\phi - m_\chi$ plane for $g = 1$. Different regions are constrained by: the collisional damping limit (dashed region and black line along the diagonal up to the orange dot), a conservative bound from the antineutrino flux at Borexino [136] (in yellow), our analysis at Super-Kamiokande (SK) described in Sec. 2.2 (in red), the analysis done in Ref. [128] using results from SK, Fréjus and Amanda (in green), and the analysis done by the SK collaboration for GeV neutrinos produced at the Galactic Centre [130] (in purple). The parameters that give rise to the right relic abundance (brown line) are shown as a reference. The dashed line refers to the DM mass lower bound derived from $N_{\rm eff}$ in [105, 108] as discussed in Sec. 1.5.1.

introduces another scalar doublet, η, that mixes with the scalar DM singlet, ϕ, there are tight, though model-dependent, constraints on the effective DM-ν coupling from the requirement that $2 \to 2$ scalar processes must be unitary [182]. In the following chapter, we will study the possibility of generating an effective DM-ν coupling via neutrino mixing with an additional right-handed fermion singlet.

Annihilation cross section. Dirac particles annihilate via a constant cross section while the cross section is v^2-dependent for Majorana particles. Nevertheless, both models can explain the observed DM abundance if the value of their annihilation cross section is of the order of $\langle \sigma v_{\rm r} \rangle \simeq 3 \times 10^{-26}$ cm^3/s and $\langle \sigma v_{\rm r} \rangle \simeq 6 \times 10^{-26}$ cm^3/s, respectively, represented by the brown lines in Fig. 3.1. For the parameters below that line, the annihilation cross section is larger than the thermal value. Hence, χ's

cannot constitute all the DM unless one invokes a different production mechanism, such as the decay of an unstable heavy particle (see Ref. [183] for a recent review of non-thermal DM production mechanisms) or a regeneration mechanism [171]. In contrast, configurations above the brown line over-predict the DM abundance and require, e.g., additional annihilation channels to explain the observed abundance.

We note that, in these fermion DM scenarios, the mediator needs to be light if the DM is weakly coupled to neutrinos, i.e., $g \ll 1$. Furthermore, the DM cannot be too heavy. Indeed the stability condition, $m_\chi < m_\phi$, leads to an upper limit on the DM mass of $m_\chi < 10^4$ (100) MeV for $g = 10^{-1}$ (10^{-2}) (see Fig. 3.2). If we further impose the limit on $N_{\rm eff}$ and require thermal DM, then any coupling smaller than $g \ll 10^{-2}$ is ruled out.

As expected from the velocity-dependence of the cross section, indirect detection searches are much more sensitive to Dirac DM candidates than Majorana DM particles (see Fig. 3.1). Dirac DM candidates strongly coupled to neutrinos ($g \sim 1$ and $\langle \sigma v_{\rm r} \rangle > 10^{-26}$ cm^3/s) are excluded by a combination of low-energy neutrino detectors (such as Borexino) and high-energy experiments, including SK, even when their mass is up to ~ 100 GeV. As such, limits from future neutrino detectors combined with those from CMB and gamma-ray observations [6, 54, 133, 184–217] could rule out the entire thermal DM region below ~ 100 GeV.

The bounds derived above become significantly weaker when the value of the coupling g becomes smaller (see Fig. 3.2). In fact there is no observable signal at SK (and at future neutrino detectors) when g becomes smaller than $g = 10^{-1}$ (10^{-2}) if the DM mass is a few GeV (MeV). Note however, that, since the annihilation cross section controls both the thermal relic density and the indirect detection constraints, it is always possible to test thermal DM candidates in future neutrino experiments as long as $g \geq 10^{-2}$.

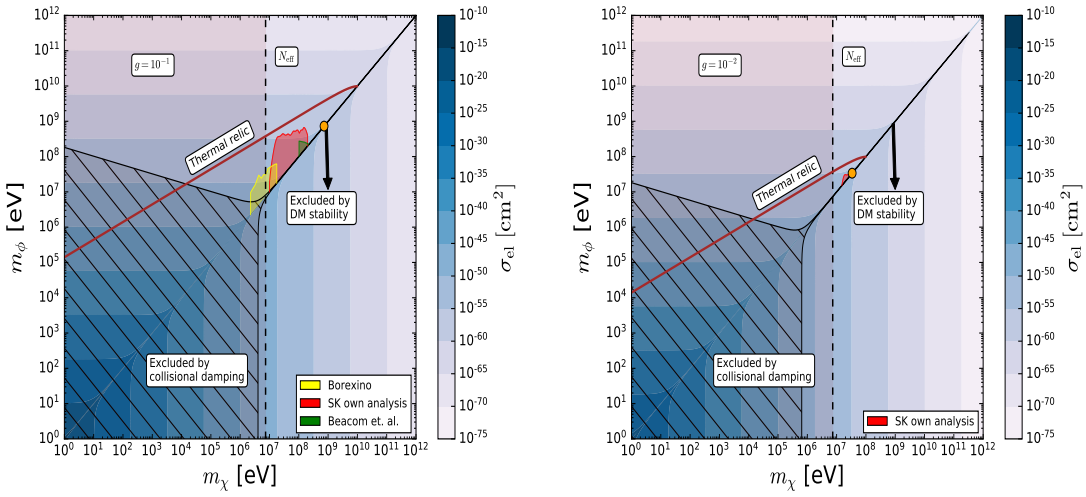

Figure 3.2: Same as left panel of Fig. 3.1 but for $g = 10^{-1}$ (left panel) and for $g = 10^{-2}$ (right panel).

Elastic scattering cross section. The elastic scattering cross section is similar for Majorana and Dirac DM. It reads

$$\sigma_{\rm el} \simeq 1.1\,(2.2)\,\times 10^{-41}\; g^4\; \left(\frac{E_\nu}{T_0}\right)^2\; \left(\frac{m_\phi}{\rm MeV}\right)^{-4}\; \left(1-\left(\frac{m_\chi}{m_\phi}\right)^2\right)^{-2}\; {\rm cm}^2, \qquad (3.2.2)$$

for Dirac (Majorana) DM candidates, where $T_0 = 2.35 \times 10^{-4}$ eV is the photon temperature today. The difference stems from the additional s- channel diagram in the Majorana case. When the DM and mediator masses are degenerated, the elastic scattering cross section in the low-energy regime becomes

$$\sigma_{\rm el} = 1\,(2) \times g^4\; \frac{1}{32\;\pi\; m_\chi^2} \simeq 4\;(8) \times 10^{-24}\; g^4\; \left(\frac{m_\chi}{\rm MeV}\right)^{-2}\; {\rm cm}^2, \qquad (3.2.3)$$

for Dirac (Majorana) DM candidates. Therefore, the collisional damping constraint can only exclude masses below $\sim \mathcal{O}(10)$ GeV. In general, collisional damping bounds require rather large values of the elastic scattering cross section, i.e., light mediators, ($m_\phi \in [\mathcal{O}(10), \mathcal{O}(10^3)]$ MeV), and light DM particles (with a mass in the sub–10 MeV range), or degenerate values of the DM and mediator masses between $m_\chi \sim [10, 10^4]$ MeV for $g = 1$, to enhance the elastic scattering cross section. Given the $N_{\rm eff}$ bound on the DM mass and the Borexino constraints, the first possibility (light DM and light mediators) is mostly excluded for any value of the coupling.

The second option (degenerate masses) is ruled out by the other indirect detection searches for a large coupling ($g = 1$).

The exclusion region for fermion DM candidates weakly coupled to neutrinos (i.e., $g \ll 1$) is shown in Fig. 3.2. As one can see, the regions excluded by indirect detection searches and the collisional damping mechanism become smaller. As a result, Dirac DM candidates heavier than a few GeVs are now allowed.

One can obtain an expression for the elastic scattering cross section that is independent of the coupling g by combining the elastic scattering and annihilation cross sections when $m_\phi \gg m_\chi$. The latter reads

$$\sigma_{\rm el} \simeq 2.6\,(19) \times 10^{-54} \left(\frac{E_\nu}{T_0}\right)^2 \left(\frac{m_\chi}{\rm MeV}\right)^{-2} \left(\frac{\langle\sigma v_{\rm r}\rangle}{3\times 10^{-26}\,{\rm cm}^3/{\rm s}}\right) \,{\rm cm}^2\,, \qquad (3.2.4)$$

for Dirac (Majorana) DM, assuming $v_{\rm CM} \simeq 1/3$ at freeze-out. This expression can be used to set a lower bound on the DM mass from the collisional damping constraint in Eq. (1.5.3) and requiring DM annihilations into neutrinos to explain the observed DM abundance. As can be readily seen from Eq. (3.2.4), thermal candidates must be heavier than $m_\chi > 14$ keV or $m_\chi > 34$ keV for Dirac or Majorana DM candidates, respectively. These constraints are not as stringent as the limits from $N_{\rm eff}$ described in Sec. 1.5.1, which impose $m_\chi > 10$ MeV for Dirac DM and $m_\chi > 3.5$ MeV for Majorana DM [105, 108]. However, unlike the $N_{\rm eff}$ constraint, the collisional damping bound remains valid in the case of asymmetric DM candidates, and also enables to constrain the mediator mass. Furthermore, it is worth recalling that we have used a conservative limit from collisional damping, which may improve with a better knowledge of the matter distribution in the early Universe and an improved understanding of the role of baryonic physics in galaxy formation.

Finally, the lower limit on the DM mass that we have found by combining the annihilation and scattering cross sections should remain the same when $g \ll 1$, because both the annihilation and elastic scattering cross sections scale in the same way with respect to the coupling g.

Other scenarios where the mediator is either a fermion or a scalar, show a similar

behaviour to the one discussed here if no lepton number violating (LNV) process occurs. Specifically, scenarios in which a vector DM candidate is coupled to a Dirac mediator would have a very similar behaviour to the case of a Dirac DM particle coupled to a scalar mediator. Indeed, the leading term in the annihilation cross section is velocity-independent and features the same DM and mediator mass dependence. The scenario with a complex scalar DM coupled to a Dirac mediator is analogous to the Majorana DM case, and given the v^2-dependence of the annihilation cross section, indirect DM searches are less sensitive to it. The only case which is somewhat different is the real scalar DM and Dirac mediator scenario, since the annihilation cross section scales as v^4. Therefore, finding evidence for this scenario using indirect detection searches would be very challenging. In this case, unless $m_\chi \sim m_{\rm N}$, the elastic cross section is severely suppressed, as it varies as E_ν^4. Therefore, for this scenario we only expect sizable collisional damping when the mediator and DM masses are similar and in the $\sim [4, 10^4]$ MeV range, i.e., above the $N_{\rm eff}$ bound (see Appendix A in Ref. [3] for the relevant results of the remaining scenarios).

3.2.2 Scalar DM and Majorana mediators

When the mediator is a Majorana particle, LNV processes are allowed and change the phenomenology significantly. In fact, LNV processes may constitute the dominant annihilation channels. This is the case for example when the DM is a spin-0 or a spin-1 particle that interacts with active neutrinos through the exchange of a Majorana fermion $N_{\rm R}$. We will focus here on the spin-0 DM scenario for concreteness, but similar conclusions apply to a spin-1 DM candidate. The term in the Lagrangian describing this interaction corresponds to

$$\mathcal{L}_{\rm int} \supset - g\, \chi\, \overline{N_{\rm R}}\, \nu_{\rm L} \,+\, \text{h.c.}\,, \tag{3.2.5}$$

and applies regardless of whether the DM candidate, χ, is a real or a complex scalar. Note that the same interaction term can also lead to neutrino masses at loop level [85, 218–220].

Annihilation cross section. The two dominant annihilation channels are $\chi\chi^* \to \nu\nu$ and $\chi\chi^* \to \bar{\nu}\bar{\nu}$, which violate lepton number by two units. We ignore annihilations into $\chi\chi^* \to \nu\bar{\nu}$, even though they also take place in LNV scenarios because the associated cross section is v^2-suppressed. This scenario provides a natural implementation of thermal light DM candidates while keeping the mass of the mediator very heavy. The annihilation cross section is proportional to

$$\langle \sigma v_{\rm r} \rangle \propto g^4 \, \frac{m_{\rm N}^2}{\left(m_\chi^2 + m_{\rm N}^2\right)^2} \propto \frac{g^4}{m_{\rm N}^2} \ , \tag{3.2.6}$$

when $m_{\rm N} \gg m_\chi$. The relic density does not constrain the DM mass, but only the mediator mass and the coupling g, satisfying the relation

$$m_{\rm N} \simeq \mathcal{O}(1)\, g^2 \left(\frac{\langle \sigma v_{\rm r} \rangle}{3 \times 10^{-26}\, {\rm cm}^3/{\rm s}} \right)^{-\frac{1}{2}} \ {\rm TeV}. \tag{3.2.7}$$

Hence, the DM candidate could be light while the mediator could be very heavy, i.e., with a mass of a few TeVs for $g = 1$. Since the leading term in the annihilation cross section is velocity-independent, we expect a copious production of neutrinos in the galactic halo. As a result, indirect detection searches set significant constraints and exclude a large fraction of the parameter space for DM particles with a mass in between $[2, 10^4]$ MeV.

Elastic scattering cross section. The elastic scattering is mostly controlled by the mediator mass and E_ν, and reads

$$\sigma_{\rm el} \simeq 1.2 \times 10^{-41} \ g^4 \ \left(\frac{E_\nu}{T_0} \right)^2 \ \left(\frac{m_{\rm N}}{\rm MeV} \right)^{-4} \ \left(1 - \left(\frac{m_\chi}{m_{\rm N}} \right)^2 \right)^{-2} \ {\rm cm}^2 \ , \tag{3.2.8}$$

assuming $m_{\rm N} \gg m_\chi$. As for the previous scenario, this cross section can be significantly enhanced if both the mediator and DM masses are degenerate.

Observable collisional damping effects require either very light DM particles, $m_\chi < 2$ MeV or degenerate DM and mediator masses with values below $m_\chi < 10$ GeV. This is however excluded by the $N_{\rm eff}$ bound and indirect DM searches, respectively. Furthermore, if the DM candidate is a real scalar, the elastic scattering cross section scales as E_ν^4 and it is therefore very suppressed. Consequently, there is no room for significant collisional damping in this case.

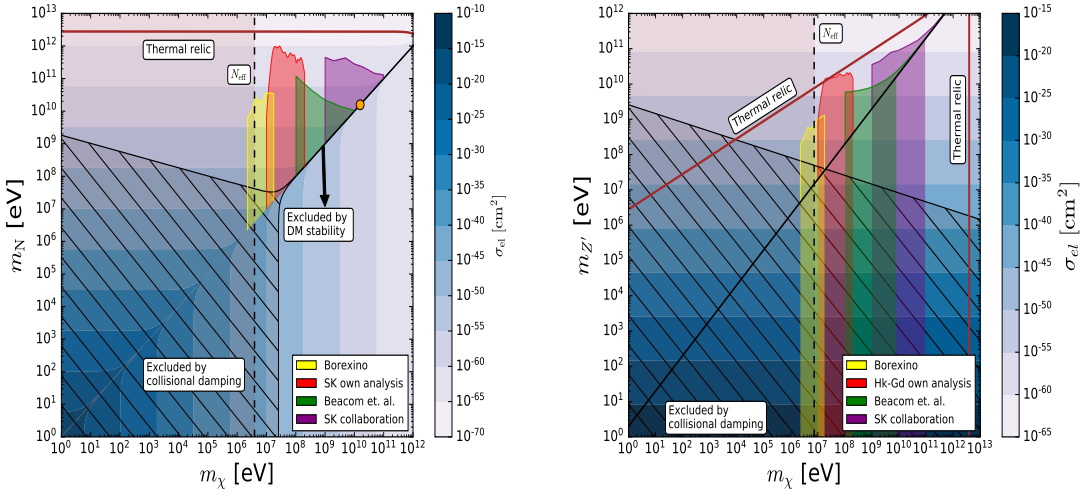

Figure 3.3: Same as Fig. 3.1 but for complex DM with a Majorana mediator (left panel) and for Dirac DM with a vector mediator (right panel).

3.3 Results for a vector mediator

We now discuss scenarios where the mediator is a spin-1 particle. There are four possible Lagrangians to describe DM-ν interactions in presence of such a mediator, which are shown in Table 3.1. For concreteness, let us focus on scenarios with a spin-0 or spin-1/2 (Dirac) DM candidate. The associated Lagrangians read

$$\mathcal{L}_{\rm int} \supset \begin{cases} -g_\nu \overline{\nu_{\rm L}} \gamma^\mu Z'_\mu \nu_{\rm L} - g_\chi Z'^\mu \left((\partial_\mu \chi) \chi^\dagger - (\partial_\mu \chi)^\dagger \chi \right), \\ -g_\nu \overline{\nu_{\rm L}} \gamma^\mu Z'_\mu \nu_{\rm L} - g_{\chi_{\rm L,R}} \overline{\chi_{\rm L,R}} \gamma^\mu Z'_\mu \chi_{\rm L,R} \ . \end{cases} \tag{3.3.1}$$

In both cases, the first term represents the coupling of the spin-1 particle to active neutrinos while the second term represents the spin-1 coupling to the DM particle. The top and the bottom lines correspond to a vector mediator which couples to a complex scalar or a Dirac DM candidate respectively. This type of interaction was initially introduced in Refs. [113, 172] as an attempt to build viable models of sub-GeV DM candidates and illustrates the new collisional damping effects described in Refs. [111, 113].

More recently, models where the DM is coupled to a light spin-1 mediator have been proposed in the context of self-interacting DM [221] and models with both self-interactions and DM-ν interactions (all mediated by a spin-1 boson) have also been

considered in Refs. [222–224]. In these references, collisional damping – that stems from early DM interactions – is neglected and the thermal-production assumption has been relaxed.

The phenomenology of these scenarios with spin-1 mediators is different from that associated with spin-0 and spin-1/2 mediators. Firstly, the absence of a direct coupling between the DM candidate and neutrinos ensures the stability of the DM candidate. Mediators lighter than the DM are allowed (unlike for the spin-0 and spin-1/2 mediator cases). Secondly, since DM can be heavier than the mediator, DM particles can also annihilate into two spin-1 particles. This process may actually be the dominant annihilation channel, depending on the exact value of the couplings.

Annihilation cross section. For concreteness, we shall consider Dirac DM candidates coupled to vector boson mediators, i.e., $g_{\chi_{\rm L}} = g_{\chi_{\rm R}} = g_\chi$. When the mediator is heavier than the DM particles, the only possible annihilation channel is a neutrino/antineutrino pair. The associated cross section is given by

$$\langle \sigma v_{\rm r} \rangle = \frac{g_\chi^2\, g_\nu^2}{2\,\pi} \frac{m_\chi^2}{(4\,m_\chi^2 - m_{\rm Z'}^2)^2} \simeq \frac{g_\chi^2\, g_\nu^2}{2\,\pi} \frac{m_\chi^2}{m_{\rm Z'}^4} \ , \tag{3.3.2}$$

which can become resonant since it proceeds via an s- channel diagram. We do not illustrate the impact of the resonance on the parameter space but a smaller value of the coupling would be required to explain the observed DM abundance[4].

When the mediator is lighter than the DM particles, annihilations can be both i) into neutrino/antineutrino pairs, with a cross section of the order of

$$\langle \sigma v_{\rm r} \rangle_{\nu\bar{\nu}} \simeq \frac{g_\chi^2\, g_\nu^2}{32\,\pi} \frac{1}{m_\chi^2} \ , \tag{3.3.3}$$

and ii) into two vector bosons, with a cross section of the order of

$$\langle \sigma v_{\rm r} \rangle_{Z'\,Z'} = \frac{g_\chi^4}{8\,\pi\, m_\chi^2} \sqrt{1 - \frac{m_{\rm Z'}^2}{m_\chi^2}} \simeq \frac{g_\chi^4}{8\,\pi} \frac{1}{m_\chi^2} \ , \tag{3.3.4}$$

[4]In fact, using the Breit-Wigner form of the propagator, a DM mass of the order of $\mathcal{O}(100)$ TeV would be needed to explain the observed DM abundance for $g_\chi = 1$.

which does not have a resonant structure since the Z' are produced via a t- channel diagram.

Both final states eventually contribute to the relic density calculations. However one may dominate over the other one, depending on the relative strength of g_χ and g_ν (hence the two thermal lines in Fig. 3.3). One expects a lower limit on the Z' mass if Z''s are copiously produced by DM annihilations and decay into neutrinos after the standard neutrino decoupling, as this would lead to an increase in $N_{\rm eff}$. To avoid such a limit, one can invoke additional Z' decay channels to suppress the branching fraction into neutrinos.

Here, we only consider the $\chi\bar{\chi} \to \nu\bar{\nu}$ channel in order to derive the constraints from indirect detection searches. For mediators lighter than the DM mass, the DM annihilation into two vector bosons could also yield a signal in neutrino detectors if the produced Z' bosons decay into neutrino/antineutrino pairs. This signal would however generate a box-shaped energy spectrum that depends on the Z' branching ratio into neutrinos and on the $m_\chi/m_{Z'}$ ratio [225, 226]. For simplicity, we do not consider this case.

Note that the Sommerfeld enhancement of the annihilation cross section when $m_{Z'} \ll m_\chi$ at the time of freeze-out is expected to be small and consequently, we disregard this effect[5]. However, the Sommerfeld effect might be important at late-times and it might increase the neutrino production in the galactic halo, in particular for v^2-dependent cross sections and DM masses above 1 TeV [229, 230]. Nevertheless, our analysis focuses on smaller DM masses and we do not consider the effects of such enhancements, although this might rule out tiny DM mass regions between the 1–100 TeV regime, depending on the particular scenario [226].

The scalar and Majorana DM case is similar except that the annihilation cross section is v^2-dominated and therefore suppressed with respect to the Dirac DM case. Yet, despite the v^2-dependent suppression, indirect detection searches rule out

[5]We expect order $\mathcal{O}(1)$ corrections to our relic density results [227, 228].

the parameter space where large collisional damping effects would be expected (see Appendix C in Ref. [3]).

Elastic scattering cross section. The elastic scattering cross section for spin-1 mediator scenarios is independent of the DM mass. It reads

$$\sigma_{\rm el} \simeq 4.4 \times 10^{-41}\, g_\nu^2\, g_\chi^2 \left(\frac{E_\nu}{T_0}\right)^2 \left(\frac{m_{Z'}}{\rm MeV}\right)^{-4} {\rm cm}^2 \,, \tag{3.3.5}$$

which proceeds via a t- channel diagram and is proportional to E_ν^2, in contrast to previous scenarios in which the cross section is energy-independent in the regime of degenerate DM and mediator masses. Moreover, contrary to scenarios with a spin-0 and a spin-1/2 mediator, the $m_{Z'} < m_\chi$ region could give rise to measurable collisional damping for $m_\chi >$ few MeV. However, for constant annihilation cross sections, indirect detection constraints imply that only DM masses above $\gtrsim 100$ GeV and mediators between $[1, 10]$ MeV would produce sizable collisional damping for $g_\nu = g_\chi = 1$. This is alleviated if the DM annihilation cross section is velocity-dependent (for Majorana, scalar and vector DM candidates). In such cases, collisional damping could be important for $m_\chi \sim [1, 10]$ MeV and $m_\chi \gtrsim 100$ MeV with $m_{Z'} \sim [1, 100]$ MeV. Moreover, for $g_\chi \sim g_\nu \ll 1$ indirect detection constraints weaken, allowing for sizable collisional damping for $m_\chi \sim [0.4, 1]$ GeV and $\mathcal{O}$(few) MeV mediators masses for $g = 10^{-1}$, while $m_\chi \gtrsim 100$ MeV and sub-MeV mediators are required for $g = 10^{-2}$.

For a thermal DM candidate and $m_\chi \ll m_{Z'}$,

$$\sigma_{\rm el} \simeq 7.7 \times 10^{-55} \left(\frac{E_\nu}{T_0}\right)^2 \left(\frac{m_\chi}{\rm MeV}\right)^{-2} \left(\frac{\langle \sigma v_{\rm r} \rangle}{3 \times 10^{-26}\ {\rm cm}^3/{\rm s}}\right) {\rm cm}^2 \,, \tag{3.3.6}$$

so that, using the collisional damping and relic density constraints, we obtain a lower limit on the DM mass independent of the DM coupling to the mediator and neutrinos (g_χ and g_ν, respectively). More specifically, we find $m_\chi \geq 9.2$ keV. This lower bound is again less constraining than the one derived by the change in $N_{\rm eff}$, which in turn, also excludes observable collisional damping for light DM candidates and $m_{Z'} \sim [10, 10^3]$ MeV. Nevertheless, indirect constraints could still constrain a

large region of the parameter space when $g_\nu \ll 1$ if one considers the annihilation channel into a pair of Z' and its subsequent decay into neutrinos for a strongly coupled dark sector ($g_\chi \simeq 1$).

Finally, if the DM candidate is heavier than the mediator, to produce the correct DM relic density assuming only DM-ν interactions, Eq. (3.3.1), requires $m_\chi \simeq 4\, g_\chi^2 \left(1 + \frac{1}{4}\left(\frac{g_\nu}{g_\chi}\right)^2\right)^{\frac{1}{2}}$ TeV. Therefore, in the $m_\chi \gg m_{Z'}$ limit and for a thermal DM candidate, the elastic cross section is

$$\sigma_{\rm el} \simeq 1.2 \times 10^{-47}\, g_\nu^2 \left(1 + \frac{1}{4}\left(\frac{g_\nu}{g_\chi}\right)^2\right)^{-\frac{1}{2}} \left(\frac{E_\nu}{T_0}\right)^2 \left(\frac{m_\chi}{\rm MeV}\right) \left(\frac{m_{Z'}}{\rm MeV}\right)^{-4} \tag{3.3.7}$$

$$\times \left(\frac{\langle \sigma v_{\rm r}\rangle}{3 \times 10^{-26}\ {\rm cm}^3/{\rm s}}\right)^{\frac{1}{2}} {\rm cm}^2\ , \tag{3.3.8}$$

which, when compared to the collisional damping constraint, Eq. (1.5.3), sets a lower bound in the mediator mass of $m_{Z'} \geq 2\, g_\nu^{\frac{1}{2}} \left(1 + \frac{1}{4}\left(\frac{g_\nu}{g_\chi}\right)^2\right)^{-\frac{1}{8}} \simeq 2$ MeV, for $g_\nu = g_\chi = 1$.

3.4 Conclusions

In this chapter, we have investigated the viability of scenarios in which DM is coupled to active neutrinos, by evaluating their cosmological effects (collisional damping and relic density) and their implications for indirect DM searches with neutrino detectors.

Using a simplified model approach and considering only dimension 4 terms in the Lagrangian, we have identified twelve different scenarios. Many of these share some common properties and can be grouped according to the nature of the particle that mediates the interactions. For all these scenarios we have computed the elastic scattering and DM annihilation cross sections. The full expressions are given in Appendix B in Ref. [3] while their dominant terms are given in Table 3.1. We have not explicitly assumed thermal DM. However, we do show the DM and mediator masses that lead to a thermal annihilation cross section of $\langle \sigma v_{\rm r}\rangle \simeq 3 \times 10^{-26}\, {\rm cm}^3/{\rm s}$ (or $\langle \sigma v_{\rm r}\rangle \simeq 6 \times 10^{-26}\, {\rm cm}^3/{\rm s}$ for v^2-dependent cross sections). For each of these

scenarios, we constrain the parameter space by imposing the stability of the DM candidate and also that i) the DM-ν interactions are compatible with small scales Lyman-α forest data, ii) there are no anomalous neutrino signals at Borexino and SK experiments and finally iii) DM annihilations into neutrinos do not significantly change the CMB angular power spectrum.

We find that, generically, for scalar and fermion mediators that are much heavier than the DM particle, the annihilation cross section is either constant or velocity-dominated and scales as the square of the DM mass (except if LNV annihilation channels dominate, which occurs when the mediator is a Majorana particle). While the velocity dependence is not particularly important at the time of the DM freeze-out, it is crucial for annihilations in the Milky Way, as it significantly suppresses the neutrino signal. Therefore, only scalar DM-Majorana mediator, Dirac DM-scalar mediator and vector DM-Dirac mediator scenarios have strong indirect detection constraints. These bounds are not far from the values required for a thermal DM candidate. Hence, future neutrino experiments have the potential to significantly improve these constraints and exclude a large fraction of the thermal DM parameter space (assuming the DM annihilates into SM particles). This conclusion remains valid as long as $g \gg 10^{-2}$, since the relic density line and the indirect constraints are both proportional to g^4. Couplings of this magnitude can be achieved in specific UV-complete models as we will discuss in the following chapter.

The elastic cross section typically scales as the neutrino energy squared and can be resonantly enhanced if the DM and mediator masses are nearly degenerate. Observable collisional damping requires very large values of this cross section, which implies sub-MeV DM masses or the quasi-degenerate DM-mediator mass regime. The first possibility is, however, excluded by constraints from $N_{\rm eff}$, using CMB data [105, 108]. The second case is viable, but only for velocity-dependent annihilation cross sections (scalar DM-Dirac mediator and Majorana DM-scalar mediator), so that the indirect detection bounds are weak and leave significant portions of the parameter space unconstrained, in particular, DM masses in the $\sim [100, 10^4]$ MeV range for $g = 1$.

The real scalar DM-Dirac mediator case is an exception, as the annihilation and the elastic scattering cross sections are suppressed by v^4 and E_ν^4 terms respectively, which in turn, might produce observable collisional damping if the mediator and DM masses are degenerate and in the $\sim [4, 10^4]$ MeV range.

If the mediator is a vector, the phenomenology is different because it can be lighter than the DM particle and moreover, when the DM and mediator particles are degenerate in mass, the annihilation cross section can be resonantly enhanced. If the DM particle is heavier than the vector mediator, the annihilation channel into two vectors is open and could dominate, depending on the value of the parameters. The indirect DM searches apply to both mass regimes: if DM is lighter than the mediator, the constraints are similar to those obtained for the previous cases, i.e., strong and close to the thermal relic line for Dirac DM and significantly weaker for complex, Majorana and vector DM, due to the velocity dependence of the cross section. In the opposite case, i.e., DM heavier than the mediator, DM can annihilate both into neutrinos and into Z', which can subsequently decay into neutrinos. Depending on the relative strength of the couplings g_ν and g_χ, either of the two channels can dominate and lead to significant constraints on the parameter space. The values of the elastic cross section needed for collisional damping can be achieved even for heavy DM, if the mediator mass is in the $\sim [1 - 10]$ MeV range.

In summary, we find that DM-ν interactions can have a strong impact on the early and present Universe and that the complementarity between cosmological and astrophysical constraints can test large areas of the allowed parameter space. These bounds should be taken into account when considering a particular UV-complete model that generates interactions between DM and neutrinos and would be particularly relevant for models that generate neutrino masses while providing a DM candidate.

Chapter 4

Towards a gauge-invariant model of dark matter-neutrino interactions

> *-But, Friedrich, to reach the truth, we, scientists, have to get rid of all illusions don't we?*
> *-Oh, TRUTH -said Nietzsche- I forgot, Josef, that scientists still need to learn that TRUTH is also an illusion, yet an illusion without which we could not survive.*
>
> — from *When Nietzsche Wept* by Irvin D. Yalom

In the previous chapter, we have investigated the phenomenology of strong neutrino-DM interactions and the possibility to probe DM through neutrinos both via its cosmological implications as well as through indirect detection searches. However, it is not straightforward to envision a scenario in which the DM phenomenology is dominated by its interaction with neutrinos. Naively, gauge invariance dictates that the interactions of the left-handed (LH) SM neutrinos with DM will be equal to those of their charged lepton counterparts in the $SU(2)$ doublets. In this case,

the best window to DM would instead be the charged leptons rather than the more elusive neutrinos.

In this chapter, we will investigate some gauge-invariant SM extensions that lead to sizeable neutrino-DM interactions, exploring if neutrino probes could dominate our sensitivity to the dark sector. This is actually a rather natural possibility. In fact, if DM does not participate in any of the SM gauge interactions, the natural expectation is that the strongest connection to DM will be via singlets of the SM gauge group. Indeed, if non-singlet fields were involved instead, the dimensionality of the operators linking the two sectors would have to increase in order to comply with gauge invariance. This reasoning leads to the three well-known SM portals to the dark sector: the "gauge boson portal" [231], the "Higgs portal" [232, 233], and the "neutrino portal" [180, 234, 235]. The neutrino portal includes the addition of right-handed (RH) neutrinos N_R, which makes this option particularly appealing in connection to the evidence of neutrino masses and mixing from neutrino oscillations, as discussed in Sec. 1.4.

Since the neutrino portal relies on the mixing between N_R and the light SM neutrinos to connect the neutrino and DM sectors, this mixing needs to be sizeable. In the "canonical" seesaw mechanism [72, 74, 236–238], the smallness of neutrino masses is explained through a large Majorana mass for N_R and the mixings are then similarly suppressed by the large scale. An interesting alternative is to explain the smallness of neutrino masses via a symmetry argument instead [82, 83, 239–242]. Indeed, in models with an approximate lepton number (L) symmetry such as the linear [82, 83] or inverse [84] seesaw mechanisms, neutrino masses are suppressed by the small L-breaking parameters while light neutrino mixing with N_R is unsuppressed. In the present study, we will assume relatively large mixing angles noting that they can be compatible with neutrino masses, but we will not specify a concrete neutrino mass generation mechanism, since these small lepton number violating parameters, and hence light neutrino masses, will have no significant impact on the DM-related phenomenology.

We will consider fermion DM and, more specifically, Dirac DM, which has the richest phenomenology when interacting with SM neutrinos. Indeed, as we showed in the previous chapter, the dominant term in the annihilation cross section to neutrinos is not velocity suppressed and DM annihilations therefore lead to interesting signatures at neutrino detectors. Alternative scenarios with a Majorana, scalar, or vector DM candidate will lead to a velocity dependent annihilation cross section to neutrinos (see Table 3.1). While such possibilities are viable, they are difficult to probe experimentally at neutrino detectors, since, as it was already mention, the small DM velocity in the halo today significantly reduces the annihilation rate to neutrinos.

4.1 Naive gauge invariance

In this section, we will study the simplest scenario, in which the neutrino-DM interaction arises from a direct coupling to the full SM $SU(2)$ lepton doublet. In order to avoid specifying the nature of the mediator, we will adopt an effective field theory approach, simply adding a $D = 6$, 4-fermion interaction.

4.1.1 Model

Since the 4-fermion operator needs to involve two LH SM lepton doublets $L_\alpha = (\nu_{\alpha L}, \ell_{\alpha L})^T$, $\alpha = e, \mu, \tau$, its Lorentz structure is fixed to be $\overline{L_\alpha}\gamma^\mu L_\alpha$. For definiteness we will assume a vector structure for the DM part. An axial coupling would instead lead to a velocity-suppressed DM annihilation cross section to neutrinos for both DM relic abundance and indirect searches. The cross section for DM annihilation to charged leptons would however have an additional term only suppressed by the lepton mass, and thus, it would tend to dominate over the annihilation cross section to neutrinos. Therefore, we will not consider this option in what follows.

The Lagrangian describing the neutrino-DM interaction is thus given by

$$\mathcal{L} = \mathcal{L}_{\rm SM} + \overline{\chi}\left(i\partial\!\!\!/ - m_\chi\right)\chi + \frac{c_\alpha}{\Lambda^2}\,\overline{\chi}\gamma_\mu\chi\,\overline{L_\alpha}\gamma^\mu L_\alpha\,, \tag{4.1.1}$$

where χ is a Dirac fermion DM particle, and flavour diagonal couplings c_α/Λ^2 between DM and the lepton doublets have been assumed in order to avoid new sources of flavour violation. For the effective description to be consistent we will require that $\Lambda^2/c_\alpha \gg m_\chi^2$.

The Lagrangian in Eq. (4.1.1) implies that, in this naive gauge-invariant scenario, the coupling between the SM neutrinos and DM will be accompanied by a DM-charged lepton coupling of the same strength. Therefore, the strongest constraints on this model will typically come from indirect searches for DM annihilations to charged leptons. The DM relic abundance will also be set by its annihilation into leptons, either neutrinos or charged leptons, with the annihilation cross section given by

$$\langle \sigma v_r \rangle \approx \frac{c_\alpha^2 m_\chi^2}{2\pi\Lambda^4}\left(1-\frac{m_\alpha^2}{4m_\chi^2}\right)\sqrt{1-\frac{m_\alpha^2}{m_\chi^2}}\,, \tag{4.1.2}$$

where m_α is the lepton mass for the different α flavour.

4.1.2 Results

In Fig. 4.1, we show regions in the parameter space of the DM mass m_χ and the new physics scale Λ excluded by different experiments. The blue line corresponds to the correct DM relic density $\Omega_{\rm DM}h^2 = 0.120 \pm 0.001$ [7] obtained through the thermal freeze-out mechanism. This line has been computed with `micrOMEGAs` [243]. In the upper hatched region, the DM-lepton interaction would be too weak, leading to overclosure of the Universe ($\Omega_{\rm DM}h^2 > 0.12$). In the region below the blue line, the relic density is smaller than the observed DM abundance. If there are additional production mechanisms contributing to the DM density, this region is also viable.

The constraints from indirect DM searches are shown as different shaded regions. The light green (Planck [7, 54]) and orange (Fermi satellite [55]) regions correspond to the bounds from DM annihilation to charged leptons described in Sec. 1.3.2. The remaining shaded regions correspond to the constraints from DM annihilation to neutrinos as searched for in neutrino detectors and summarised in Chapter 2. In

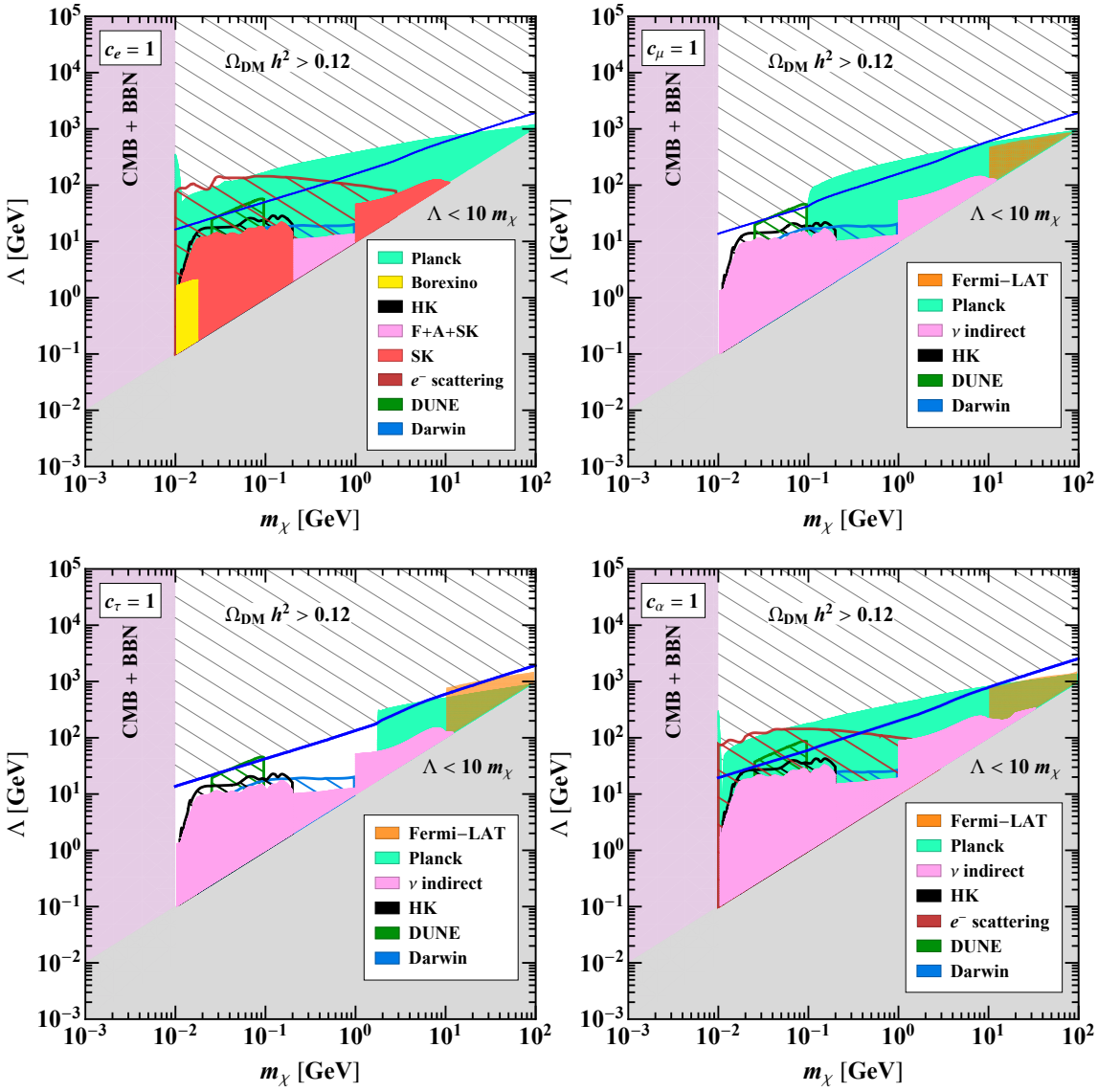

Figure 4.1: Constraints on the DM mass m_χ and the new physics scale Λ. The upper and bottom-left panels correspond to couplings to only one of the lepton doublets (electron, muon, or tau), while the bottom-right panel corresponds to all three couplings being of equal strength. Along the blue line we recover the correct DM relic abundance from thermal freeze-out. The coloured shaded regions are excluded by different experiments, while the hatched areas correspond to prospective sensitivities of future experiments. The lower bound $m_\chi \gtrsim 10$ MeV is set by observations of the CMB and BBN. See text for further details.

the upper-left panel of Fig. 4.1, we show in different colours the bounds coming from different neutrino experiments. The SK analysis [3, 130] are shown in red while the Borexino bounds [136] are displayed in yellow). The pink colour corresponds to the bounds from [128] obtained by combining the atmospheric neutrino data.[1] The dark red hatched region corresponds to prospective sensitivity of experiments on DM-electron scattering [41], while the blue, black, and green hatched regions correspond to prospects from different neutrino experiments as also described in Chapter 2. In the following panels and in the rest of the chapter we show all present indirect detection constraints from neutrino experiments in pink colour.

As can be seen in Fig. 4.1, the strongest constraints come from DM annihilation to charged leptons as probed by Fermi-LAT [55] for $\chi\overline{\chi} \to \tau^+\tau^-$, $\mu^+\mu^-$ and from Planck [7, 54] for $\chi\overline{\chi} \to \ell^+\ell^-$, $\ell = e, \mu, \tau$. Indirect searches at neutrino detectors will always play a sub-leading role as long as annihilation to charged leptons is possible. Indeed, present constraints from DM annihilation to charged leptons are strong enough to rule out the entire allowed region of the parameter space that could lead to the correct DM relic density as long as the coupling to electrons is sizeable. However, if DM dominantly couples to the heavier lepton generations, allowed windows open up for $m_\chi < m_\mu$ (m_τ) (see the upper-right and bottom-left panels of Fig. 4.1). In this case, the DM relic density would be set by its annihilation to neutrinos, and the most relevant present constraints come from the results of SK and Borexino. The prospects for HK and DUNE would be very promising in these scenarios, allowing to probe most of the parameter space up to and beyond where the relic density is entirely explained by freeze-out based on neutrino interactions.

Regarding the constraints that could be set by the DM effects in the spectrum or isotropy of high energy cosmic neutrinos as observed by IceCube [124], these would lie in the region of the parameter space already excluded by the number of relativistic degrees of freedom in the early Universe [96, 105].

From Fig. 4.1 it is clear that, barring the ad hoc choice of light DM coupling

[1] "F+A+SK" in the corresponding legend stands for Fréjus + AMANDA + SK.

exclusively to the heavier leptons, this option for a neutrino-DM coupling is mostly ruled out by DM-charged lepton interactions.

4.2 Coupling via the neutrino portal

Given the results of the previous section, we will now explore whether the neutrino portal option is able to lead to a rich DM-neutrino phenomenology without being in conflict with indirect searches involving charged leptons. The first necessary ingredient is to have sizeable mixing between the SM neutrinos and the new sterile neutrinos that will mediate the DM interaction. Therefore, the sterile-light neutrino mixing should not scale with the light neutrino masses, unlike in the canonical seesaw mechanism. Therefore, we will instead attribute the smallness of neutrino masses to an approximate lepton number (or $B-L$) symmetry rather than to a hierarchy of scales between the Dirac and Majorana masses. The new singlets will thus form pseudo-Dirac pairs since lepton number violation will necessarily be very small to account for the lightness of SM neutrinos. This is the case for instance in the popular "linear" [82, 83] and "inverse" [84] seesaw mechanisms based on such a symmetry.

As a simplifying assumption we will here consider the addition of only one Dirac sterile neutrino that will serve as portal between the SM neutrinos and DM. As discussed in Sec. 1.4, neglecting this small lepton number violation, the couplings between the SM and the new Dirac singlet neutrino are given by

$$\mathcal{L} = \mathcal{L}_{\rm SM} + \overline{N}\left(i\partial\!\!\!/ - m_N\right) N - \lambda_\alpha \overline{L_\alpha}\tilde{H} N_R \,, \tag{4.2.1}$$

where N is the Dirac sterile neutrino and $\tilde{H} = i\sigma_2 H^*$, with H being the Higgs doublet.

Electroweak symmetry breaking gives rise to the neutrino Dirac mass term

$$\left(\overline{\nu_{\alpha L}},\, \overline{N_L}\right) M_\nu N_R + \text{h.c.}\,, \tag{4.2.2}$$

where $M_\nu = (\lambda_\alpha v/\sqrt{2},\, m_N)^T$ is the neutrino mass matrix and $v = \langle H^0 \rangle = 246$ GeV is the Higgs vacuum expectation value (vev). Diagonalising $M_\nu M_\nu^\dagger$ with a 4×4

unitary matrix U,

$$U^\dagger M_\nu M_\nu^\dagger U = \text{diag}\left(m_1^2, m_2^2, m_3^2, m_4^2\right), \tag{4.2.3}$$

we find the mass of the heavy neutrino to be

$$m_4 = \sqrt{m_N^2 + \sum_\alpha |\lambda_\alpha|^2 v^2/2}\,. \tag{4.2.4}$$

As expected, the lepton number symmetry forbids light neutrino masses. In order to account for neutrino masses, small breaking of this symmetry via terms such as $\mu\,\overline{N_L} N_L^c$ (inverse seesaw), or $\lambda'_\alpha \overline{L_\alpha}\tilde{H} N_L^c$ (linear seesaw) can be added. Since these small parameters would have negligible impact in the phenomenology of neutrino-DM interactions, we will not consider them in what follows.

The neutrino mixing matrix U, which relates LH flavour neutrino fields and the neutrino fields with definite masses as

$$\begin{pmatrix} \nu_{\alpha L} \\ \\ N_L \end{pmatrix} = U \begin{pmatrix} \nu_{iL} \\ \\ \nu_{4L} \end{pmatrix}, \quad \alpha = e, \mu, \tau\,, \quad i = 1, 2, 3\,, \tag{4.2.5}$$

has the form

$$U = \begin{pmatrix} U_{\alpha i} & U_{\alpha 4} \\ \\ U_{si} & U_{s4} \end{pmatrix}. \tag{4.2.6}$$

The upper-left 3×3 block $U_{\alpha i}$ would correspond to the PMNS matrix (see Sec. 1.4) once the small lepton number-breaking terms that induce neutrino masses are taken into account. Note that this matrix, being a 3×3 sub-block of a larger unitary matrix will, in general, not be unitary. The upper-right 3×1 block $U_{\alpha 4}$ describes the mixing between the active flavour neutrinos and the LH component of the heavy neutrino with mass m_4. The last row of the matrix U specifies the admixture of each ν_{jL}, $j = 1, 2, 3, 4$, in the LH sterile neutrino N_L. As we will see in what follows, the DM-related phenomenology is driven by the mixing of active-heavy mixing matrix elements $U_{\alpha 4}$. We will use the unitarity deviations of the PMNS matrix to constrain these mixings [244]. The mixing elements of interest are given by

$$U_{\alpha 4} = \frac{\theta_\alpha}{\sqrt{1 + \sum_\alpha |\theta_\alpha|^2}}\,, \qquad U_{s4} = \frac{1}{\sqrt{1 + \sum_\alpha |\theta_\alpha|^2}}\,, \qquad \sum_{i=1}^{3} |U_{si}|^2 = \sum_{\alpha=e}^{\tau} |U_{\alpha 4}|^2\,, \tag{4.2.7}$$

with $\theta_\alpha = \lambda_\alpha v/(\sqrt{2}m_N)$. Note that, even though the SM neutrino masses have been neglected, the mixing with the extra singlet neutrino that will act as portal can still be sizeable. For definiteness we will fix the mixing to the different flavours to their 1σ limit from Ref. [244], namely:

$$|\theta_e| = 0.031\,, \quad |\theta_\mu| = 0.011\,, \quad |\theta_\tau| = 0.044\,. \tag{4.2.8}$$

In the following sections, we will explore two possible ways in which these Dirac neutrinos could couple to the dark sector and become portals between it and the SM neutrinos.

4.3 Sterile neutrino portal with a scalar mediator

In this first example, we will assume that DM is composed of a new fermion, singlet under the SM gauge group, and that a new scalar mediates the Dirac neutrino-DM interactions.

4.3.1 Model

The Lagrangian of the model we will consider is given by

$$\begin{aligned}\mathcal{L} = \mathcal{L}_{\rm SM} &+ \overline{\chi}\left(i\partial\!\!\!/ - m_\chi\right)\chi + \overline{N}\left(i\partial\!\!\!/ - m_N\right)N + \partial_\mu S^* \partial^\mu S \\ &- \left[\lambda_\alpha \overline{L_\alpha}\tilde{H} N_R + \overline{\chi}\left(y_L N_L + y_R N_R\right) S + \text{h.c.}\right] \\ &- \mu_S^2 |S|^2 - \lambda_S |S|^4 - \lambda_{SH} |S|^2 H^\dagger H\,,\end{aligned} \tag{4.3.1}$$

where χ is a Dirac fermion DM candidate and S is a complex scalar. The fields χ and S form the dark sector of the model (they are SM singlets), while N serves as a mediator between the dark sector and the SM. The Lagrangian in Eq. (4.3.1) respects a global $U(1)_L$ lepton number symmetry under which L_α, N, and S^* have the same charge and which protects the SM neutrino masses. Moreover, the Lagrangian respects a global $U(1)_D$ dark symmetry, under which χ and S have equal charges.

This preserved symmetry ensures the stability of χ, if $m_\chi < m_S$, where $m_S^2 = \mu_S^2 + \lambda_{SH} v^2/2$ is the mass squared of the scalar S.

This model was previously considered in Refs. [117,245]. However, we will go beyond these works by performing a comprehensive analysis of the sensitivity of neutrino experiments to the parameter space of this model.

We will limit ourselves to the case in which DM is lighter than the heavy neutrino,[2] i.e., $m_\chi < m_4$. This is the so-called direct annihilation regime [246], since DM annihilates through the mediator directly to SM particles. As intended, the only channel for DM annihilation at tree-level is the one into light neutrinos. This process occurs via a diagram involving a t-channel exchange of the scalar mediator S. In the opposite regime, which is usually referred to as secluded [246], DM annihilates to heavy neutrinos, which subsequently decay. The phenomenology of this regime has been studied in Refs. [247–250].

Neglecting velocity-suppressed terms, we find the following thermally averaged cross section for DM annihilation to neutrinos:

$$\langle \sigma v_r \rangle \approx \frac{y_L^4}{32\pi} \left(\sum_{i=1}^{3} |U_{si}|^2 \right)^2 \frac{m_\chi^2}{\left(m_\chi^2 + m_S^2\right)^2} \approx \frac{y_L^4}{32\pi} \left(\sum_{\alpha=e,\mu,\tau} |\theta_\alpha|^2 \right)^2 \frac{m_\chi^2}{\left(m_\chi^2 + m_S^2\right)^2} \,. \tag{4.3.2}$$

The product $y_L \sqrt{\sum_\alpha |\theta_\alpha|^2}$ controls $\langle \sigma v_r \rangle$ and, in order to allow for sufficient annihilation to reproduce the observed relic density, it cannot be too small. The value of the coupling y_L is limited by the requirement of perturbativity. We will restrict ourselves to $y_L < 4\pi$. Since the coupling y_R does not enter Eq. (4.3.2), and thus, does not affect the tree-level DM-neutrino interactions, in what follows we set it to zero for simplicity. Regarding the mixing parameters θ_α, the bounds on them depend on the mass of the heavy neutrino. For definiteness we will assume that the heavy neutrino has a mass above the electroweak scale. At this scale the bounds on heavy neutrino mixing derived in the global analysis of flavour and electroweak precision data performed in Ref. [244] apply. If smaller masses were instead considered,

[2] Otherwise the $\chi\overline{\chi} \to \nu_i \overline{\nu_4}$ or $\chi\overline{\chi} \to \nu_4 \overline{\nu_4}$ channels would dominate the annihilation cross section and only sub-dominant DM interactions with the 3 light SM neutrinos ν_i would be allowed.

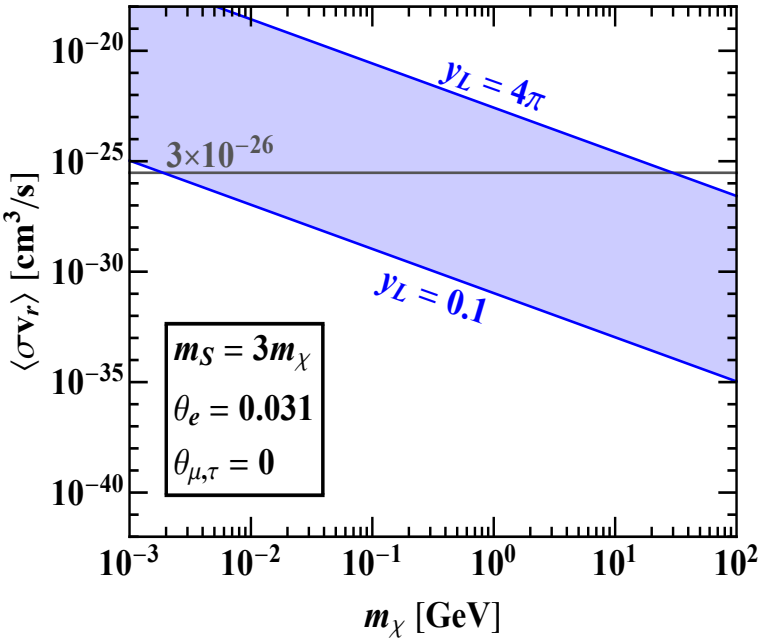

Figure 4.2: Thermally averaged annihilation cross section multiplied by the relative velocity for $\chi\overline{\chi} \to \nu\overline{\nu}$. We have fixed $m_S = 3m_\chi$, $\theta_e = 0.031$, $\theta_\mu = \theta_\tau = 0$, and varied y_L between 0.1 and 4π.

more stringent constraints from collider and beam-dump searches and, eventually, production in meson and beta decays could potentially apply [251] (see discussion in Sec. 4.4.3). In any case, all the observables relevant to DM phenomenology have a sub-leading dependence on m_4. We also consider the case where the coupling $\lambda_{SH} = 0$, ensuring the neutrino portal regime. In Refs. [117, 245], the radiative generation of the $|S|^2 H^\dagger H$ operator was considered and its effects on m_S as well as on the invisible width of the Higgs boson were found to be negligible.

In Fig. 4.2, we show the region of the parameter for which the correct thermal relic abundance is obtained. This region spans DM masses up to 100 GeV for $|\theta_e| = 0.031$, $\theta_\mu = \theta_\tau = 0$, and y_L between 0.1 and 4π while keeping $m_S = 3m_\chi$ as a benchmark.

Annihilation of DM into charged lepton-antilepton pairs $\ell^+\ell^-$ ($\ell = e, \mu, \tau$), proceeds via the one-loop diagrams[3] shown in Fig. 4.3 (in unitary gauge).

The dominant contribution comes from the first and second diagrams, while the contribution from the last diagram is suppressed by the small Yukawa couplings of

[3]The Feynman diagrams in this chapter are produced with the `TikZ-Feynman` package [252].

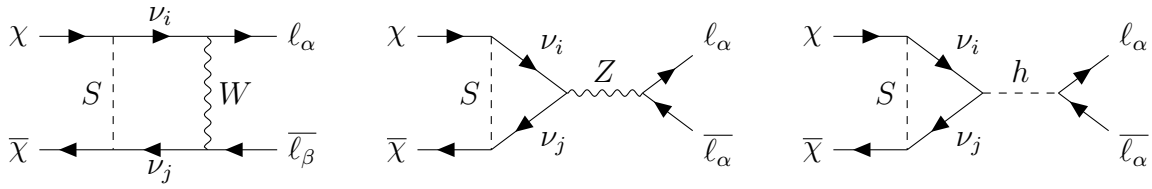

Figure 4.3: One-loop diagrams (in unitary gauge) contributing to annihilation of DM into charged lepton-antilepton pairs $\ell_\alpha\overline{\ell_\beta}$, $\alpha, \beta = e, \mu, \tau$. The indices i and j run from 1 to 4.

the charged leptons. The first diagram leads to the following effective operator:

$$\mathcal{L} \supset -a_{SW}\frac{g^2}{m_W^2}\overline{\chi}\gamma^\mu P_R\chi\,\overline{\ell_\alpha}\gamma_\mu P_L\ell_\beta\,, \tag{4.3.3}$$

where g is the weak coupling constant. Neglecting external momenta, the effective coupling a_{SW} is given by

$$a_{SW} = |U_{s4}|^2 U_{\alpha 4}U^*_{\beta 4}\frac{y_L^2}{(4\pi)^2}G\left(\frac{m_S^2}{m_4^2}\right), \tag{4.3.4}$$

where the loop function $G(x)$ reads

$$G(x) = \frac{x - 1 - \ln x}{4\,(1-x)^2}\,. \tag{4.3.5}$$

The second diagram in Fig. 4.3 leads to the following effective interaction of DM with the Z boson:

$$\mathcal{L} \supset -a_Z\frac{g}{\cos\theta_W}\overline{\chi}\gamma^\mu P_R\chi Z_\mu\,, \tag{4.3.6}$$

where θ_W is the Weinberg angle and a_Z is the effective coupling, which in the limit of zero external momenta is given by

$$a_Z = |U_{s4}|^2\left(1 - |U_{s4}|^2\right)\frac{y_L^2}{(4\pi)^2}G\left(\frac{m_S^2}{m_4^2}\right). \tag{4.3.7}$$

These contributions have been also computed using a combination of packages: `FeynRules` [253, 254] to produce a model file, `FeynArts` [255] for generating the diagrams and `FormCalc` [256] for computing their numerical contributions. For numerical evaluation of the Passarino-Veltman functions we have used `LoopTools` [256]. We have also considered the limit of zero external momenta, which effectively corresponds to the limit of small DM and charged lepton masses, and confronted the analytical results obtained in this approximation using the package `ANT` [257] with

the `LoopTools` results. For the DM masses between 1 MeV and 100 GeV that we are interested in, the approximation works very well. The availability of analytical expressions allows for an easier exploration of the parameter space.

In Fig. 4.4, we present the cross sections for annihilation of DM into e^+e^-, $\mu^+\mu^-$, and $\tau^+\tau^-$ for benchmark values of the model parameters. We fix $m_S = 3m_\chi$, $m_4 = 400$ GeV, $y_L = 1$, $\theta_e = 0.031$, and $\theta_{\mu,\tau} = 0$. As can be seen from the left panel, the annihilation cross sections to charged leptons are several orders of magnitude smaller than the cross section for DM annihilation into neutrinos. The difference in the cross sections becomes smaller when the DM mass approaches $m_Z/2$, and the cross sections for $\chi\overline{\chi} \to \ell^+\ell^-$ exhibit a resonant behaviour due to the second diagram in Fig. 4.3. In the right panel, we show the indirect detection constraints from Planck [7, 54] and Fermi-LAT [55]. Note that those constraints assume a 100% annihilation rate into a single SM channel. Even for $y_L = 4\pi$ the resulting annihilation cross sections into charged leptons are well below the experimental constraints. Thus, the considered realisation of the neutrino portal does provide an example of a gauge-invariant model in which the neutrino-DM interactions dominate DM phenomenology.

At one-loop level DM also interacts with quarks via diagrams involving Z and h, which are analogous to those in Fig. 4.3. The corresponding effective DM-nucleon spin-independent scattering cross section reads [245]

$$\sigma_n = \frac{\mu_n^2}{\pi} \frac{\left(Z f_p + (A - Z) f_n\right)^2}{A^2}\,, \tag{4.3.8}$$

where μ_n is the reduced mass of the nucleon, A is the total number of nucleons in a nuclei, Z is the number of protons,

$$f_p = \left(4\sin^2\theta_W - 1\right)\frac{G_F a_Z}{\sqrt{2}}\,, \qquad f_n = \frac{G_F a_Z}{\sqrt{2}}\,, \tag{4.3.9}$$

with a_Z given in Eq. (4.3.7), and G_F being the Fermi constant. The radiative coupling of DM to the Higgs, $\overline{\chi}\chi h$, would also give a contribution to direct detection searches. This contribution is however suppressed by the small quark Yukawa couplings.

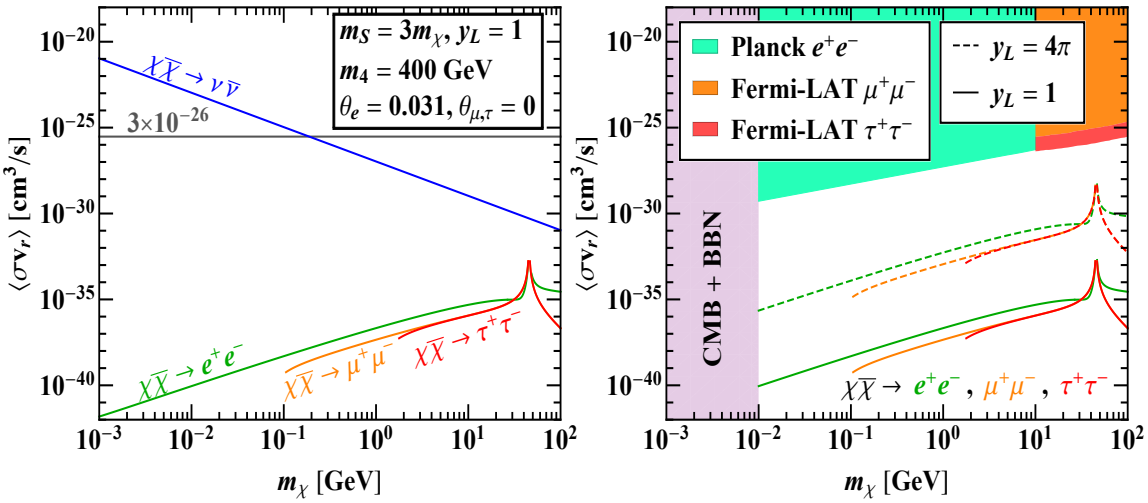

Figure 4.4: Thermally averaged annihilation cross section multiplied by the relative velocity for DM annihilation into e^+e^-, $\mu^+\mu^-$, and $\tau^+\tau^-$. We have fixed $m_S = 3m_\chi$, $m_4 = 400$ GeV, $y_L = 1$, $\theta_e = 0.031$, and $\theta_{\mu,\tau} = 0$. The *left* panel provides comparison with $\langle\sigma v_r\rangle$ for DM annihilation into neutrinos assuming the same set of model parameters. The *right* panel displays the indirect detection constraints coming from Planck and Fermi-LAT. The lower bound $m_\chi \gtrsim 10$ MeV is set by observations of the CMB and BBN. See text for further details.

The most stringent constraint on DM-nucleon spin-independent cross section for $m_\chi \gtrsim 10$ GeV comes from XENON1T [45]. As we will see in the next subsection, this constraint is strong enough to probe the loop-suppressed scattering process if the value of the coupling y_L is sufficiently large. We have also considered DM scattering off electrons and found that the corresponding cross section is much smaller than the projected sensitivities of silicon, germanium, and xenon experiments derived in Ref. [41]. Thus, DM-electron scattering cannot provide an additional probe of the considered neutrino portal model.

4.3.2 Results

In this subsection, we explore the parameter space to find regions that satisfy all direct and indirect detection constraints and in which the DM phenomenology could be dominated by its interactions with SM neutrinos. We show our results in the $m_\chi - m_S$ plane to determine the masses of the DM and the dark scalar that are presently allowed and could lead to the correct relic abundance (see Fig. 4.5).

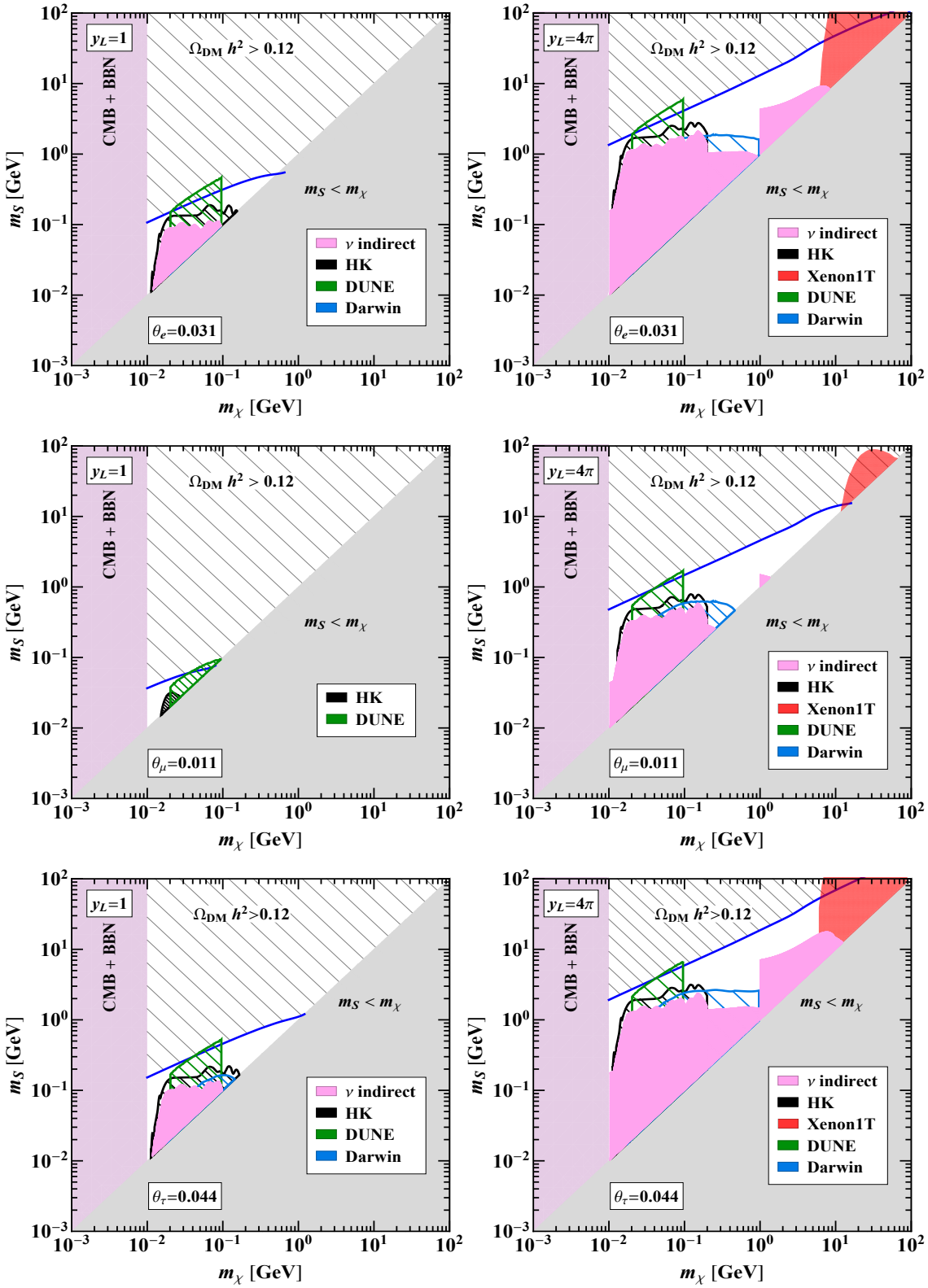

Figure 4.5: Constraints on the DM mass m_χ and the dark scalar mass m_S. We have fixed $\theta_e = 0.031$, $\theta_{\mu,\tau} = 0$; $\theta_\mu = 0.011$, $\theta_{e,\tau} = 0$; and $\theta_\tau = 0.044$, $\theta_{e,\mu} = 0$ (from top to bottom), considering $y_L = 1$ and 4π. Along the blue line the DM relic density matches the observed value. The coloured shaded regions are excluded by different experiments, while the hatched areas correspond to prospective sensitivities of future experiments. The lower bound $m_\chi \gtrsim 10$ MeV is set by observations of the CMB and BBN. See text for further details.

In Fig. 4.5 the triangular region $m_S < m_\chi$ is forbidden by DM stability. Along the blue line(s) computed with `micrOMEGAs`,[4] the DM relic density matches the observed value $\Omega_{\rm DM}h^2 = 0.120 \pm 0.001$ [7]. Above this line (the upper hatched region), the DM relic density is bigger than the measured value, i.e., DM overcloses the Universe. Below this line, the relic abundance would be smaller than the observed value. However, if there is an additional production mechanism, the relic abundance could also be compatible with this region.

As can be seen in the figure indirect searches for annihilation to neutrinos, together with direct detection bounds by XENON1T for large DM masses, are the only probes that are presently constraining the allowed parameter space. The prospects to explore the remaining allowed regions through annihilation to neutrinos are very promising. In particular DUNE would be able to detect the neutrino signal in the range $25 - 100$ MeV if the DM abundance is entirely due to the DM annihilation to neutrinos.

In Fig. 4.6, we fix m_S to several representative values, namely $m_S = 0.04$, 0.2, 1, and 5 GeV, and show the lines corresponding to the correct relic abundance in the $m_\chi - y_L$ plane. These results have been obtained with `micrOMEGAs`. Small values of y_L are ruled out since they do not lead to efficient DM annihilation. As can be seen, a lighter dark scalar allows for smaller values of y_L. For $m_S \gtrsim 500$ MeV, values of $y_L \gtrsim 1$ are required to yield the observed relic density.

Overall, the cosmologically allowed parameter space of the model is already constrained by the current neutrino detectors as well as XENON1T. Moreover, the next generation of neutrino experiments, in particular DUNE, will be able to probe thermal MeV Dirac DM in the considered scenario.

[4]We have implemented the effective DM couplings to the Z boson and to the charged leptons via exchange of the W boson (see Fig. 4.3) to the `FeynRules` model file.

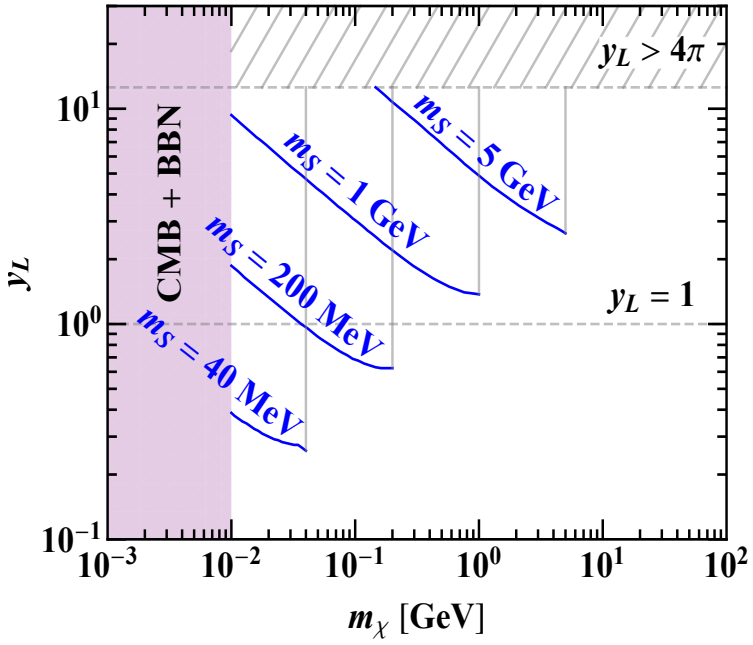

Figure 4.6: Values of the DM mass m_χ and the coupling y_L required to reproduce the observed relic abundance. We have fixed $m_S = 0.04$, 0.2, 1, and 5 GeV, and have considered the representative case of $\theta_e = 0.031$, while keeping $\theta_{\mu,\tau} = 0$. Along (above) the blue lines the DM relic density matches (is less than) the observed value. The lower bound $m_\chi \gtrsim 10$ MeV is set by observations of the CMB and BBN.

4.4 Neutrino portal with a vector mediator

In this second example, we will again assume that DM is composed of a new Dirac fermion, this time coupled to a new massive vector boson. The Dirac singlet neutrino will also interact with this boson so as to provide the neutrino-DM interaction.

4.4.1 Model

The Lagrangian of the model is given by

$$\begin{aligned}\mathcal{L} = \mathcal{L}_{\rm SM} &+ \overline{\chi}\left(i\partial\!\!\!/ - m_\chi\right)\chi + \overline{N}\left(i\partial\!\!\!/ - m_N\right)N \\ &+ \left[g'\overline{\chi_R}\gamma^\mu\chi_R Z'_\mu + g'\overline{N_L}\gamma^\mu N_L Z'_\mu - \lambda_\alpha\overline{L_\alpha}\tilde{H}N_R + \text{h.c.}\right] \\ &- \frac{1}{4}Z'_{\mu\nu}Z'^{\mu\nu} + \frac{1}{2}m^2_{Z'}Z'_\mu Z'^\mu\,,\end{aligned} \tag{4.4.1}$$

where χ is a Dirac fermion DM candidate, Z' is a new vector boson mediating the interaction between neutrinos and DM, and N is the Dirac sterile neutrino connecting the dark and visible sectors through its mixing with the active neutrinos. This

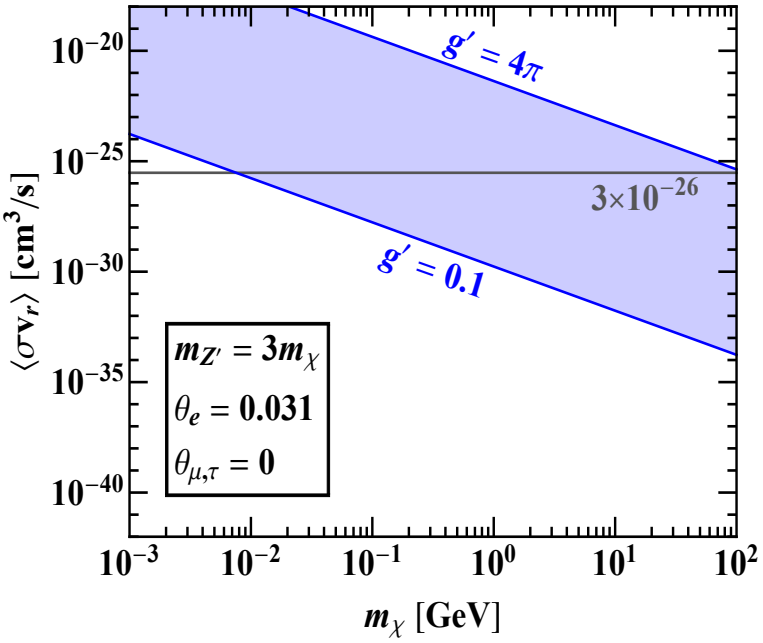

Figure 4.7: Thermally averaged annihilation cross section multiplied by the relative velocity for $\chi\overline{\chi} \to \nu\overline{\nu}$. We have fixed $m_{Z'} = 3m_\chi$, $\theta_e = 0.031$, $\theta_\mu = \theta_\tau = 0$, and varied g' between 0.1 and 4π.

Lagrangian could for instance describe a new $U(1)'$ gauge symmetry spontaneously broken by the vev of a scalar SM singlet charged under it, that would induce masses for the Z' as well as for the heavy neutrino N and the DM. The particular mechanism is not relevant for the rest of the discussion and will not be elaborated further. We will also assume there is an additional conserved charge (e.g., a $\mathbb{Z}_2$ symmetry) not shared between the neutrino and the DM that prevents their mixing. Note that in order to keep the Lagrangian in Eq. (4.4.1) anomaly free without introducing new fields, the simplest option is to couple the LH part of the Dirac sterile neutrino and the RH part of the DM to the new gauge boson with the same coupling g'.

As in the previous scenario, we will assume that the DM mass $m_\chi < m_4$ so that the dominant DM annihilation channel is to the three light SM neutrinos. This is a tree-level process and its cross section is given by

$$\langle\sigma v_r\rangle \approx \frac{g'^4}{8\pi}\left(\sum_{i=1}^{3}|U_{si}|^2\right)^2 \frac{m_\chi^2}{(4m_\chi^2 - m_{Z'}^2)^2} \approx \frac{g'^4}{8\pi}\left(\sum_{\alpha=e,\mu,\tau}|\theta_\alpha|^2\right)^2 \frac{m_\chi^2}{(4m_\chi^2 - m_{Z'}^2)^2}\,. \tag{4.4.2}$$

Note however that, for $m_{Z'} \lesssim m_\chi$, the tree-level DM annihilation to a pair of Z'

bosons is allowed. When this channel is open, it will dominate over the direct annihilation into neutrinos, since the latter is suppressed by neutrino mixing. This is the so-called secluded annihilation regime [246], which we do not consider in the present study.

In this scenario, as can be seen from Fig. 4.7, the correct relic abundance can be obtained purely from annihilation to the SM neutrinos for values of the new gauge coupling g' between 0.1 and 4π, and DM masses in the $0.01 - 100$ GeV range. In this figure, we have fixed $m_{Z'} = 3m_\chi$, $|\theta_e| = 0.031$, and $\theta_\mu = \theta_\tau = 0$ as benchmark values.

A direct coupling between the Z' boson and the charged leptons will also be induced through the loop diagrams in Fig. 4.8. Neglecting external momenta for the charged leptons, the effective vertex from the first loop diagram is given by

$$\mathcal{L} \supset -a_W g' \overline{\ell_\alpha} \gamma^\mu P_L \ell_\beta Z'_\mu \,, \tag{4.4.3}$$

where

$$a_W = |U_{s4}|^2 U_{\alpha 4} U^*_{\beta 4} \frac{g^2}{(4\pi)^2} \frac{m_4^2}{2m_W^2} \,. \tag{4.4.4}$$

4.4.2 Mixing with the Z boson

Since the neutrino mass eigenstates have components that couple both to the Z and the Z', mixing between the two gauge bosons will be induced at loop level [231] through the second diagram in Fig. 4.8. The kinetic and mass mixings are described by the effective Lagrangian

$$\mathcal{L}_{Z'Z} = -\frac{\sin\epsilon}{2} Z'_{\mu\nu} Z^{\mu\nu} + \delta m^2 Z'_\mu Z^\mu \,. \tag{4.4.5}$$

Notice that these two terms could be present already at the Lagrangian level after gauge symmetry breaking. These would represent additional free parameters of the Lagrangian. However, these parameters do not contribute to the neutrino portal of interest here. Conversely, the neutrino mixing required for the neutrino portal does induce the Z-Z' mixing at the loop level. Barring fine-tuned cancellations

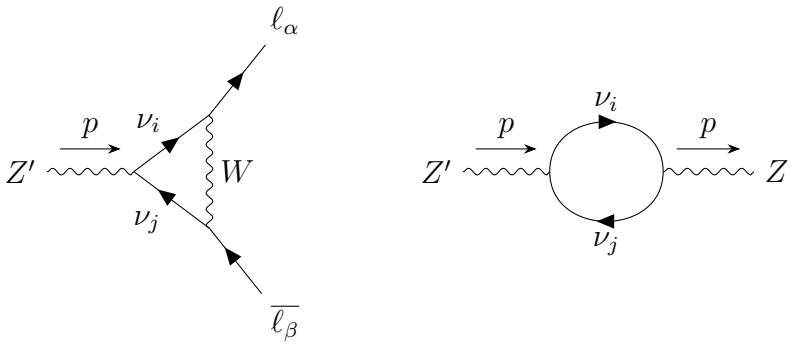

Figure 4.8: One-loop diagrams contributing to the coupling of the Z' boson to charged leptons (*left*) and to kinetic and mass mixing between the Z' and Z bosons (*right*).

between the allowed free parameters at the Lagrangian level and the loop-induced contributions from neutrino mixing, the minimum contribution present in our set-up will be the latter. We will therefore set the tree-level parameters to zero and require that the loop-induced contributions are below the present experimental constraints on Z-Z' mixing. We find the following results for the mixing parameters:

$$\delta m^2 = \frac{2}{(4\pi)^2} g' \frac{g}{\cos\theta_W} |U_{s4}|^2 \left(1 - |U_{s4}|^2\right) m_4^2 \, f_1 \,, \tag{4.4.6}$$

$$\sin\epsilon = \frac{2}{(4\pi)^2} g' \frac{g}{\cos\theta_W} |U_{s4}|^2 \left(1 - |U_{s4}|^2\right) f_2 \,, \tag{4.4.7}$$

where f_1 and f_2 are functions of $x \equiv m_4^2/p^2$, namely,

$$f_1(x) = \frac{1}{12}\Bigg\{ 4x^2 \left(1 - x^{-1}\right)^3 \coth^{-1}(1-2x) + 2x - x^{-1}\ln(x) - 2\sqrt{x\left(4 - x^{-1}\right)^3}\arctan\left((4x-1)^{-1/2}\right)\Bigg\}, \tag{4.4.8}$$

$$f_2(x) = -\frac{x^2}{6}\Bigg\{ 4\left(2x - 3 + x^{-2}\right)\coth^{-1}(1-2x) + 4 + x^{-2}\ln(x) - 2\sqrt{x^{-1}(4-x^{-1})}\left(2 + x^{-1}\right)\arctan\left((4x-1)^{-1/2}\right)\Bigg\}. \tag{4.4.9}$$

For the purposes of this work $p^2 \sim m_\chi^2$, and thus, f_1 and f_2 will only depend on the ratio of the masses of the heavy neutrino and the DM particle. Following Ref. [258], we first diagonalise the kinetic term through a non-unitary transformation and then perform a rotation to diagonalise the mass term. The mass eigenstates Z_1 and Z_2 have masses given by

$$m_{Z_{1,2}}^2 = \frac{\sec^2\epsilon}{2}\left(m_Z^2 + m_{Z'}^2 - 2\delta m^2 \sin\epsilon \mp \Delta\right), \tag{4.4.10}$$

where

$$\Delta = \mathrm{sgn}\left(m_{Z'}^2 - m_Z^2\left(1-2\sin^2\epsilon\right) - 2\delta m^2 \sin\epsilon\right) \times \sqrt{m_Z^4 + m_{Z'}^4 + 4\delta m^4 - 4\left(m_Z^2 + m_{Z'}^2\right)\delta m^2 \sin\epsilon - 2m_Z^2 m_{Z'}^2\left(1-2\sin^2\epsilon\right)} \tag{4.4.11}$$

From Eq. (4.4.10), one can easily verify that in the limit of small mass and kinetic mixing, i.e., $\delta m^2 \to 0$ and $\sin\epsilon \to 0$, the masses $m_{Z_1} \to m_Z$ and $m_{Z_2} \to m_{Z'}$. After the full diagonalisation, we can write the Z and Z' in terms of the mass eigenstates Z_1 and Z_2 as follows:

$$Z_\mu = \left(\cos\xi - \tan\epsilon\sin\xi\right) Z_{1\mu} - \left(\sin\xi + \tan\epsilon\cos\xi\right) Z_{2\mu}\,, \tag{4.4.12}$$

$$Z'_\mu = \sec\epsilon\left(\sin\xi\, Z_{1\mu} + \cos\xi\, Z_{2\mu}\right), \tag{4.4.13}$$

where ξ is the angle related to the mass diagonalisation, which is defined through

$$\tan(2\xi) = \frac{2\cos\epsilon\left(m_Z^2\sin\epsilon - \delta m^2\right)}{m_{Z'}^2 - m_Z^2\left(1-2\sin^2\epsilon\right) - 2\delta m^2\sin\epsilon}\,. \tag{4.4.14}$$

The two angles ξ and ϵ will control the phenomenology associated to the Z-Z' mixing and consequently, the possible Z' couplings to fermions.

The loop-induced kinetic mixing parameter ϵ depends solely on the ratio $x \approx m_4^2/m_\chi^2$, providing the coupling g' and the element U_{s4} of the neutrino mixing matrix are fixed (see Eqs. (4.4.7) and (4.4.9)), and increases with it. Fixing $|\theta_e| = 0.031$ and $\theta_{\mu,\tau} = 0$, we find that for $x = 4$, which is the lowest value preventing the $\chi\overline{\chi} \to \nu_i\overline{\nu_4}$, $i = 1,2,3$, channels, and $g' = 1$ (4π), the mixing parameter $|\sin\epsilon|$ is of order of 10^{-6} (10^{-5}). For values of x as large as 10^4 and $g' = 1$ (4π), the value of $|\sin\epsilon|$ does not exceed approximately 10^{-5} (10^{-4}). Generally, these values can be probed in beam dump and fixed target experiments searching for visible decay products (electrons and muons) of the Z_2 boson with mass between approximately 1 MeV and 1 GeV (see, e.g., [259, 260]). However, in the considered model the Z_2 decays mostly invisibly, either to a pair of the SM neutrinos or, if it is heavy enough, to a pair of DM particles, while its decays to charged leptons are suppressed. Thus, the bounds from fixed target experiments will not apply in this case. Constraints on the kinetic mixing parameter from the anomalous cooling of supernovas cover nearly the same

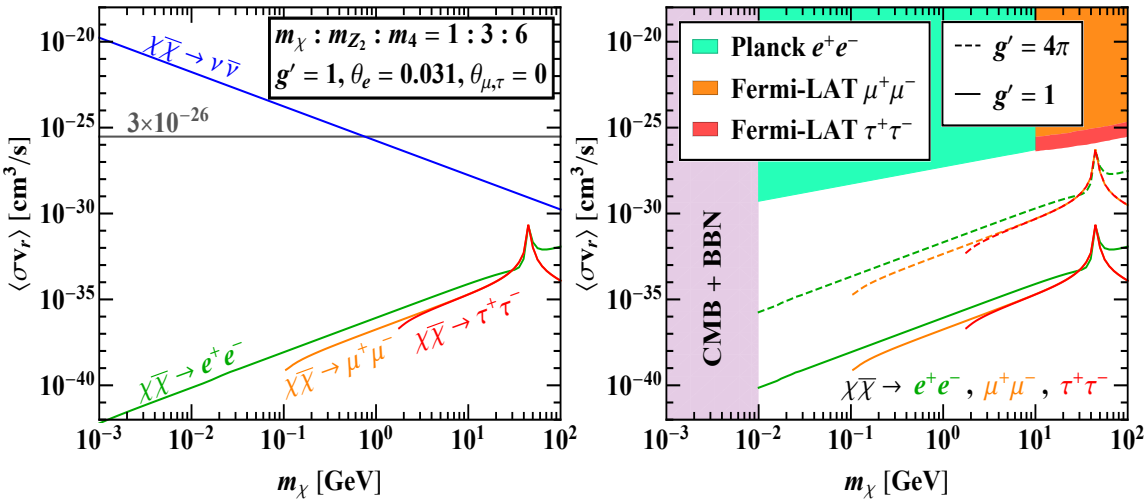

Figure 4.9: Thermally averaged annihilation cross section multiplied by the relative velocity for DM annihilation into e^+e^-, $\mu^+\mu^-$, and $\tau^+\tau^-$. We have fixed $m_\chi : m_{Z_2} : m_4 = 1 : 3 : 6$, $g' = 1$, $\theta_e = 0.031$, and $\theta_{\mu,\tau} = 0$. The *left* panel provides comparison with $\langle\sigma v_r\rangle$ for DM annihilation into neutrinos assuming the same set of model parameters. The *right* panel displays the indirect detection constraints coming from Planck and Fermi-LAT. The lower bound $m_\chi \gtrsim 10$ MeV is set by observations of the CMB and BBN. See text for further details.

Z_2 masses, but a different range of $\epsilon \sim 10^{-10} - 10^{-7}$ [259] and consequently, are also avoided. For larger Z_2 masses, up to 100 GeV, collider experiments place the best constraints on $\epsilon \sim 10^{-4} - 10^{-3}$ (see, e.g., Ref. [260]). These constraints are above the values of the loop-induced kinetic mixing parameter in our model.

Together with the first diagram in Fig. 4.8, the size of ξ and ϵ will determine how relevant the DM annihilation to a pair of charged leptons is. We find that the tree-level annihilation to neutrinos dominates over that to charged leptons. In Fig. 4.9, we show a particular example of this behaviour for $m_4 = 2m_{Z_2}$, $m_{Z_2} = 3m_\chi$, $g' = 1$, $|\theta_e| = 0.031$, and $\theta_\mu = \theta_\tau = 0$. It is clear from this figure that the annihilation to charged leptons is unconstrained by current experimental searches. Note that the Planck and Fermi-LAT constraints shown in the right panel of Fig. 4.9 assume a 100% annihilation rate into a single SM channel.

4.4.3 Results

The allowed region of the parameter space in the $m_\chi - m_{Z_2}$ plane that satisfy cosmological, indirect and direct detection constraints for this model are presented in Fig. 4.10 for $g' = 1$ and 4π, setting $\theta_\alpha \neq 0$ one at a time and keeping two other mixing angles fixed to zero. For definiteness, in the figure we set $m_4 = 2m_{Z_2}$. Notice that this choice is not relevant for the interaction between the SM neutrinos and DM and only plays a role in the loop-induced processes that are sub-dominant. Nevertheless, if the Z_2 originates from a new $U(1)'$ gauge group, its mass m_{Z_2}, as well as that of the Dirac neutrino m_4, are generated after the breaking of the symmetry. Thus, the natural expectation is that m_4 is not much heavier than m_{Z_2} as long as the new gauge coupling g' is $\mathcal{O}(1)$. Hence, unlike for the scalar example, it is not appropriate to set m_4 to a value above the electroweak scale while exploring (sub-)GeV Z_2 boson masses.

Below the electroweak scale constraints on the neutrino mixing parameters θ_α are *a priori* much more stringent [251]. However, in the model under investigation the heavy neutrino decays mostly invisibly to either a SM neutrino and the Z_2 (if $m_4 > m_{Z_2}$), or a SM neutrino and a pair of the DM particles (if $m_4 < m_{Z_2}$), assuming $g' \gtrsim 1$. This implies that the existing collider and beam dump constraints[5] should be rescaled with the corresponding branching ratios and become even weaker than the non-unitarity constraints imposed previously for the scalar realisation. The bounds from peak searches in leptonic decays of pions and kaons will however apply, since they rely entirely on the kinematics of a two-body decay. Thus, the non-unitarity constraints actually dominate down to $m_4 \approx m_K \approx 0.5$ GeV, where m_K is the kaon mass. In the region $m_4 \sim 0.01 - 0.4$ GeV, the bounds on U_{e4} and $U_{\mu 4}$ from peak searches are very stringent. We do not display them explicitly in Fig. 4.10, because they are m_4-dependent, while all the constraints shown in the figures have an extremely sub-leading dependence on m_4, as outlined above. Thus, Fig. 4.10 is

[5]If the heavy neutrino decays before reaching the detector, the constraints from beam dump experiments will not apply at all.

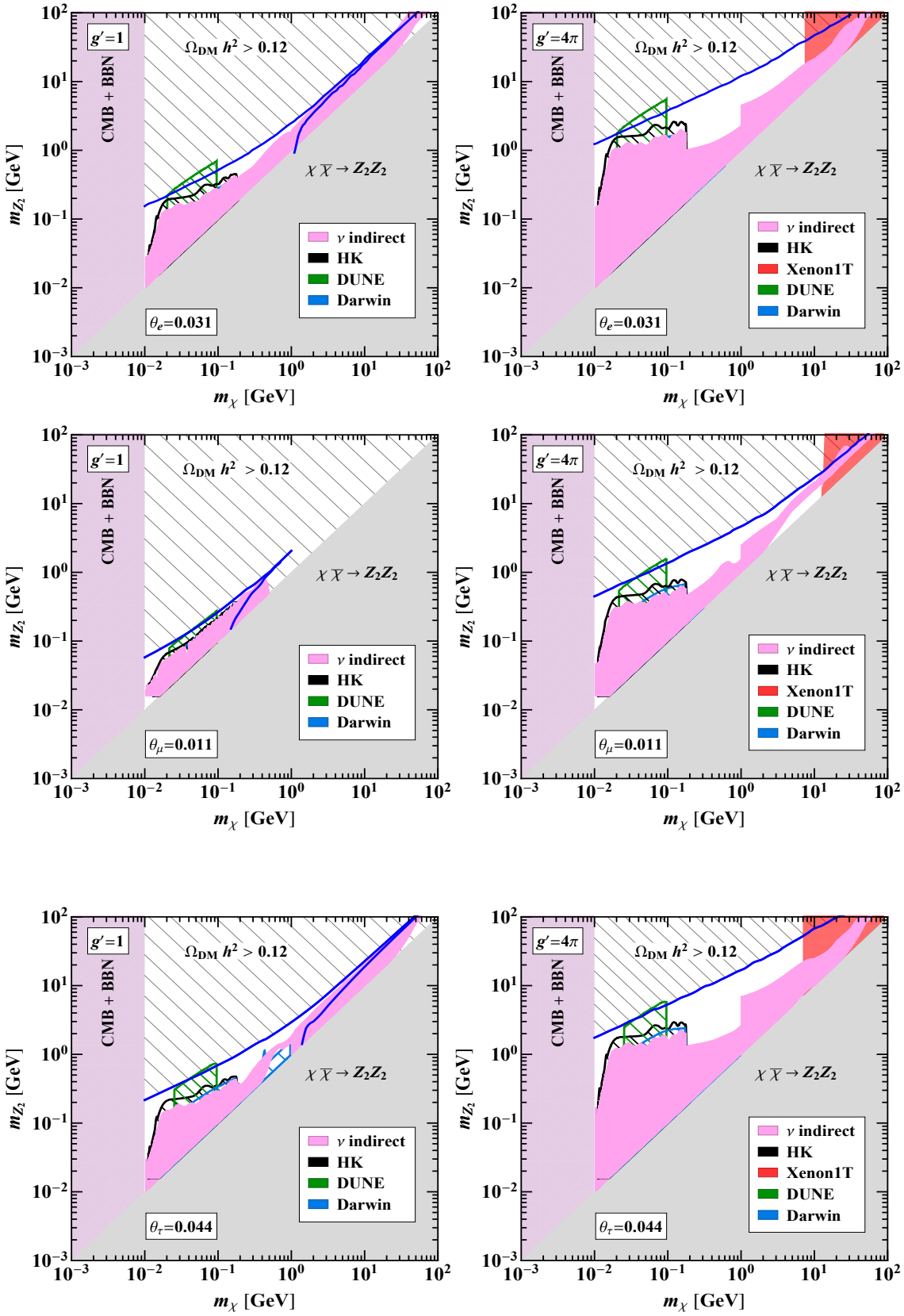

Figure 4.10: Constraints on the DM mass m_χ and m_{Z_2}. Along the blue lines, computed with `micrOMEGAs`, the DM relic density matches the observed value. The coloured shaded regions are excluded by different experiments. The lower bound $m_\chi \gtrsim 10$ MeV is set by observations of the CMB and BBN. See text for further details.

to be interpreted as generally valid for any neutrino mass $m_4 > m_K$.

The blue line was calculated with `micrOMEGAs` and represents the DM and vector boson masses that will produce the correct relic abundance in a thermal scenario, while the masses in the upper hatched area would generate too much DM. A key difference with respect to the previous model is that here the DM annihilation cross section to neutrinos proceeds via an s-channel and thus is enhanced for $m_{Z_2} \sim 2m_\chi$, as can be seen from Eq. (4.4.2). This explains the second branch of the blue line below the resonant condition in the panels with $g' = 1$. A line where the relic abundance can be obtained below $m_{Z_2} = 2m_\chi$ also occurs for $g' = 4\pi$ but, since the cross section is larger, the relic abundance is achieved for $m_\chi > 100$ GeV, which is ruled out by XENON1T. This resonant effect also explains the shape of the indirect detection constraints which follow the same trend.

Similar to the previous model in Sec. 4.3, the direct detection constraints from XENON1T become relevant at large DM masses for $g' = 4\pi$. However, even for values of the gauge coupling this large, we have checked that direct detection constraints from the elastic DM scattering off electrons are negligible.

The complementarity between cosmological observables, DM, and neutrino experiments allows us to set very strong bounds on the DM and Z_2 masses for this particular realisation, ruling out significant portions of the parameter space. There are still allowed regions for larger values of the gauge coupling consistent with a thermal DM candidate. However, future neutrino experiments such as DUNE will be able to probe down to the value for which the correct relic abundance is obtained in some parts of the parameter space.

It is worth noticing that the sensitivity of present and future neutrino detectors to DM annihilations into neutrinos is largely independent of the flavour to which the sterile neutrino dominantly couples. Indeed, as discussed in Sec. 1.4 regardless of the original flavour composition produced by the DM annihilations, neutrino oscillations will tend to populate all flavours with similar fractions when the flux arrives to the detector. The main differences between the three rows in Fig. 4.10 are due to

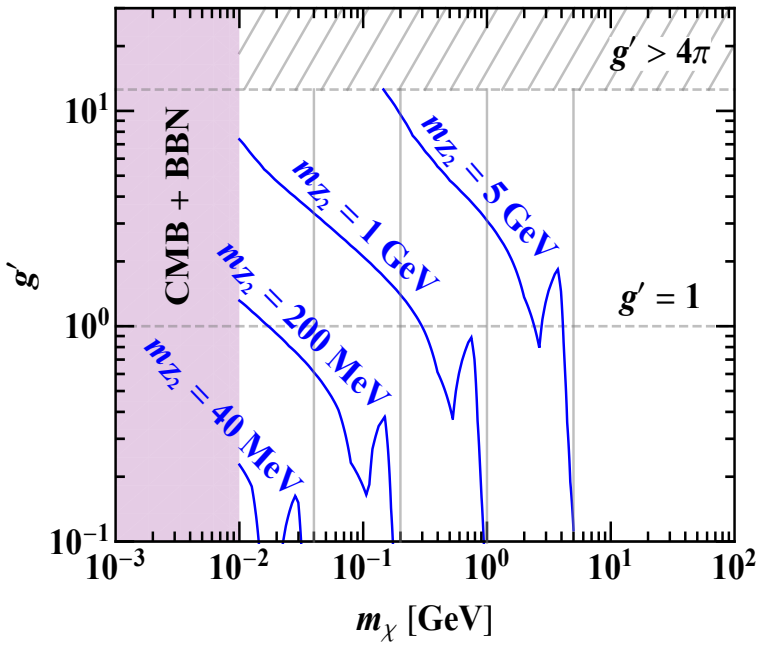

Figure 4.11: Values of the DM mass m_χ and the coupling g' required to reproduce the observed relic abundance. We have fixed $m_{Z_2} = 0.04$, 0.2, 1, and 5 GeV, and have considered the representative case of $\theta_e = 0.031$, while keeping $\theta_{\mu,\tau} = 0$. Along (above) the blue lines the DM relic density matches (is less than) the observed value. We do not consider $m_\chi > m_{Z_2}$ to ensure the neutrino portal regime. The lower bound $m_\chi \gtrsim 10$ MeV is set by observations of the CMB and BBN.

the different magnitude of the mixing allowed to the different flavours, with more stringent constraints applying for the mixing with muon neutrinos.

Finally, in Fig. 4.11, we fix m_{Z_2} to several values, namely, $m_{Z_2} = 0.04$, 0.2, 1, and 5 GeV, and show the lines corresponding to the correct relic abundance in the $m_\chi - g'$ plane. These results were obtained using `micrOMEGAs`. Small values of g' are ruled out except for DM masses in the proximity of the resonance, i.e., when $m_\chi \approx m_{Z_2}/2$. As can be seen from this figure, a lighter dark vector boson allows for smaller values of g'. For $m_{Z_2} \gtrsim 1$ GeV, values of $g' \gtrsim 1$ are required to yield the observed relic density, except for the resonant region. The dip towards $m_\chi \approx m_{Z_2}$ corresponds to the opening of new DM annihilation channels at tree level.

4.5 Conclusions

Due to $SU(2)$ gauge invariance, one expects that neutrinos share all their interactions with their charged lepton counterparts, which are much easier to detect. Consequently, the usual concern when studying neutrino-DM interactions is whether they actually provide with any additional information relevant to the DM phenomenology. In this chapter, we have explored whether a dominant neutrino-DM interaction is allowed in simple gauge-invariant models without conflicting with searches through charged leptons.

We first studied the simplest scenario, in which DM couples to the full lepton doublet. We verified that, as long as the DM is heavier than the charged lepton(s) it couples to, the bounds from DM annihilation to charged leptons preclude DM-neutrino couplings sizeable enough to be probed. In fact, in this regime, charged lepton constraints are so strong that they rule out all of the parameter space that would not lead to overclosure of the Universe. Alternatively, if DM couples to τ (μ) and is lighter than the charged lepton, its phenomenology is dominated by the interaction with neutrinos. This region is constrained by present neutrino detectors and will be fully probed for certain DM masses by future experiments.

We have then explored the option of the neutrino portal to DM and showed, as an example, two specific realisations with scalar and vector couplings, respectively. In the neutrino portal DM couples directly to new heavy neutrinos. Indeed, their singlet nature makes them natural candidates to probe the dark sector since they are allowed to interact with it via relevant or marginal operators. These right-handed neutrinos are also a natural addition to the SM particle content so as to account for the evidence for neutrino masses and mixings. The mixing between the SM neutrinos and the new singlets will induce DM-neutrino interactions at tree-level, but DM-charged lepton couplings only at loop level.

In the two realisations considered we find that it is indeed possible for neutrino detectors to place the most stringent and competitive bounds through searches for

DM annihilations to neutrinos. Present searches at Super-Kamiokande, Fréjus, or Borexino are ruling out large areas of the parameter space. Interestingly, future projects such as Hyper-Kamiokande, DARWIN, or DUNE will be able to probe the cross section very close and beyond the value required to explain the DM abundance solely by annihilation to SM neutrinos.

Chapter 5

Raising the neutrino floor with new physics

Experimental confirmation of a prediction is merely a measurement. An experiment disproving a prediction is a discovery.

— Enrico Fermi

In the previous chapters, we have examined how useful neutrinos are in order to deepen our understanding of the DM nature. However, neutrinos can also become a challenging obstacle in this quest. In fact, future DM direct detection experiments will soon be sensitive to a new source of background, due to coherent elastic neutrino-nucleus scattering (CEνNS), which proceeds through the exchange of a Z boson in the SM [261]. Neutrinos with energies in the $1 - 100$ MeV range are quite abundant, cannot be shielded against, and could induce keV scale nuclear recoils which would be difficult to distinguish from those caused by DM particles. For example, the recoil spectrum expected from the ^{8}B solar neutrino flux would resemble that of a 6 GeV DM particle (with a specific scattering cross-section) [262]. This is interpreted as a "neutrino floor" [263] in the DM-nucleus scattering cross section and DM mass

parameter space, which corresponds to the threshold below which the number of neutrino events is expected to be much larger than the number of DM events, which prevents to identify DM events with certainty. Discriminating these signals would require exploiting their different contributions to annual modulation [262,264], using a combination of complementary targets [265] and directional detectors [266,267] or employing detectors with improved energy resolution [268].

Despite the extremely small energy deposition and weak scale cross section, CEνNS has recently been observed by the COHERENT collaboration [269] for the first time, using neutrinos from a spallation source. Direct detection experiments will soon be sensitive to the CEνNS from solar neutrinos, which takes place at lower energies, thereby providing complementary information on this process. For example, the xenon based LZ [270], currently under construction, expects to observe approximately seven neutrino events in a three-year run. This also offers the possibility of studying different solar models [271], and it is perhaps a unique opportunity to measure neutrinos from the CNO cycle [272,273] and thus estimate the solar metallicity [272].

New physics in the neutrino sector (described in terms of new mediators between neutrinos and electrons and/or quarks, or in terms of non standard effective interactions) can increase the CEνNS scattering cross-section at low energies (as well as the elastic neutrino-electron scattering) [259,274–285]. This can raise the neutrino floor, inevitably affecting the search for light DM particles in upcoming experiments, especially in those that will explore the low-mass DM window. In this chapter we study a range of simplified models with emphasis on low-mass mediators in the neutrino sector to which we apply the most recent constraints in order to determine how high the neutrino floor can be. This information is crucial in order to correctly interpret a future signal in direct DM detectors.

We have found that the CEνNS floor can be raised by several orders of magnitude in the region with DM mass below 10 GeV when a new scalar mediator is assumed. However, the impact that such a mediator could have on the equation of state of a supernovae core would require further analysis. The increase is only by a

factor of approximately 2 for a new vector mediator. This result already affects the background predictions for xenon based experiments such as XENON1T [45] and, more importantly, it has deep implications for future results from detectors that explore the low-mass DM window, such as SuperCDMS SNOLAB [286] and NEWS-G [287].

5.1 The CEνNS floor in the presence of new hysics

The total number of expected events from CEνNS in a direct DM detection experiment with a given exposure, ϵ, can be computed by integrating the CEνNS cross section, $d\sigma_{\nu N}/dE_R$, and the incoming flux of neutrinos, $d\phi_\nu/dE_\nu$, over the resulting nuclear recoil energy,

$$N_{\text{CE}\nu\text{NS}} = \frac{\epsilon}{m_N}\int_{E_T}^{E_{\max}} dE_R \int_{E_\nu^{\min}} dE_\nu \frac{d\phi_\nu}{dE_\nu}\frac{d\sigma_{\nu N}}{dE_R}, \tag{5.1.1}$$

where m_N is the nuclear mass, and $E_\nu^{\min}$ is the minimum neutrino energy to produce a nuclear recoil of energy E_R. In the SM, the coherent scattering of neutrinos off nuclei takes place through the exchange of a Z boson, and the resulting cross section reads [261]

$$\frac{d\sigma_{\nu N}}{dE_R} = \frac{G_F^2}{4\pi} Q_{vN}^2 m_N \left(1 - \frac{m_N E_R}{2E_\nu^2}\right) F^2(E_R), \tag{5.1.2}$$

where G_F is the Fermi constant, $Q_{vN} = N - (1 - 4\sin^2\theta_w)Z$ is the weak hypercharge of a target nucleus containing N neutrons and Z protons, and $F^2(E_R)$ is the nuclear form factor, for which we have taken the parametrisation given by Helm [288]. The scattering cross section benefits from a coherence factor that scales as the total number of nucleons squared $Q_{vN}^2 \sim A^2$. The neutrino flux at low energies is dominated by solar neutrinos, and the relevant fluxes used in this work can be found in Refs. [289, 290]. At higher energies, atmospheric neutrinos are the most important source, although their flux is substantially smaller [291]. As a side note, although there are systematic and statistical uncertainties of the order of $1 - 10\%$

associated to the flux of solar neutrinos, we will neglect these in calculating the neutrino floor. As we will show below, the effect of new physics can be much larger than such uncertainties.

We construct the neutrino floor as follows, based on Ref. [262]. For a given target nucleus, a minimum energy threshold E_T is set and, using Eq. (5.1.1), the exposure required to give 1 expected count of CEνNS is calculated. Using this value of the exposure, one can compute the minimum spin-independent WIMP-nucleon elastic cross section, $\sigma_{\chi n}^{SI}$, that can be excluded at the 90% confidence level for each value of the DM particle mass, m_χ. For a background-free analysis, this lies along the 2.3 DM event isovalue contour. The threshold energy is then varied across the relevant range and, by taking a lower envelope on $\sigma_{\chi n}^{SI}$, we obtain the contour in parameter space along which, given an optimal choice of the threshold to minimise the neutrino background, there will be as many CEνNS events as WIMP events. Alternatively, it is also possible to define the neutrino floor as a DM discovery limit using spectral information and including uncertainties in the solar neutrino fluxes [262]. The neutrino floor can also be generalised to other types of DM-nucleus effective field theory operators [292], but in this work we assume only a spin-independent WIMP-nucleon interaction. In our calculation of the DM signature we have assumed a Standard Halo Model with a local density of 0.4 GeV cm^{-3}, a central velocity of 230 km/s, and a velocity dispersion of 156 km/s.

Disentangling DM and neutrino signals in the region of parameter space below this line is not impossible, but the CEνNS floor serves as an indication of the point at which neutrinos become a significant obstacle to DM direct detection. New physics in the neutrino sector can contribute to the predicted CEνNS cross section, thus shifting the neutrino floor. These contributions are larger for light mediators [275, 276, 278, 283, 292, 293].

5.1.1 New physics models

We have considered a set of low scale simplified models in which the SM structure is extended by the inclusion of a new light mediator [184, 294] between the neutrinos and quarks (and/or leptons). An obvious concern of dealing with simplified models at low scales is the difficulty in realizing such models in UV complete frameworks. This concern is justified as such models typically have chiral anomalies, requiring extra light fermion content to fix it, or non-trivial scalar sectors associated to the breaking of some symmetry at low scales. To mitigate this worry, we will focus on low scale simplified models that may have a clear UV completion: gauged $B - L$ [259, 295], gauged $B - L(3)$ of the third family [296], sequential Z' [297] and scalar mediators (see e.g. Ref. [298]).

- **Vector/Axial Vector Mediator:**

  The introduction of a new vector field, Z', that couples to SM fermions gives rise to new terms in the SM Lagrangian of the form

  $$\mathcal{L} \supset -\left(g_{Z'} J^{\mu}_{Z'} - \frac{g}{c_W}\epsilon' J^{\mu}_{\rm Z} - e\epsilon J^{\mu}_{\rm em}\right) Z'_{\mu} \ , \tag{5.1.3}$$

  where $g_{Z'}$ is the gauge coupling of the new gauge group; $J_{Z'}$, $J_{\rm em}$, and J_Z are the Z', electromagnetic, and Z currents; and ϵ and ϵ' parametrize the Z' mixing with the photon and the Z boson, respectively. Here we will not study any model with kinetic mixing[1], so we can disregard the last term in eq. (5.1.3). To ease the notation, we parametrise the Lagrangian as

  $$\mathcal{L} \supset -\sum_f c_f \bar{f}\gamma^{\mu} f Z'_{\mu} + \text{h.c.} \ , \tag{5.1.4}$$

  where the sum runs over all left- and right-handed fermion fields, that is $f = Q_L, u_R, d_R, L, e_R$ for each flavour. For the $B - L$ case, $c_f = g_{B-L}/3$ for quarks and $c_f = -g_{B-L}$ for leptons. In the sequential Z', all couplings come

[1] If the $U(1)$ studied here is a subgroup of a non-Abelian gauge group, kinetic mixing is forbidden at tree level, although it will be induced at loop level. The loop contribution depends on the fermion content of the UV theory, but generically we expect it to be suppressed by a factor of $\epsilon \sim g_{B-L}e/16\pi^2 \sim 2 \times 10^{-3} g_{B-L}$, and is therefore negligible.

from the mass mixing to the SM Z boson, ϵ', and thus c_f are given by $g_{Z'}\epsilon'$ times the Z couplings of each fermion. In the $B-L(3)$ model, the couplings to the third family are identical to the $B-L$, while the coupling to the first two comes from $Z-Z'$ mass mixing. The resulting CEνNS cross section can be written as

$$\frac{d\sigma_{\nu N}}{dE_R} = \frac{d\sigma_{\nu N}^{SM}}{dE_R} - \left(\frac{G_F m_N Q_{\nu N} Q'_{\nu N,v} (2E_\nu^2 - E_R m_N)}{2\sqrt{2}\pi E_\nu^2 \left(2E_R m_N + m_{Z'}^2\right)} - \frac{Q'^2_{\nu N,v} m_N (2E_\nu^2 - E_R m_N)}{4\pi E_\nu^2 \left(2E_R m_N + m_{Z'}^2\right)^2} \right) F^2(E_R), \tag{5.1.5}$$

where the SM cross section is given in Eq. (5.1.2). Here $Q_{\nu N}$ and $Q'_{\nu N,v}$ are the coherence factors of the cross section, the latter being given by

$$Q'_{\nu N,v} = \left[(2Z+N)\frac{(c_{Q_L} + c_{u_R})}{2} + (Z+2N)\frac{(c_{Q_L} + c_{d_R})}{2} \right] c_\nu \ . \tag{5.1.6}$$

Eq.(5.1.4) assumes a vector mediator. However we did check the case of an axial coupling. Typically, axial interactions contribute less significantly to the CEνNS cross section than vector interactions, as the former couple to the overall spin of the nucleus [299–302]. The coherence factor for an axial interaction is proportional to the nuclear angular momentum, and does not benefit from the $\sim A^2$ enhancement. Since the couplings c_ν are still affected by the constraints from electron interactions, one should not expect a large contribution from the axial component for heavy nuclei. However, this contribution can be significant for light targets provided they have non-vanishing nuclear angular momentum. In our study, we have considered Ge and Xe (which are heavy targets), and He (which has zero spin), for all of which the contribution from axial couplings is negligible, and thus has been dropped out in Eq. (5.1.6).

To obtain the CEνNS cross section for any of the models considered here, we simply need to identify the corresponding c_f couplings. Different models have different couplings to quarks and leptons, leading to distinct constraints on the values of the gauge coupling and mediator mass: the constraints used in

this chapter for the $B-L(3)$ model are taken from Ref. [260, 296, 303] for the case $\tan\beta = 10$, which leads to $\epsilon' \simeq 0.01 g_{B-L(3)}$; while the constraints on the $B-L$ model are a combination of those used in Refs. [259, 275, 304, 305] and Big Bang nucleosynthesis (BBN) constraints given in Ref [306]. The Sequential SM turns out to be extremely constrained and the resulting contribution to the neutrino floor is very small, thus we will not discuss it further.

- **Scalar/Pseudoscalar mediator:**

  The other scenario of interest which may impact the neutrino floor is constituted by a light scalar mediator that interacts with SM fermions [85, 172]. We consider here a simple extension of the form

$$\mathcal{L} = -y_\nu \bar{\nu}_L^c \phi \nu_L - \sum_{f\neq\nu} y_f \bar{f} \phi f - \sum_{f\neq\nu} y_f^5 \bar{f} \phi i\gamma_5 f + \text{h.c.} \,, \tag{5.1.7}$$

  where the sum runs over all charged fermions. Note that in this scenario the scalar coupling violates lepton number[2]. For simplicity, we assume that all SM particles have the same coupling $y_f = y$ to ϕ. We also neglect y_f^5, as this pseudoscalar coupling leads to a very small contribution to the coherent scattering cross section (see e.g. [302]). The resulting CEνNS cross section reads

$$\frac{d\sigma_{\nu N}}{dE_R} = \frac{d\sigma_{\nu N}^{SM}}{dE_R} + \frac{y^4 Q'^2_{\nu N,s} m_N^2 E_R}{4\pi E_\nu^2 (2E_R m_N + m_\phi^2)^2} F^2(E_R) \,, \tag{5.1.8}$$

  where m_ϕ is the mass of the scalar mediator and the new coherence factor $Q'_{\nu N,s} = 13.8A - 0.02Z$ is computed using Refs. [307–310] to calculate the scalar-quark form factors.

  Compared with the models with a vector mediator discussed above, the specific couplings of this scalar model are less motivated by theory. It therefore has fewer model specific constraints. In this work, we have considered the bounds from astrophysical and cosmological sources discussed in Ref. [311], and the results of the COHERENT experiment [269].

[2]One could also work with a lepton number conserving model, at the expense of including right-handed neutrinos. The predictions for CEνNS would not change but this scenario is more affected by supernova constraints, which limit the contribution to the neutrino floor.

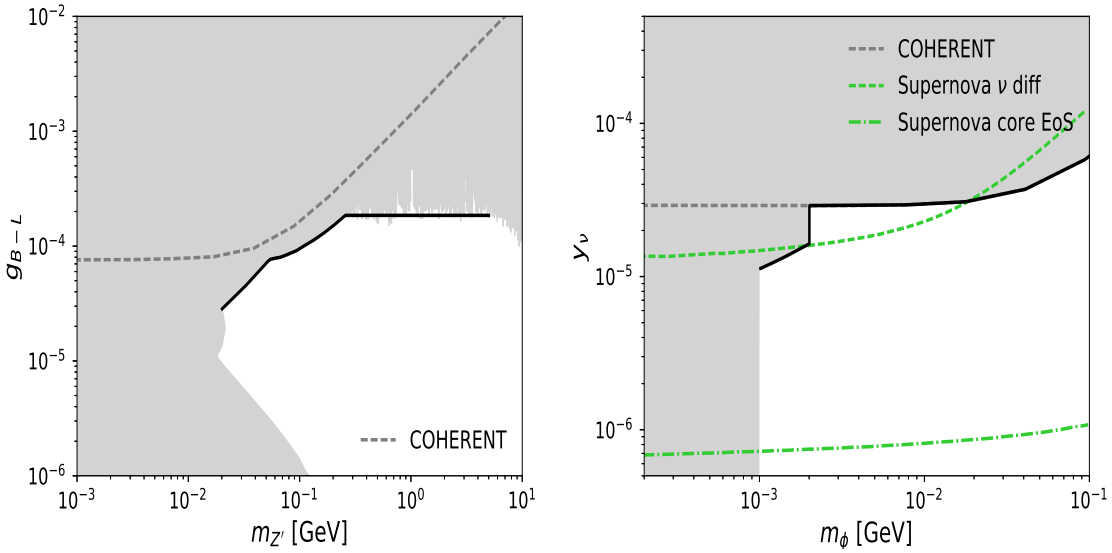

Figure 5.1: The gray areas represent the regions excluded in the case of a vector (left panel) and scalar (right panel) mediator. The solid black line represents the values of the mediator coupling that we have used to determine the maximum contribution to the neutrino floor in both cases. In the scalar case we include constraints from supernovae in green: both those from neutrino diffusion (dashed) and the core equation of state (dot-dashed).

Fig. 5.1 represents the areas in the mediator mass and coupling parameter space that are available for models with new vector (left panel) and scalar (right panel) mediators. Gray regions are excluded by various astrophysical and cosmological limits, as well as bounds from neutrino and neutron scattering experiments. The upper bound on new physics couplings obtained from the COHERENT observation [269] is shown by means of a dashed gray line [282, 311, 312]. The green dashed and green dot-dashed lines for scalar mediators indicate the values of the neutrino coupling for which the neutrino diffusion rate and the core equation of state in supernovae could be significantly altered and need to be reevaluated. Vector mediators are extremely constrained by a combination of bounds from neutrino experiments (mainly Borexino, GEMMA and TEXONO) as well as astrophysical constraints (on supernovae and other stellar systems), fixed target and beam dump experiments (CHARM, U70 and E317) and e^+e^- colliders (such as BaBar and Belle). Contrariwise, models with extra scalar mediators are in principle more flexible (with the caveat that supernovae limits might have to be reevaluated).

5.2 Results

For each simplified model described in Sec. 5.1, we have considered the largest possible values of the neutrino couplings as a function of the mediator mass that is allowed by the various experimental constraints (represented as a solid black line in Fig. 5.1), and we have used these to determine the maximum contribution to the CEνNS cross section. The height and shape of the CEνNS floor vary for different target nuclei. Here we consider three different materials. Germanium and xenon have qualitatively similar shapes, but we include both as they are common targets in low and high mass searches respectively, such as SuperCDMS [286], XENON1T [45], LZ [270], and DARWIN [148]. We also include helium, as an example of a very light target, which has been proposed as a way of probing very low DM masses in a future phase of the NEWS-G experiment [287]. The sensitivity line for NEWS-G has been extracted from Ref. [313]. The very low mass of the He nucleus allows solar ^{8}B neutrinos to generate much higher energy recoils. The resulting flattening of the recoil spectrum prevents us from distinguishing ^{8}B neutrinos from higher mass DM simply by choosing a higher energy threshold, and so the neutrino floor is noticeably flatter than it is for heavier targets.

Figure 5.2 represents the resulting CEνNS floor for the two vector mediated models discussed in Sec 5.1.1. For comparison, the SM contribution is shown as a solid grey line. We can observe that the new physics contribution can be greater than a factor of 2 for DM masses below 10 GeV. The $B-L$ model (black dashed line) has a greater enhancement at low masses than the $B-L(3)$ (black dot-dashed line) due to less stringent constraints on the mediator mass. However, at higher energies the $B-L(3)$ enhancement is comparable, as larger couplings to the third generation are allowed with higher mediator masses. We also observe that current direct detection experiments are beginning to probe the region of parameter space below the "new" neutrino floor, suggesting that future detectors could be used to put competitive limits on the properties of these new vector mediators. It should be noted that

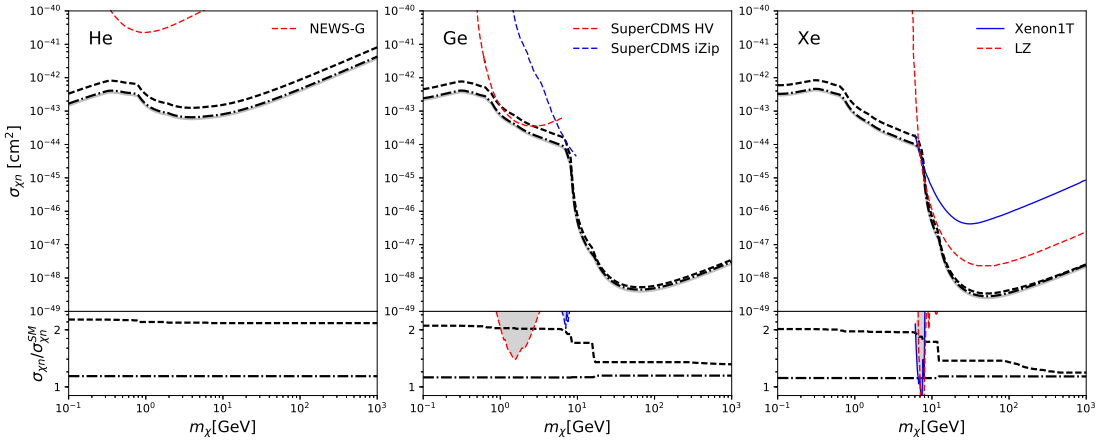

Figure 5.2: Upper: CEνNS floor for a new vector mediator, computed for direct detection experiments utilising, from left to right, He, Ge, and Xe. The SM neutrino floor (solid, grey) is compared with the maximum level reached in a $B-L$ (dashed, black) and a $B-L(3)$ (dot-dashed, black) model. For comparison, the sensitivities of some current (solid) and future (dashed) direct detection experiments are shown in color. Lower: Ratio of the new neutrino floor to the SM result. The sensitivities of representative direct detection experiments are also shown in this parameter space.

astrophysical uncertainties in the parameters that describe the DM halo can lead to a greater effect in the DM discovery limit over the neutrino floor [314].

As expected, models with scalar mediators allow for a much larger enhancement of the neutrino floor, represented by a dashed line in Fig. 5.3. However, the spectacular increase of several orders of magnitude for DM masses below 10 GeV is subject to the reevaluation of supernovae constraints in this kind of lepton-violating models. As pointed out in Ref. [311], it is uncertain whether this range of mediator masses and couplings can induce changes in the equation of state that describes the supernova core and the physics of neutrino diffusion. To account for these effects, in Fig. 5.3 we also show the results when neutrino diffusion are limits included (dot-dashed line) and when a strict limit on the supernova core equation of state is also added (dotted line). The spectacular enhancement of the neutrino floor at small DM masses corresponds to very light new mediators (with masses in the MeV range) [85, 172], while for heavier mediators, such as those considered in Ref. [276], the increase is much more moderate.

The new scalar mediator gives very little enhancement to the neutrino floor at higher

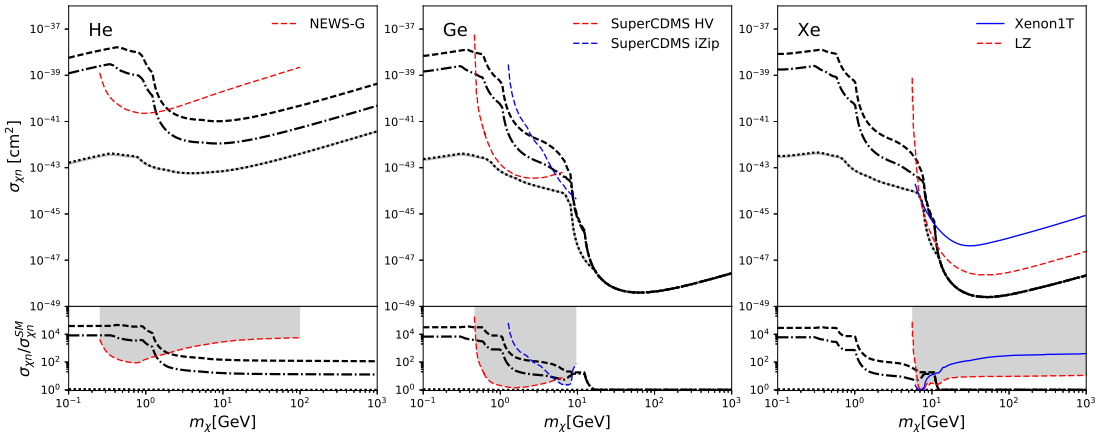

Figure 5.3: As in Fig. 5.2, but for a scalar mediator. For the constraints on our model, we consider three different cases discussed in Sec 5.1.1: one in which supernova constraints are neglected (dashed), one in which supernova diffraction constraints are included but bounds from the SN core EoS are ignored (dot-dashed) and one in which all supernova constraints are included (dotted).

WIMP masses, since the region of heavy mediators is more constrained from particle physics bounds, meaning that the best prospects to constrain such models come from experiments with low energy thresholds such as SuperCDMS SNOLAB.

The shape and height of the neutrino floor depend on the nature of the DM interaction, and thus they change significantly for different EFT operators [292], especially when these feature non-trivial momentum or velocity dependence. However, we have checked explicitly that the ratio by which the neutrino floor is raised with respect to its SM value is only slightly distorted. In particular, the maximum increase in the neutrino floor at small DM masses is insensitive to the choice of EFT operator. Therefore, the lower panels of Figures 5.2 and 5.3 are a useful guide to the results for all other EFT operators.

5.3 Conclusions

In this chapter, we have determined the contribution from new physics models to the coherent neutrino scattering (CEνNS) floor, which is expected to be within the reach of next-generation DM direct detection experiments. We have considered a collection

of simplified models that include a new vector or scalar mediator between the SM neutrino and the SM quarks and leptons. We have incorporated the most recent constraints from various sources of experiments and astrophysical observations and used them to determine the maximum reach of the neutrino floor in the parameter space of elastic spin-independent DM scattering. In doing this, we have payed particular attention to the limits on new physics that can be derived from the recent observation of CEνNS by the COHERENT collaboration.

We have observed that, in the case of vector mediators embedded in UV complete frameworks, the CEνNS floor can be raised by approximately a factor of two for small DM masses (below 10 GeV, where the main contribution is due to solar neutrinos) and by a factor of 1.3 for large DM masses (where atmospheric neutrinos dominate). Experimental limits from neutrino and beam dump experiments are the main obstacle that limits the height of the neutrino floor in these scenarios.

In the case of new scalar mediators, the neutrino floor can be raised by several orders of magnitude in the region of low-mass DM (below 10 GeV), a feature that is definitely within the reach of upcoming experiments such as SuperCDMS SNOLAB and NEWS-G. However, this spectacular enhancement is subject to the re-examination of supernovae bounds, as new physics can induce changes in the equation of state of the supernova core that must be carefully analysed. If these bounds turn out to be as strong as suggested in Ref. [311], the maximum enhancement of the neutrino floor due to a light scalar mediator would be quite small.

In conclusion, our results indicate that the expected CEνNS background in the recent XENON1T results could increase by a factor of two or even more. More importantly, future claims by DM experiments in the low-mass window must be carefully examined to discriminate neutrino and DM signals well above the expected SM neutrino floor.

Chapter 6

Conclusions: Neutrinos as a tool to unveil the dark matter mystery

> *In eternity there is no time, only an instant long enough for a joke.*
>
> — from *Steppenwolf* by Hermann Hesse

The unknown origin of neutrino masses and mixing together with the existence of the DM component of the Universe constitute the most significant experimental evidence for physics beyond the SM and therefore, the best windows to explore new physics. Neutrinos and DM also share an elusive nature with very weak interactions with the other SM particles. Indeed, neutrinos only participate in the weak interaction of the SM while all direct and indirect searches for DM interactions with the SM, other than gravity, are so far negative or inconclusive. A tantalising avenue of investigation is the possibility of a stronger connection between these two sectors. In this case, the best way to probe DM would be through the neutrino sector.

Non-vanishing DM-neutrino interactions have several important cosmological and astrophysical consequences. They can explain the observed DM relic density if DM

has been thermally produced and annihilations into neutrinos are the dominant channel. They can also lead to DM indirect detection signatures if DM annihilates or decays into neutrinos in the galaxy. In Chapter 2 we have seen how, in the absence of a DM signal, indirect detection searches can set strong constraints on the annihilation cross section of DM to neutrinos across several orders of magnitude in the DM mass. Furthermore, future neutrino experiments like DUNE or HK doped with gadolinium will be able to rule out thermal DM candidates for DM masses between $10-100$ MeV. We exploit these searches to study different simplified models in which DM couples to neutrinos in Chapter 3. We found that the complementarity between cosmological and astrophysical constraints can be used to test large areas of the allowed parameter space for such models.

Nevertheless, $SU(2)$ gauge invariance would naively dictate that neutrinos share all their interactions with their charged lepton counterparts, which are much easier to detect. We have therefore explored in Chapter 4 whether a dominant neutrino-DM interaction is allowed in simple gauge-invariant models without conflicting with searches involving charged leptons. In fact, if DM couples to the full leptonic doublet, we have found that the bounds from DM annihilation to charged leptons preclude DM-neutrino couplings sizeable enough to be probed, even ruling out all of the parameter space that would not lead to overclosure of the Universe. However, if DM couples directly to new sterile neutrinos, the mixing between the SM neutrinos and the new singlets will induce DM-neutrino interactions at tree-level, while DM-charged lepton couplings only at loop-level. We have discussed two possible realisations with a scalar and a vector mediator between the DM and the right-handed neutrinos and we found that it is indeed possible for neutrino detectors to place the most stringent and competitive bounds through searches for DM annihilations to neutrinos. It would be very interesting to study whether generating light neutrino masses can set complementary constraints on the parameter space by invoking a mass mechanism such as the one presented in [315]. Together with indirect detection constraints from future experiments such as HK, DARWIN, or DUNE, these bounds will effectively

cover most of the parameter space, probing if the right-handed singlet fermions that can explain the origin of neutrino masses also represent the best window to the discovery of the dark matter sector.

At the same time, direct detection experiments are becoming so sensitive that it is possible to study neutrino physics with them. In Chapter 5 we have determined the contribution from new physics models to the coherent neutrino scattering (CEνNS) floor. By considering two simplified models with a vector and a scalar mediator between the neutrinos and the charged leptons and quarks, we have seen that, for DM masses below ~ 10 GeV, the neutrino floor can be raised by a factor of 2 or by several orders of magnitude for a vector and a scalar mediator respectively. This implies that potential future discovery claims by DM detectors for low DM masses should be carefully studied to understand whether they correspond to a DM signal or to new physics in the neutrino sector. Furthermore, if we were able to discriminate such signals, it would be intriguing to see whether one can set competitive constraints on the new physics parameters.

Some interesting continuation of this work would be to study the constraints that neutrino detectors can set on decaying DM models. This analysis would be very similar to the one performed in 2 but it would require the use of a different energy spectrum. Similarly, DM models with a vector mediator could be further constraint by studying the neutrinos produced in the $\chi + \bar{\chi} \to 2Z' \to 2\nu + 2\bar{\nu}$ annihilation channel. This is more challenging since the spectrum changes significantly but the results could allow us to rule out certain DM models.

In conclusion, neutrinos play a very important role in our understanding of DM. Recognising what the nature of DM is will only be possible through the complementarity between different observables at distinct energy scales. I hope the work presented in this thesis helps us to further our understanding about what DM is, or at least, what it cannot be.

Bibliography

[1] C. A. Arguelles, A. Kheirandish, A. Olivares-Del Campo, I. Safa and A. C. Vincent, *Constraining DM annihilation into neutrinos: the most invisible channel, to appear*, .

[2] A. Olivares-Del Campo, S. Palomares-Ruiz and S. Pascoli, *Implications of a Dark Matter-Neutrino Coupling at Hyper-Kamiokande*, in *53rd Rencontres de Moriond on Electroweak Interactions and Unified Theories (Moriond EW 2018) La Thuile, Italy, March 10-17*, 2018, 1805.09830.

[3] A. Olivares-Del Campo, C. Bœhm, S. Palomares-Ruiz and S. Pascoli, *Dark matter-neutrino interactions through the lens of their cosmological implications*, *Phys. Rev.* **D97** (2018) 075039, [1711.05283].

[4] M. Blennow, E. Fernandez-Martinez, A. O.-D. Campo, S. Pascoli, S. Rosauro-Alcaraz and A. V. Titov, *Neutrino Portals to Dark Matter*, 1903.00006.

[5] C. Bœhm, D. G. Cerdeño, P. A. N. Machado, A. O.-D. Campo and E. Reid, *How high is the neutrino floor?*, *JCAP* **1901** (2019) 043, [1809.06385].

[6] Planck collaboration, P. A. R. Ade et al., *Planck 2015 results. XIII. Cosmological parameters*, *Astron. Astrophys.* **594** (2016) A13, [1502.01589].

[7] Planck collaboration, N. Aghanim et al., *Planck 2018 results. VI. Cosmological parameters*, 1807.06209.

[8] M. Milgrom, *A Modification of the Newtonian dynamics as a possible alternative to the hidden mass hypothesis*, *Astrophys. J.* **270** (1983) 365–370.

[9] M. Milgrom, *A Modification of the Newtonian dynamics: Implications for galaxies*, *Astrophys. J.* **270** (1983) 371–383.

[10] M. Milgrom, *A Modification of the Newtonian Dynamics - Implications for Galaxy Systems*, *ApJ* **270** (July, 1983) 384.

[11] S. Dodelson, *The Real Problem with MOND*, *Int. J. Mod. Phys.* **D20** (2011) 2749–2753, [1112.1320].

[12] L. Bergström, *Nonbaryonic dark matter: Observational evidence and detection methods*, *Rept. Prog. Phys.* **63** (2000) 793, [hep-ph/0002126].

[13] G. Bertone and D. Hooper, *History of dark matter*, *Rev. Mod. Phys.* **90** (2018) 045002, [1605.04909].

[14] K. Garrett and G. Duda, *Dark Matter: A Primer*, *Adv. Astron.* **2011** (2011) 968283, [1006.2483].

[15] K. Freese, *Status of Dark Matter in the Universe*, *Int. J. Mod. Phys.* **1** (2017) 325–355, [1701.01840].

[16] M. Bauer and T. Plehn, *Yet Another Introduction to Dark Matter*, 1705.01987.

[17] K. C. Freeman, *On the Disks of Spiral and S0 Galaxies*, *ApJ* **160** (June, 1970) 811.

[18] V. C. Rubin and W. K. Ford, Jr., *Rotation of the Andromeda Nebula from a Spectroscopic Survey of Emission Regions*, *ApJ* **159** (Feb., 1970) 379.

[19] D. Clowe, A. Gonzalez and M. Markevitch, *Weak lensing mass reconstruction of the interacting cluster 1E0657-558: Direct evidence for the existence of dark matter*, *Astrophys. J.* **604** (2004) 596–603, [astro-ph/0312273].

[20] D. Clowe, M. Bradac, A. H. Gonzalez, M. Markevitch, S. W. Randall, C. Jones et al., *A direct empirical proof of the existence of dark matter*, *Astrophys. J.* **648** (2006) L109–L113, [astro-ph/0608407].

[21] P. J. E. Peebles, *Recombination of the Primeval Plasma*, *ApJ* **153** (July, 1968) 1.

[22] A. A. Penzias and R. W. Wilson, *A Measurement of excess antenna temperature at 4080-Mc/s*, *Astrophys. J.* **142** (1965) 419–421.

[23] G. F. e. a. Smoot, *Structure in the COBE differential microwave radiometer first-year maps*, *ApJ* **396** (Sept., 1992) L1–L5.

[24] J. F. Navarro, C. S. Frenk and S. D. M. White, *The Structure of cold dark matter halos*, *Astrophys. J.* **462** (1996) 563–575, [astro-ph/9508025].

[25] V. Springel et al., *Simulating the joint evolution of quasars, galaxies and their large-scale distribution*, *Nature* **435** (2005) 629–636, [astro-ph/0504097].

[26] F. D. Albareti, C. Allende Prieto, A. Almeida, F. Anders, S. Anderson, B. H. Andrews et al., *The 13th Data Release of the Sloan Digital Sky Survey: First Spectroscopic Data from the SDSS-IV Survey Mapping Nearby Galaxies at Apache Point Observatory*, *ApJS* **233** (Dec., 2017) 25, [1608.02013].

[27] C. Boehm, J. A. Schewtschenko, R. J. Wilkinson, C. M. Baugh and S. Pascoli, *Using the Milky Way satellites to study interactions between cold dark matter and radiation*, *Mon. Not. Roy. Astron. Soc.* **445** (2014) L31–L35, [1404.7012].

[28] J. de Swart, G. Bertone and J. van Dongen, *How Dark Matter Came to Matter*, 1703.00013.

[29] G. Arcadi, M. Dutra, P. Ghosh, M. Lindner, Y. Mambrini, M. Pierre et al., *The waning of the WIMP? A review of models, searches, and constraints*, *Eur. Phys. J.* **C78** (2018) 203, [1703.07364].

[30] L. Roszkowski, E. M. Sessolo and S. Trojanowski, *WIMP dark matter candidates and searches—current status and future prospects*, *Rept. Prog. Phys.* **81** (2018) 066201, [1707.06277].

[31] J. L. Feng, *Dark Matter Candidates from Particle Physics and Methods of Detection*, *Annual Review of Astronomy and Astrophysics* **48** (2010) 495–545, [https://doi.org/10.1146/annurev-astro-082708-101659].

[32] K. Griest and D. Seckel, *Three exceptions in the calculation of relic abundances*, *Phys. Rev.* **D43** (1991) 3191–3203.

[33] M. Srednicki, R. Watkins and K. A. Olive, *Calculations of Relic Densities in the Early Universe*, *Nucl. Phys.* **B310** (1988) 693.

[34] F. Giacchino, L. Lopez-Honorez and M. H. G. Tytgat, *Scalar Dark Matter Models with Significant Internal Bremsstrahlung*, *JCAP* **1310** (2013) 025, [1307.6480].

[35] I. G. Irastorza and J. Redondo, *New experimental approaches in the search for axion-like particles*, *Prog. Part. Nucl. Phys.* **102** (2018) 89–159, [1801.08127].

[36] S. Knapen, T. Lin and K. M. Zurek, *Light dark matter: Models and constraints*, *Phys. Rev. D* **96** (Dec, 2017) 115021.

[37] M. Frigerio, A. Pomarol, F. Riva and A. Urbano, *Composite Scalar Dark Matter*, *JHEP* **07** (2012) 015, [1204.2808].

[38] XENON collaboration, E. Aprile et al., *The XENON1T Dark Matter Experiment*, *Eur. Phys. J.* **C77** (2017) 881, [1708.07051].

[39] M. Battaglieri et al., *US Cosmic Visions: New Ideas in Dark Matter 2017: Community Report*, 1707.04591.

[40] R. Essig, T. Volansky and T.-T. Yu, *New Constraints and Prospects for sub-GeV Dark Matter Scattering off Electrons in Xenon*, *Phys. Rev.* **D96** (2017) 043017, [1703.00910].

[41] R. Essig, M. Sholapurkar and T.-T. Yu, *Solar Neutrinos as a Signal and Background in Direct-Detection Experiments Searching for Sub-GeV Dark Matter With Electron Recoils*, *Phys. Rev.* **D97** (2018) 095029, [1801.10159].

[42] M. J. Dolan, F. Kahlhoefer and C. McCabe, *Directly detecting sub-GeV dark matter with electrons from nuclear scattering*, *Phys. Rev. Lett.* **121** (2018) 101801, [1711.09906].

[43] LUX collaboration, D. S. Akerib et al., *Results from a search for dark matter in the complete LUX exposure*, *Phys. Rev. Lett.* **118** (2017) 021303, [1608.07648].

[44] PandaX-II collaboration, X. Cui et al., *Dark Matter Results From 54-Ton-Day Exposure of PandaX-II Experiment*, *Phys. Rev. Lett.* **119** (2017) 181302, [1708.06917].

[45] XENON collaboration, E. Aprile et al., *Dark Matter Search Results from a One Tonne× Year Exposure of XENON1T*, 1805.12562.

[46] K. M. Zurek, *Asymmetric Dark Matter: Theories, Signatures, and Constraints*, *Phys. Rept.* **537** (2014) 91–121, [1308.0338].

[47] F. Stoehr, S. D. M. White, V. Springel, G. Tormen and N. Yoshida, *Dark matter annihilation in the halo of the Milky Way*, *Mon. Not. Roy. Astron. Soc.* **345** (2003) 1313, [astro-ph/0307026].

[48] M. Benito, N. Bernal, N. Bozorgnia, F. Calore and F. Iocco, *Particle Dark Matter Constraints: the Effect of Galactic Uncertainties*, *JCAP* **1702** (2017) 007, [1612.02010].

[49] M. Benito, A. Cuoco and F. Iocco, *Handling the Uncertainties in the Galactic Dark Matter Distribution for Particle Dark Matter Searches*, 1901.02460.

[50] E. V. Karukes, M. Benito, F. Iocco, R. Trotta and A. Geringer-Sameth, *Bayesian reconstruction of the Milky Way dark matter distribution*, 1901.02463.

[51] D. Hooper and L. Goodenough, *Dark Matter Annihilation in The Galactic Center As Seen by the Fermi Gamma Ray Space Telescope*, *Phys. Lett.* **B697** (2011) 412–428, [1010.2752].

[52] Fermi-LAT collaboration, M. Ajello et al., *Fermi-LAT Observations of High-Energy γ-Ray Emission Toward the Galactic Center*, *Astrophys. J.* **819** (2016) 44, [1511.02938].

[53] M.-Y. Cui, Q. Yuan, Y.-L. S. Tsai and Y.-Z. Fan, *Possible dark matter annihilation signal in the AMS-02 antiproton data*, *Phys. Rev. Lett.* **118** (2017) 191101, [1610.03840].

[54] T. R. Slatyer, *Indirect dark matter signatures in the cosmic dark ages. I. Generalizing the bound on s-wave dark matter annihilation from Planck results*, *Phys. Rev.* **D93** (2016) 023527, [1506.03811].

[55] MAGIC and Fermi-LAT collaboration, M. L. Ahnen et al., *Limits to dark matter annihilation cross-section from a combined analysis of MAGIC and Fermi-LAT observations of dwarf satellite galaxies*, *JCAP* **1602** (2016) 039, [1601.06590].

[56] S. Palomares-Ruiz, *Model-Independent Bound on the Dark Matter Lifetime*, *Phys. Lett.* **B665** (2008) 50–53, [0712.1937].

[57] K. Murase and J. F. Beacom, *Constraining Very Heavy Dark Matter Using Diffuse Backgrounds of Neutrinos and Cascaded Gamma Rays*, *JCAP* **1210** (2012) 043, [1206.2595].

[58] ATLAS collaboration, G. Aad et al., *Search for dark matter candidates and large extra dimensions in events with a jet and missing transverse momentum with the ATLAS detector*, *JHEP* **04** (2013) 075, [1210.4491].

[59] CMS collaboration, S. Chatrchyan et al., *Search for dark matter and large extra dimensions in monojet events in pp collisions at* $\sqrt{s} = 7$ *TeV*, *JHEP* **09** (2012) 094, [1206.5663].

[60] A. Boveia and C. Doglioni, *Dark Matter Searches at Colliders*, *Ann. Rev. Nucl. Part. Sci.* **68** (2018) 429–459, [1810.12238].

[61] R. Contino, A. Falkowski, F. Goertz, C. Grojean and F. Riva, *On the Validity of the Effective Field Theory Approach to SM Precision Tests*, *JHEP* **07** (2016) 144, [1604.06444].

[62] J. Abdallah et al., *Simplified Models for Dark Matter Searches at the LHC*, *Phys. Dark Univ.* **9-10** (2015) 8–23, [1506.03116].

[63] Super-Kamiokande collaboration, Y. Fukuda et al., *Evidence for oscillation of atmospheric neutrinos*, *Phys. Rev. Lett.* **81** (1998) 1562–1567, [hep-ex/9807003].

[64] B. Pontecorvo, *Mesonium and anti-mesonium*, *Sov. Phys. JETP* **6** (1957) 429.

[65] B. Pontecorvo, *Inverse beta processes and nonconservation of lepton charge*, *Sov. Phys. JETP* **7** (1958) 172–173.

[66] Z. Maki, M. Nakagawa and S. Sakata, *Remarks on the Unified Model of Elementary Particles*, *Progress of Theoretical Physics* **28** (11, 1962) 870–880.

[67] Particle Data Group collaboration, C. Patrignani et al., *Review of Particle Physics*, *Chin. Phys.* **C40** (2016) 100001.

[68] S. Bilenky, J. Hošek and S. Petcov, *On the oscillations of neutrinos with dirac and majorana masses*, *Physics Letters B* **94** (1980) 495 – 498.

[69] V. Barger, K. Whisnant and R. J. N. Phillips, *Cp nonconservation in three-neutrino oscillations*, *Phys. Rev. Lett.* **45** (Dec, 1980) 2084–2088.

[70] M. C. Gonzalez-Garcia, M. Maltoni, J. Salvado and T. Schwetz, *Global fit to three neutrino mixing: critical look at present precision*, *JHEP* **12** (2012) 123, [1209.3023].

[71] I. Esteban, M. C. Gonzalez-Garcia, A. Hernandez-Cabezudo, M. Maltoni and T. Schwetz, *Global analysis of three-flavour neutrino oscillations: synergies and tensions in the determination of $\theta_2 3, \delta_C P$, and the mass ordering*, *JHEP* **01** (2019) 106, [1811.05487].

[72] P. Minkowski, *$\mu \to e\gamma$at a Rate of One Out of 1-Billion Muon Decays?*, *Phys. Lett.* **B67** (1977) 421.

[73] T. Yanagida, *Horizontal Symmetry and Masses of Neutrinos*, *Progress of Theoretical Physics* **64** (09, 1980) 1103–1105.

[74] M. Gell-Mann, P. Ramond and R. Slansky, *Complex Spinors and Unified Theories*, in *Proceedings of Supergravity Workshop, Stony Brook, New York, September 27–28, 1979*, pp. 315–321, 1979, 1306.4669.

[75] M. Magg and C. Wetterich, *Neutrino Mass Problem and Gauge Hierarchy*, *Phys. Lett.* **94B** (1980) 61–64.

[76] *Quark, lepton and neutrino masses in grand unified theories with local generation group*, *Nuclear Physics B* **292** (1987) 443 – 460.

[77] R. N. Mohapatra and G. Senjanović, *Neutrino masses and mixings in gauge models with spontaneous parity violation*, *Phys. Rev. D* **23** (Jan, 1981) 165–180.

[78] R. Foot, H. Lew, X. G. He and G. C. Joshi, *Seesaw Neutrino Masses Induced by a Triplet of Leptons*, *Z. Phys.* **C44** (1989) 441.

[79] A. Zee, *Quantum Numbers of Majorana Neutrino Masses*, *Nucl. Phys.* **B264** (1986) 99–110.

[80] K. S. Babu, *Model of 'Calculable' Majorana Neutrino Masses*, *Phys. Lett.* **B203** (1988) 132–136.

[81] Y. Cai, J. Herrero-García, M. A. Schmidt, A. Vicente and R. R. Volkas, *From the trees to the forest: a review of radiative neutrino mass models*, *Front.in Phys.* **5** (2017) 63, [1706.08524].

[82] R. Mohapatra and J. Valle, *Neutrino Mass and Baryon Number Nonconservation in Superstring Models*, *Phys. Rev.* **D34** (1986) 1642.

[83] J. Bernabeu, A. Santamaria, J. Vidal, A. Mendez and J. Valle, *Lepton Flavor Nonconservation at High-Energies in a Superstring Inspired Standard Model*, *Phys. Lett.* **B187** (1987) 303.

[84] M. Malinsky, J. Romao and J. Valle, *Novel supersymmetric SO(10) seesaw mechanism*, *Phys. Rev. Lett.* **95** (2005) 161801, [hep-ph/0506296].

[85] C. Boehm, Y. Farzan, T. Hambye, S. Palomares-Ruiz and S. Pascoli, *Is it possible to explain neutrino masses with scalar dark matter?*, *Phys. Rev.* **D77** (2008) 043516, [hep-ph/0612228].

[86] J. W. F. Valle, "Neutrino mass and new physics." 2017.

[87] R. Ichimasa, R. Nakamura, M. Hashimoto and K. Arai, *Big-Bang Nucleosynthesis in comparison with observed helium and deuterium abundances: possibility of a nonstandard model*, *Phys. Rev.* **D90** (2014) 023527, [1404.4831].

[88] R. A. Alpher, H. Bethe and G. Gamow, *The origin of chemical elements*, *Phys. Rev.* **73** (Apr, 1948) 803–804.

[89] K. Enqvist, K. Kainulainen and V. Semikoz, *Neutrino annihilation in hot plasma*, *Nucl. Phys.* **B374** (1992) 392–404.

[90] E. W. Kolb, M. S. Turner and T. P. Walker, *The Effect of Interacting Particles on Primordial Nucleosynthesis*, *Phys. Rev.* **D34** (1986) 2197.

[91] P. D. Serpico and G. G. Raffelt, *MeV-mass dark matter and primordial nucleosynthesis*, *Phys. Rev.* **D70** (2004) 043526, [astro-ph/0403417].

[92] F. Iocco, G. Mangano, G. Miele, O. Pisanti and P. D. Serpico, *Primordial Nucleosynthesis: from precision cosmology to fundamental physics*, *Phys. Rept.* **472** (2009) 1–76, [0809.0631].

[93] C. M. Ho and R. J. Scherrer, *Limits on MeV Dark Matter from the Effective Number of Neutrinos*, *Phys. Rev.* **D87** (2013) 023505, [1208.4347].

[94] Z. Berezhiani, A. Dolgov and I. Tkachev, *BBN with light dark matter*, *JCAP* **1302** (2013) 010, [1211.4937].

[95] K. M. Nollett and G. Steigman, *BBN And The CMB Constrain Light, Electromagnetically Coupled WIMPs*, *Phys. Rev.* **D89** (2014) 083508, [1312.5725].

[96] K. M. Nollett and G. Steigman, *BBN And The CMB Constrain Neutrino Coupled Light WIMPs*, *Phys. Rev.* **D91** (2015) 083505, [1411.6005].

[97] T. L. Smith, S. Das and O. Zahn, *Constraints on neutrino and dark radiation interactions using cosmological observations*, *Phys. Rev.* **D85** (2012) 023001, [1105.3246].

[98] J. Hamann, S. Hannestad, G. G. Raffelt and Y. Y. Y. Wong, *Sterile neutrinos with eV masses in cosmology: How disfavoured exactly?*, *JCAP* **1109** (2011) 034, [1108.4136].

[99] M. Archidiacono, E. Calabrese and A. Melchiorri, *The Case for Dark Radiation*, *Phys. Rev.* **D84** (2011) 123008, [1109.2767].

[100] J. Hamann, *Evidence for extra radiation? Profile likelihood versus Bayesian posterior*, *JCAP* **1203** (2012) 021, [1110.4271].

[101] K. M. Nollett and G. P. Holder, *An analysis of constraints on relativistic species from primordial nucleosynthesis and the cosmic microwave background*, 1112.2683.

[102] C. Bœhm, M. J. Dolan and C. McCabe, *Increasing Neff with particles in thermal equilibrium with neutrinos*, *JCAP* **1212** (2012) 027, [1207.0497].

[103] G. Steigman, *Equivalent Neutrinos, Light WIMPs, and the Chimera of Dark Radiation*, *Phys. Rev.* **D87** (2013) 103517, [1303.0049].

[104] M. Archidiacono, E. Giusarma, A. Melchiorri and O. Mena, *Neutrino and dark radiation properties in light of recent CMB observations*, *Phys. Rev.* **D87** (2013) 103519, [1303.0143].

[105] C. Bœhm, M. J. Dolan and C. McCabe, *A Lower Bound on the Mass of Cold Thermal Dark Matter from Planck*, *JCAP* **1308** (2013) 041, [1303.6270].

[106] E. Di Valentino, A. Melchiorri and O. Mena, *Dark radiation sterile neutrino candidates after Planck data*, *JCAP* **1311** (2013) 018, [1304.5981].

[107] E. Di Valentino, S. Gariazzo, M. Gerbino, E. Giusarma and O. Mena, *Dark Radiation and Inflationary Freedom after Planck 2015*, *Phys. Rev.* **D93** (2016) 083523, [1601.07557].

[108] R. J. Wilkinson, A. C. Vincent, C. Bœhm and C. McCabe, *Ruling out the light weakly interacting massive particle explanation of the Galactic 511 keV line*, *Phys. Rev.* **D94** (2016) 103525, [1602.01114].

[109] M. Escudero, *Neutrino decoupling beyond the Standard Model: CMB constraints on the Dark Matter mass with a fast and precise $N_{\rm eff}$ evaluation*, *JCAP* **1902** (2019) 007, [1812.05605].

[110] C. Bœhm, P. Fayet and R. Schaeffer, *Constraining dark matter candidates from structure formation*, *Phys. Lett.* **B518** (2001) 8–14, [astro-ph/0012504].

[111] C. Bœhm and R. Schaeffer, *Constraints on dark matter interactions from structure formation: Damping lengths*, *Astron. Astrophys.* **438** (2005) 419–442, [astro-ph/0410591].

[112] G. Mangano, A. Melchiorri, P. Serra, A. Cooray and M. Kamionkowski, *Cosmological bounds on dark matter-neutrino interactions*, *Phys. Rev.* **D74** (2006) 043517, [astro-ph/0606190].

[113] C. Bœhm, A. Riazuelo, S. H. Hansen and R. Schaeffer, *Interacting dark matter disguised as warm dark matter*, *Phys. Rev.* **D66** (2002) 083505, [astro-ph/0112522].

[114] M. Escudero, O. Mena, A. C. Vincent, R. J. Wilkinson and C. Bœhm, *Exploring dark matter microphysics with galaxy surveys*, *JCAP* **1509** (2015) 034, [1505.06735].

[115] E. Di Valentino, C. Boehm, E. Hivon and F. R. Bouchet, *Reducing the H_0 and σ_8 tensions with Dark Matter-neutrino interactions*, 1710.02559.

[116] R. J. Wilkinson, C. Bœhm and J. Lesgourgues, *Constraining Dark Matter-Neutrino Interactions using the CMB and Large-Scale Structure*, *JCAP* **1405** (2014) 011, [1401.7597].

[117] B. Bertoni, S. Ipek, D. McKeen and A. E. Nelson, *Constraints and consequences of reducing small scale structure via large dark matter-neutrino interactions*, *JHEP* **04** (2015) 170, [1412.3113].

[118] J. A. Schewtschenko, R. J. Wilkinson, C. M. Baugh, C. Bœhm and S. Pascoli, *Dark matter–radiation interactions: the impact on dark matter haloes*, *Mon. Not. Roy. Astron. Soc.* **449** (2015) 3587–3596, [1412.4905].

[119] J. A. Schewtschenko, C. M. Baugh, R. J. Wilkinson, C. Bœhm, S. Pascoli and T. Sawala, *Dark matter–radiation interactions: the structure of Milky Way*

satellite galaxies, *Mon. Not. Roy. Astron. Soc.* **461** (2016) 2282–2287, [1512.06774].

[120] A. Fattahi et al., *The cold dark matter content of Galactic dwarf spheroidals: no cores, no failures, no problem*, 1607.06479.

[121] J. Stadler, C. Bœhm and O. Mena, *First numerical study of Neutrino-Dark Matter Mixed Damping*, 1903.00540.

[122] Y. Farzan and S. Palomares-Ruiz, *Dips in the Diffuse Supernova Neutrino Background*, *JCAP* **1406** (2014) 014, [1401.7019].

[123] T. Franarin, M. Fairbairn and J. H. Davis, *JUNO Sensitivity to Resonant Absorption of Galactic Supernova Neutrinos by Dark Matter*, 1806.05015.

[124] C. A. Argüelles, A. Kheirandish and A. C. Vincent, *Imaging Galactic Dark Matter with High-Energy Cosmic Neutrinos*, *Phys. Rev. Lett.* **119** (2017) 201801, [1703.00451].

[125] S. Karmakar, S. Pandey and S. Rakshit, *Are We Looking at Neutrino Absorption Spectra at IceCube?*, 1810.04192.

[126] S. Pandey, S. Karmakar and S. Rakshit, *Interactions of Astrophysical Neutrinos with Dark Matter: A model building perspective*, *JHEP* **01** (2019) 095, [1810.04203].

[127] J. F. Beacom, N. F. Bell and G. D. Mack, *General Upper Bound on the Dark Matter Total Annihilation Cross Section*, *Phys. Rev. Lett.* **99** (2007) 231301, [astro-ph/0608090].

[128] H. Yüksel, S. Horiuchi, J. F. Beacom and S. Ando, *Neutrino Constraints on the Dark Matter Total Annihilation Cross Section*, *Phys. Rev.* **D76** (2007) 123506, [0707.0196].

[129] S. Palomares-Ruiz and S. Pascoli, *Testing MeV dark matter with neutrino detectors*, *Phys. Rev.* **D77** (2008) 025025, [0710.5420].

[130] Super-Kamiokande collaboration, K. Frankiewicz, *Searching for Dark Matter Annihilation into Neutrinos with Super-Kamiokande*, in *Proceedings, Meeting of the APS Division of Particles and Fields (DPF 2015): Ann Arbor, Michigan, USA, 4-8 Aug 2015*, 2015, 1510.07999.

[131] F. Calore, I. Cholis and C. Weniger, *Background Model Systematics for the Fermi GeV Excess*, *JCAP* **1503** (2015) 038, [1409.0042].

[132] G. Bertone, ed., *Particle Dark Matter: Observations, Models and Searches*. Cambridge Univ. Press, Cambridge, 2010.

[133] R. Diamanti, L. Lopez-Honorez, O. Mena, S. Palomares-Ruiz and A. C. Vincent, *Constraining Dark Matter Late-Time Energy Injection: Decays and P-Wave Annihilations*, *JCAP* **1402** (2014) 017, [1308.2578].

[134] K. K. Boddy, J. Kumar and L. E. Strigari, *Effective J -factor of the Galactic Center for velocity-dependent dark matter annihilation*, *Phys. Rev.* **D98** (2018) 063012, [1805.08379].

[135] Borexino collaboration, G. Bellini et al., *Final results of Borexino Phase-I on low energy solar neutrino spectroscopy*, *Phys. Rev.* **D89** (2014) 112007, [1308.0443].

[136] Borexino collaboration, G. Bellini et al., *Study of solar and other unknown anti-neutrino fluxes with Borexino at LNGS*, *Phys. Lett.* **B696** (2011) 191–196, [1010.0029].

[137] Super-Kamiokande collaboration, Y. Fukuda et al., *The Super-Kamiokande detector*, *Nucl. Instrum. Meth.* **A501** (2003) 418–462.

[138] FREJUS collaboration, C. Berger et al., *The Frejus Nucleon Decay Detector*, *Nucl. Instrum. Meth.* **A262** (1987) 463.

[139] AMANDA collaboration, F. Halzen et al., *The AMANDA neutrino telescope*, *Nucl. Phys. Proc. Suppl.* **77** (1999) 474–485, [hep-ex/9809025].

[140] ANTARES collaboration, M. Ageron et al., *ANTARES: the first undersea neutrino telescope*, *Nucl. Instrum. Meth.* **A656** (2011) 11–38, [1104.1607].

[141] A. Albert et al., *Results from the search for dark matter in the Milky Way with 9 years of data of the ANTARES neutrino telescope*, *Physics Letters B* **769** (2017) 249–254.

[142] ANTARES collaboration, S. Adrian-Martinez et al., *Search of Dark Matter Annihilation in the Galactic Centre using the ANTARES Neutrino Telescope*, *JCAP* **1510** (2015) 068, [1505.04866].

[143] F. Halzen and S. R Klein, *Invited review article: Icecube: An instrument for neutrino astronomy*, *The Review of scientific instruments* **81** (08, 2010) 081101.

[144] IceCube collaboration, M. G. Aartsen et al., *All-flavour Search for Neutrinos from Dark Matter Annihilations in the Milky Way with IceCube/DeepCore*, *Eur. Phys. J.* **C76** (2016) 531, [1606.00209].

[145] DUNE collaboration, R. Acciarri et al., *Long-Baseline Neutrino Facility (LBNF) and Deep Underground Neutrino Experiment (DUNE)*, 1512.06148.

[146] N. Klop and S. Ando, *Constraints on MeV dark matter using neutrino detectors and their implication for the 21-cm results*, *Phys. Rev.* **D98** (2018) 103004, [1809.00671].

[147] Hyper-Kamiokande collaboration, K. Abe et al., *Hyper-Kamiokande Design Report*, 1805.04163.

[148] DARWIN collaboration, J. Aalbers et al., *DARWIN: towards the ultimate dark matter detector*, *JCAP* **1611** (2016) 017, [1606.07001].

[149] D. McKeen and N. Raj, *Monochromatic dark neutrinos and boosted dark matter in noble liquid direct detection*, 1812.05102.

[150] M. Actis et al., *Design concepts for the Cherenkov Telescope Array CTA: an advanced facility for ground-based high-energy gamma-ray astronomy*, *Experimental Astronomy* **32** (Dec., 2011) 193–316, [1008.3703].

[151] F. S. Queiroz, C. E. Yaguna and C. Weniger, *Gamma-ray Limits on Neutrino Lines*, *JCAP* **1605** (2016) 050, [1602.05966].

[152] M. Cirelli, G. Corcella, A. Hektor, G. Hutsi, M. Kadastik, P. Panci et al., *PPPC 4 DM ID: A Poor Particle Physicist Cookbook for Dark Matter Indirect Detection*, *JCAP* **1103** (2011) 051, [1012.4515].

[153] K. Griest and M. Kamionkowski, *Unitarity Limits on the Mass and Radius of Dark Matter Particles*, *Phys. Rev. Lett.* **64** (1990) 615.

[154] Super-Kamiokande collaboration, K. Bays et al., *Supernova Relic Neutrino Search at Super-Kamiokande*, *Phys. Rev.* **D85** (2012) 052007, [1111.5031].

[155] Super-Kamiokande collaboration, J. Hosaka et al., *Solar neutrino measurements in super-Kamiokande-I*, *Phys. Rev.* **D73** (2006) 112001, [hep-ex/0508053].

[156] Super-Kamiokande collaboration, J. P. Cravens et al., *Solar neutrino measurements in Super-Kamiokande-II*, *Phys. Rev.* **D78** (2008) 032002, [0803.4312].

[157] Super-Kamiokande collaboration, K. Abe et al., *Solar neutrino results in Super-Kamiokande-III*, *Phys. Rev.* **D83** (2011) 052010, [1010.0118].

[158] A. Strumia and F. Vissani, *Precise quasielastic neutrino/nucleon cross-section*, *Phys. Lett.* **B564** (2003) 42–54, [astro-ph/0302055].

[159] P. Vogel and J. F. Beacom, *Angular distribution of neutron inverse beta decay, anti-neutrino(e) + p —> e+ + n*, *Phys. Rev.* **D60** (1999) 053003, [hep-ph/9903554].

[160] R. A. Smith and E. J. Moniz, *NEUTRINO REACTIONS ON NUCLEAR TARGETS*, *Nucl. Phys.* **B43** (1972) 605.

[161] G. Battistoni, A. Ferrari, T. Montaruli and P. R. Sala, *The FLUKA atmospheric neutrino flux calculation*, *Astropart. Phys.* **19** (2003) 269–290, [hep-ph/0207035].

[162] G. Battistoni, A. Ferrari, T. Montaruli and P. R. Sala, *The atmospheric neutrino flux below 100-MeV: The FLUKA results*, *Astropart. Phys.* **23** (2005) 526–534.

[163] A. Czarnecki, M. Dowling, X. G. i. Tormo, W. J. Marciano and R. Szafron, *Michel decay spectrum for a muon bound to a nucleus*, *Phys. Rev.* **D90** (2014) 093002, [1406.3575].

[164] P. Haenggi, R. D. Viollier, U. Raff and K. Alder, *Muon decay in orbit*, *Phys. Lett.* **B51** (1974) 119–122.

[165] N. Bernal, J. Martín-Albo and S. Palomares-Ruiz, *A novel way of constraining WIMPs annihilations in the Sun: MeV neutrinos*, *JCAP* **1308** (2013) 011, [1208.0834].

[166] K. Abe et al., *Letter of Intent: The Hyper-Kamiokande Experiment — Detector Design and Physics Potential —*, 1109.3262.

[167] Super-Kamiokande collaboration, A. Renshaw, *Research and Development for a Gadolinium Doped Water Cherenkov Detector*, *Phys. Procedia* **37** (2012) 1249–1256, [1201.1017].

[168] Super-Kamiokande collaboration, K. Choi et al., *Search for neutrinos from annihilation of captured low-mass dark matter particles in the Sun by Super-Kamiokande*, *Phys. Rev. Lett.* **114** (2015) 141301, [1503.04858].

[169] IceCube collaboration, M. G. Aartsen et al., *Search for annihilating dark matter in the Sun with 3 years of IceCube data*, *Eur. Phys. J.* **C77** (2017) 146, [1612.05949].

[170] M. D. Schwartz, *Quantum Field Theory and the Standard Model*. Cambridge University Press, 2014.

[171] A. J. Williams, C. Bœhm, S. M. West and D. Albornoz Vasquez, *Regenerating WIMPs in the Light of Direct and Indirect Detection*, *Phys. Rev.* **D86** (2012) 055018, [1204.3727].

[172] C. Boehm and P. Fayet, *Scalar dark matter candidates*, *Nucl. Phys.* **B683** (2004) 219–263, [hep-ph/0305261].

[173] G. Jungman, M. Kamionkowski and K. Griest, *Supersymmetric dark matter*, *Phys. Rept.* **267** (1996) 195–373, [hep-ph/9506380].

[174] D. Hooper, J. March-Russell and S. M. West, *Asymmetric sneutrino dark matter and the Omega(b) / Omega(DM) puzzle*, *Phys. Lett.* **B605** (2005) 228–236, [hep-ph/0410114].

[175] C. Bœhm, A. Djouadi and M. Drees, *Light scalar top quarks and supersymmetric dark matter*, *Phys. Rev.* **D62** (2000) 035012, [hep-ph/9911496].

[176] E. A. Bagnaschi et al., *Supersymmetric Dark Matter after LHC Run 1*, *Eur. Phys. J.* **C75** (2015) 500, [1508.01173].

[177] A. Goudelis, B. Herrmann and O. Stal, *Dark matter in the Inert Doublet Model after the discovery of a Higgs-like boson at the LHC*, *JHEP* **09** (2013) 106, [1303.3010].

[178] J. Kopp, L. Michaels and J. Smirnov, *Loopy Constraints on Leptophilic Dark Matter and Internal Bremsstrahlung*, *JCAP* **1404** (2014) 022, [1401.6457].

[179] D. Albornoz Vasquez, C. Boehm and J. Idarraga, *Signature of Sub GeV Dark Matter particles at LHC and TEVATRON*, *Phys. Rev.* **D83** (2011) 115017, [0912.5373].

[180] M. Lindner, A. Merle and V. Niro, *Enhancing Dark Matter Annihilation into Neutrinos*, *Phys. Rev.* **D82** (2010) 123529, [1005.3116].

[181] C. Bœhm and J. Silk, *A New test of the light dark matter hypothesis*, *Phys. Lett.* **B661** (2008) 287–289, [0708.2768].

[182] A. G. Akeroyd, A. Arhrib and E.-M. Naimi, *Note on tree level unitarity in the general two Higgs doublet model*, *Phys. Lett.* **B490** (2000) 119–124, [hep-ph/0006035].

[183] H. Baer, K.-Y. Choi, J. E. Kim and L. Roszkowski, *Dark matter production in the early Universe: beyond the thermal WIMP paradigm*, *Phys. Rept.* **555** (2015) 1–60, [1407.0017].

[184] C. Boehm, T. A. Ensslin and J. Silk, *Can Annihilating dark matter be lighter than a few GeVs?*, *J. Phys.* **G30** (2004) 279–286, [astro-ph/0208458].

[185] X.-L. Chen and M. Kamionkowski, *Particle decays during the cosmic dark ages*, *Phys.Rev.* **D70** (2004) 043502, [astro-ph/0310473].

[186] N. Padmanabhan and D. P. Finkbeiner, *Detecting dark matter annihilation with CMB polarization: Signatures and experimental prospects*, *Phys.Rev.* **D72** (2005) 023508, [astro-ph/0503486].

[187] M. Mapelli, A. Ferrara and E. Pierpaoli, *Impact of dark matter decays and annihilations on reionzation*, *Mon.Not.Roy.Astron.Soc.* **369** (2006) 1719–1724, [astro-ph/0603237].

[188] L. Zhang, X.-L. Chen, Y.-A. Lei and Z.-G. Si, *The impacts of dark matter particle annihilation on recombination and the anisotropies of the cosmic microwave background*, *Phys.Rev.* **D74** (2006) 103519, [astro-ph/0603425].

[189] E. Ripamonti, M. Mapelli and A. Ferrara, *Intergalactic medium heating by dark matter*, *Mon.Not.Roy.Astron.Soc.* **374** (2007) 1067–1077, [astro-ph/0606482].

[190] L. Chuzhoy, *Impact of Dark Matter Annihilation on the High-Redshift Intergalactic Medium*, *Astrophys. J.* **679** (2008) L65, [0710.1856].

[191] D. P. Finkbeiner, N. Padmanabhan and N. Weiner, *CMB and 21-cm Signals for Dark Matter with a Long-Lived Excited State*, *Phys.Rev.* **D78** (2008) 063530, [0805.3531].

[192] A. Natarajan and D. J. Schwarz, *The effect of early dark matter halos on reionization*, *Phys.Rev.* **D78** (2008) 103524, [0805.3945].

[193] A. Natarajan and D. J. Schwarz, *Dark matter annihilation and its effect on CMB and Hydrogen 21 cm observations*, *Phys.Rev.* **D80** (2009) 043529, [0903.4485].

[194] S. Galli, F. Iocco, G. Bertone and A. Melchiorri, *CMB constraints on Dark Matter models with large annihilation cross-section*, *Phys.Rev.* **D80** (2009) 023505, [0905.0003].

[195] T. R. Slatyer, N. Padmanabhan and D. P. Finkbeiner, *CMB Constraints on WIMP Annihilation: Energy Absorption During the Recombination Epoch*, *Phys.Rev.* **D80** (2009) 043526, [0906.1197].

[196] M. Cirelli, F. Iocco and P. Panci, *Constraints on Dark Matter annihilations from reionization and heating of the intergalactic gas*, *JCAP* **0910** (2009) 009, [0907.0719].

[197] T. Kanzaki, M. Kawasaki and K. Nakayama, *Effects of Dark Matter Annihilation on the Cosmic Microwave Background*, *Prog.Theor.Phys.* **123** (2010) 853–865, [0907.3985].

[198] J. Chluba, *Could the Cosmological Recombination Spectrum Help Us Understand Annihilating Dark Matter?*, *Mon.Not.Roy.Astron.Soc.* **402** (2010) 1195–1207, [0910.3663].

[199] M. Valdes, C. Evoli and A. Ferrara, *Particle energy cascade in the Intergalactic Medium*, *Mon.Not.Roy.Astron.Soc.* **404** (2010) 1569–1582, [0911.1125].

[200] A. Natarajan and D. J. Schwarz, *Distinguishing standard reionization from dark matter models*, *Phys.Rev.* **D81** (2010) 123510, [1002.4405].

[201] S. Galli, F. Iocco, G. Bertone and A. Melchiorri, *Updated CMB constraints on Dark Matter annihilation cross-sections*, *Phys.Rev.* **D84** (2011) 027302, [1106.1528].

[202] G. Hutsi, J. Chluba, A. Hektor and M. Raidal, *WMAP7 and future CMB constraints on annihilating dark matter: implications on GeV-scale WIMPs*, *Astron.Astrophys.* **535** (2011) A26, [1103.2766].

[203] C. Evoli, M. Valdes, A. Ferrara and N. Yoshida, *Energy deposition by weakly interacting massive particles: a comprehensiv e study*, *Mon.Not.Roy.Astron.Soc.* **422** (2012) 420–433.

[204] G. Giesen, J. Lesgourgues, B. Audren and Y. Ali-Haimoud, *CMB photons shedding light on dark matter*, *JCAP* **1212** (2012) 008, [1209.0247].

[205] C. Evoli, S. Pandolfi and A. Ferrara, *CMB constraints on light dark matter candidates*, *Mon. Not. Roy. Astron. Soc.* **433** (2013) 1736, [1210.6845].

[206] T. R. Slatyer, *Energy Injection And Absorption In The Cosmic Dark Ages*, *Phys. Rev.* **D87** (2013) 123513, [1211.0283].

[207] A. R. Frey and N. B. Reid, *Cosmic microwave background constraints on dark matter models of the Galactic center 511 keV signal*, *Phys. Rev.* **D87** (2013) 103508, [1301.0819].

[208] J. M. Cline and P. Scott, *Dark Matter CMB Constraints and Likelihoods for Poor Particle Physicists*, *JCAP* **1303** (2013) 044, [1301.5908].

[209] C. Weniger, P. D. Serpico, F. Iocco and G. Bertone, *CMB bounds on dark matter annihilation: Nucleon energy-losses after recombination*, *Phys. Rev.* **D87** (2013) 123008, [1303.0942].

[210] L. Lopez-Honorez, O. Mena, S. Palomares-Ruiz and A. C. Vincent, *Constraints on dark matter annihilation from CMB observationsbefore Planck*, *JCAP* **1307** (2013) 046, [1303.5094].

[211] M. S. Madhavacheril, N. Sehgal and T. R. Slatyer, *Current Dark Matter Annihilation Constraints from CMB and Low-Redshift Data*, *Phys. Rev.* **D89** (2014) 103508, [1310.3815].

[212] T. R. Slatyer, *Indirect Dark Matter Signatures in the Cosmic Dark Ages II. Ionization, Heating and Photon Production from Arbitrary Energy Injections*, *Phys. Rev.* **D93** (2016) 023521, [1506.03812].

[213] V. Poulin, P. D. Serpico and J. Lesgourgues, *Dark Matter annihilations in halos and high-redshift sources of reionization of the universe*, *JCAP* **1512** (2015) 041, [1508.01370].

[214] M. Kawasaki, K. Nakayama and T. Sekiguchi, *CMB Constraint on Dark Matter Annihilation after Planck 2015*, *Phys. Lett.* **B756** (2016) 212–215, [1512.08015].

[215] H. Liu, T. R. Slatyer and J. Zavala, *Contributions to cosmic reionization from dark matter annihilation and decay*, *Phys. Rev.* **D94** (2016) 063507, [1604.02457].

[216] I. M. Oldengott, D. Boriero and D. J. Schwarz, *Reionization and dark matter decay*, *JCAP* **1608** (2016) 054, [1605.03928].

[217] T. R. Slatyer and C.-L. Wu, *General Constraints on Dark Matter Decay from the Cosmic Microwave Background*, *Phys. Rev.* **D95** (2017) 023010, [1610.06933].

[218] Y. Farzan, S. Pascoli and M. A. Schmidt, *AMEND: A model explaining neutrino masses and dark matter testable at the LHC and MEG*, *JHEP* **10** (2010) 111, [1005.5323].

[219] Y. Farzan, *Two-loop snail diagrams: relating neutrino masses to dark matter*, *JHEP* **05** (2015) 029, [1412.6283].

[220] A. Arhrib, C. Bœhm, E. Ma and T.-C. Yuan, *Radiative Model of Neutrino Mass with Neutrino Interacting MeV Dark Matter*, *JCAP* **1604** (2016) 049, [1512.08796].

[221] S. Tulin, H.-B. Yu and K. M. Zurek, *Beyond Collisionless Dark Matter: Particle Physics Dynamics for Dark Matter Halo Structure*, *Phys. Rev.* **D87** (2013) 115007, [1302.3898].

[222] L. G. van den Aarssen, T. Bringmann and C. Pfrommer, *Is dark matter with long-range interactions a solution to all small-scale problems of Λ CDM cosmology?*, *Phys. Rev. Lett.* **109** (2012) 231301, [1205.5809].

[223] O. G. Miranda, C. A. Moura and A. Parada, *Sterile neutrinos, dark matter, and resonant effects in ultra high energy regimes*, *Phys. Lett.* **B744** (2015) 55–58, [1308.1408].

[224] T. Bringmann, F. Kahlhoefer, K. Schmidt-Hoberg and P. Walia, *Strong constraints on self-interacting dark matter with light mediators*, *Phys. Rev. Lett.* **118** (2017) 141802, [1612.00845].

[225] A. Ibarra, S. Lopez Gehler and M. Pato, *Dark matter constraints from box-shaped gamma-ray features*, *JCAP* **1207** (2012) 043, [1205.0007].

[226] C. El Aisati, C. Garcia-Cely, T. Hambye and L. Vanderheyden, *Prospects for discovering a neutrino line induced by dark matter annihilation*, *JCAP* **1710** (2017) 021, [1706.06600].

[227] J. L. Feng, M. Kaplinghat and H.-B. Yu, *Sommerfeld Enhancements for Thermal Relic Dark Matter*, *Phys. Rev.* **D82** (2010) 083525, [1005.4678].

[228] S. Hannestad and T. Tram, *Sommerfeld Enhancement of DM Annihilation: Resonance Structure, Freeze-Out and CMB Spectral Bound*, *JCAP* **1101** (2011) 016, [1008.1511].

[229] J. Hisano, S. Matsumoto and M. M. Nojiri, *Explosive dark matter annihilation*, *Phys. Rev. Lett.* **92** (2004) 031303, [hep-ph/0307216].

[230] A. Das and B. Dasgupta, *Selection Rule for Enhanced Dark Matter Annihilation*, *Phys. Rev. Lett.* **118** (2017) 251101, [1611.04606].

[231] B. Holdom, *Two U(1)'s and Epsilon Charge Shifts*, *Phys. Lett.* **166B** (1986) 196–198.

[232] B. Patt and F. Wilczek, *Higgs-field portal into hidden sectors*, hep-ph/0605188.

[233] J. March-Russell, S. M. West, D. Cumberbatch and D. Hooper, *Heavy Dark Matter Through the Higgs Portal*, *JHEP* **07** (2008) 058, [0801.3440].

[234] A. Falkowski, J. Juknevich and J. Shelton, *Dark Matter Through the Neutrino Portal*, 0908.1790.

[235] V. Gonzalez Macias and J. Wudka, *Effective theories for Dark Matter interactions and the neutrino portal paradigm*, *JHEP* **07** (2015) 161, [1506.03825].

[236] T. Yanagida, *Horizontal Symmetry and Masses of Neutrinos*, in *Proceedings of Workshop on the Unified Theories and the Baryon Number in the Universe, Tsukuba, Japan, February 13–14, 1979*, pp. 95–99, 1979.

[237] S. L. Glashow, *The Future of Elementary Particle Physics*, *NATO Sci. Ser. B* **61** (1980) 687.

[238] R. N. Mohapatra and G. Senjanovic, *Neutrino mass and spontaneous parity nonconservation*, *Phys. Rev. Lett.* **44** (1980) 912.

[239] G. C. Branco, W. Grimus and L. Lavoura, *The Seesaw Mechanism in the Presence of a Conserved Lepton Number*, *Nucl. Phys.* **B312** (1989) 492–508.

[240] W. Buchmuller and D. Wyler, *Dilatons and majorana neutrinos*, *Phys. Lett.* **B249** (1990) 458–462.

[241] A. Pilaftsis, *Radiatively induced neutrino masses and large Higgs neutrino couplings in the standard model with Majorana fields*, *Z. Phys.* **C55** (1992) 275–282, [hep-ph/9901206].

[242] J. Kersten and A. Y. Smirnov, *Right-Handed Neutrinos at CERN LHC and the Mechanism of Neutrino Mass Generation*, *Phys. Rev.* **D76** (2007) 073005, [0705.3221].

[243] G. Belanger, F. Boudjema, A. Pukhov and A. Semenov, *MicrOMEGAs: A Program for calculating the relic density in the MSSM*, *Comput. Phys. Commun.* **149** (2002) 103–120, [hep-ph/0112278].

[244] E. Fernández-Martínez, J. Hernández-García and J. Lopez-Pavon, *Global constraints on heavy neutrino mixing*, *JHEP* **08** (2016) 033, [1605.08774].

[245] B. Batell, T. Han, D. McKeen and B. Shams Es Haghi, *Thermal Dark Matter Through the Dirac Neutrino Portal*, *Phys. Rev.* **D97** (2018) 075016, [1709.07001].

[246] M. Pospelov, A. Ritz and M. B. Voloshin, *Secluded WIMP Dark Matter*, *Phys. Lett.* **B662** (2008) 53–61, [0711.4866].

[247] M. Escudero, N. Rius and V. Sanz, *Sterile neutrino portal to Dark Matter I: The $U(1)_{B-L}$ case*, *JHEP* **02** (2017) 045, [1606.01258].

[248] M. Escudero, N. Rius and V. Sanz, *Sterile Neutrino portal to Dark Matter II: Exact Dark symmetry*, *Eur. Phys. J.* **C77** (2017) 397, [1607.02373].

[249] M. G. Folgado, G. A. Gómez-Vargas, N. Rius and R. Ruiz De Austri, *Probing the sterile neutrino portal to Dark Matter with γ rays*, *JCAP* **1808** (2018) 002, [1803.08934].

[250] P. Bandyopadhyay, E. J. Chun, R. Mandal and F. S. Queiroz, *Scrutinizing Right-Handed Neutrino Portal Dark Matter With Yukawa Effect*, *Phys. Lett.* **B788** (2019) 530–534, [1807.05122].

[251] A. Atre, T. Han, S. Pascoli and B. Zhang, *The Search for Heavy Majorana Neutrinos*, *JHEP* **05** (2009) 030, [0901.3589].

[252] J. Ellis, *TikZ-Feynman: Feynman diagrams with TikZ*, *Comput. Phys. Commun.* **210** (2017) 103–123, [1601.05437].

[253] N. D. Christensen and C. Duhr, *FeynRules - Feynman rules made easy*, *Comput. Phys. Commun.* **180** (2009) 1614–1641, [0806.4194].

[254] A. Alloul, N. D. Christensen, C. Degrande, C. Duhr and B. Fuks, *FeynRules 2.0 - A complete toolbox for tree-level phenomenology*, *Comput. Phys. Commun.* **185** (2014) 2250–2300, [1310.1921].

[255] T. Hahn, *Generating Feynman diagrams and amplitudes with FeynArts 3*, *Comput. Phys. Commun.* **140** (2001) 418–431, [hep-ph/0012260].

[256] T. Hahn and M. Perez-Victoria, *Automatized one loop calculations in four-dimensions and D-dimensions*, *Comput. Phys. Commun.* **118** (1999) 153–165, [hep-ph/9807565].

[257] P. W. Angel, Y. Cai, N. L. Rodd, M. A. Schmidt and R. R. Volkas, *Testable two-loop radiative neutrino mass model based on an $LLQd^cQd^c$ effective operator*, *JHEP* **10** (2013) 118, [1308.0463].

[258] K. S. Babu, C. F. Kolda and J. March-Russell, *Implications of generalized Z - Z-prime mixing*, *Phys. Rev.* **D57** (1998) 6788–6792, [hep-ph/9710441].

[259] R. Harnik, J. Kopp and P. A. N. Machado, *Exploring nu Signals in Dark Matter Detectors*, *JCAP* **1207** (2012) 026, [1202.6073].

[260] M. Bauer, P. Foldenauer and J. Jaeckel, *Hunting All the Hidden Photons*, *JHEP* **07** (2018) 094, [1803.05466].

[261] D. Z. Freedman, *Coherent Neutrino Nucleus Scattering as a Probe of the Weak Neutral Current*, *Phys. Rev.* **D9** (1974) 1389–1392.

[262] J. Billard, L. Strigari and E. Figueroa-Feliciano, *Implication of neutrino backgrounds on the reach of next generation dark matter direct detection experiments*, *Phys. Rev.* **D89** (2014) 023524, [1307.5458].

[263] J. D. Vergados and H. Ejiri, *Can Solar Neutrinos be a Serious Background in Direct Dark Matter Searches?*, *Nucl. Phys.* **B804** (2008) 144–159, [0805.2583].

[264] J. H. Davis, *Dark Matter vs. Neutrinos: The effect of astrophysical uncertainties and timing information on the neutrino floor*, *JCAP* **1503** (2015) 012, [1412.1475].

[265] F. Ruppin, J. Billard, E. Figueroa-Feliciano and L. Strigari, *Complementarity of dark matter detectors in light of the neutrino background*, *Phys.Rev.* **D90** (2014) 083510, [1408.3581].

[266] P. Grothaus, M. Fairbairn and J. Monroe, *Directional Dark Matter Detection Beyond the Neutrino Bound*, *Phys.Rev.* **D90** (2014) 055018, [1406.5047].

[267] C. A. J. O'Hare, A. M. Green, J. Billard, E. Figueroa-Feliciano and L. E. Strigari, *Readout strategies for directional dark matter detection beyond the neutrino background*, *Phys. Rev.* **D92** (2015) 063518, [1505.08061].

[268] J. B. Dent, B. Dutta, J. L. Newstead and L. E. Strigari, *No ν floors: Effective field theory treatment of the neutrino background in direct dark matter detection experiments*, 1602.05300.

[269] COHERENT collaboration, D. Akimov et al., *Observation of Coherent Elastic Neutrino-Nucleus Scattering*, *Science* **357** (2017) 1123–1126, [1708.01294].

[270] B. J. Mount et al., *LUX-ZEPLIN (LZ) Technical Design Report*, 1703.09144.

[271] D. T. Cumberbatch, J. Guzik, J. Silk, L. S. Watson and S. M. West, *Light WIMPs in the Sun: Constraints from Helioseismology*, *Phys. Rev.* **D82** (2010) 103503, [1005.5102].

[272] D. G. Cerdeño, J. H. Davis, M. Fairbairn and A. C. Vincent, *CNO Neutrino Grand Prix: The race to solve the solar metallicity problem*, *JCAP* **1804** (2018) 037, [1712.06522].

[273] J. L. Newstead, L. E. Strigari and R. F. Lang, *CNO Solar Neutrinos in Next-Generation Dark Matter Experiments*, 1807.07169.

[274] M. Pospelov, *Neutrino Physics with Dark Matter Experiments and the Signature of New Baryonic Neutral Currents*, *Phys. Rev.* **D84** (2011) 085008, [1103.3261].

[275] D. G. Cerdeño, M. Fairbairn, T. Jubb, P. A. N. Machado, A. C. Vincent and C. Boehm, *Physics from solar neutrinos in dark matter direct detection experiments*, *JHEP* **05** (2016) 118, [1604.01025].

[276] E. Bertuzzo, F. F. Deppisch, S. Kulkarni, Y. F. Perez Gonzalez and R. Zukanovich Funchal, *Dark Matter and Exotic Neutrino Interactions in Direct Detection Searches*, *JHEP* **04** (2017) 073, [1701.07443].

[277] B. Dutta, S. Liao, L. E. Strigari and J. W. Walker, *Non-standard interactions of solar neutrinos in dark matter experiments*, *Phys. Lett.* **B773** (2017) 242–246, [1705.00661].

[278] D. Aristizabal Sierra, N. Rojas and M. H. G. Tytgat, *Neutrino non-standard interactions and dark matter searches with multi-ton scale detectors*, *JHEP* **03** (2018) 197, [1712.09667].

[279] P. Coloma, P. B. Denton, M. C. Gonzalez-Garcia, M. Maltoni and T. Schwetz, *Curtailing the Dark Side in Non-Standard Neutrino Interactions*, *JHEP* **04** (2017) 116, [1701.04828].

[280] M. C. Gonzalez-Garcia, M. Maltoni, Y. F. Perez-Gonzalez and R. Zukanovich Funchal, *Neutrino Discovery Limit of Dark Matter Direct Detection Experiments in the Presence of Non-Standard Interactions*, *JHEP* **07** (2018) 019, [1803.03650].

[281] D. Aristizabal Sierra, V. De Romeri and N. Rojas, *COHERENT analysis of neutrino generalized interactions*, 1806.07424.

[282] D. K. Papoulias and T. S. Kosmas, *COHERENT constraints to conventional and exotic neutrino physics*, *Phys. Rev.* **D97** (2018) 033003, [1711.09773].

[283] D. K. Papoulias, R. Sahu, T. S. Kosmas, V. K. B. Kota and B. Nayak, *Novel neutrino-floor and dark matter searches with deformed shell model calculations*, 1804.11319.

[284] J. Billard, J. Johnston and B. J. Kavanagh, *Prospects for exploring New Physics in Coherent Elastic Neutrino-Nucleus Scattering*, 1805.01798.

[285] P. B. Denton, Y. Farzan and I. M. Shoemaker, *Testing large non-standard neutrino interactions with arbitrary mediator mass after COHERENT data*, *JHEP* **07** (2018) 037, [1804.03660].

[286] SuperCDMS collaboration, R. Agnese et al., *Projected Sensitivity of the SuperCDMS SNOLAB experiment*, *Phys. Rev.* **D95** (2017) 082002, [1610.00006].

[287] NEWS-G collaboration, Q. Arnaud et al., *First results from the NEWS-G direct dark matter search experiment at the LSM*, *Astropart. Phys.* **97** (2018) 54–62, [1706.04934].

[288] R. H. Helm, *Inelastic and Elastic Scattering of 187-Mev Electrons from Selected Even-Even Nuclei*, *Phys. Rev.* **104** (1956) 1466–1475.

[289] J. N. Bahcall and A. M. Serenelli, *How do uncertainties in the surface chemical abundances of the Sun affect the predicted solar neutrino fluxes?*, *Astrophys. J.* **626** (2005) 530, [astro-ph/0412096].

[290] N. Vinyoles, A. Serenelli and F. L. Villante, *The Sun and solar neutrinos*, *J. Phys. Conf. Ser.* **888** (2017) 012006.

[291] G. Battistoni, A. Ferrari, T. Montaruli and P. R. Sala, *The atmospheric neutrino flux below 100-MeV: The FLUKA results*, *Astropart. Phys.* **23** (2005) 526–534.

[292] J. B. Dent, B. Dutta, J. L. Newstead and L. E. Strigari, *Dark matter, light mediators, and the neutrino floor*, *Phys. Rev.* **D95** (2017) 051701, [1607.01468].

[293] M. Lindner, W. Rodejohann and X.-J. Xu, *Coherent Neutrino-Nucleus Scattering and new Neutrino Interactions*, *JHEP* **03** (2017) 097, [1612.04150].

[294] C. Boehm, *Implications of a new light gauge boson for neutrino physics*, *Phys. Rev.* **D70** (2004) 055007, [hep-ph/0405240].

[295] A. E. Nelson and J. Walsh, *Short Baseline Neutrino Oscillations and a New Light Gauge Boson*, *Phys. Rev.* **D77** (2008) 033001, [0711.1363].

[296] K. S. Babu, A. Friedland, P. A. N. Machado and I. Mocioiu, *Flavor Gauge Models Below the Fermi Scale*, *JHEP* **12** (2017) 096, [1705.01822].

[297] H. Davoudiasl, H.-S. Lee and W. J. Marciano, *Muon $g-2$, rare kaon decays, and parity violation from dark bosons*, *Phys. Rev.* **D89** (2014) 095006, [1402.3620].

[298] S. Gabriel and S. Nandi, *A New two Higgs doublet model*, *Phys. Lett.* **B655** (2007) 141–147, [hep-ph/0610253].

[299] J. M. Alarcon, J. Martin Camalich and J. A. Oller, *The chiral representation of the πN scattering amplitude and the pion-nucleon sigma term*, *Phys. Rev.* **D85** (2012) 051503, [1110.3797].

[300] J. M. Alarcon, L. S. Geng, J. Martin Camalich and J. A. Oller, *The strangeness content of the nucleon from effective field theory and phenomenology*, *Phys. Lett.* **B730** (2014) 342–346, [1209.2870].

[301] M. Cirelli, E. Del Nobile and P. Panci, *Tools for model-independent bounds in direct dark matter searches*, *JCAP* **1310** (2013) 019, [1307.5955].

[302] R. J. Hill and M. P. Solon, *Standard Model anatomy of WIMP dark matter direct detection II: QCD analysis and hadronic matrix elements*, *Phys. Rev.* **D91** (2015) 043505, [1409.8290].

[303] P. Ilten, Y. Soreq, M. Williams and W. Xue, *Serendipity in dark photon searches*, *JHEP* **06** (2018) 004, [1801.04847].

[304] S. Bilmis, I. Turan, T. M. Aliev, M. Deniz, L. Singh and H. T. Wong, *Constraints on Dark Photon from Neutrino-Electron Scattering Experiments*, *Phys. Rev.* **D92** (2015) 033009, [1502.07763].

[305] E. Rrapaj and S. Reddy, *Nucleon-nucleon bremsstrahlung of dark gauge bosons and revised supernova constraints*, *Phys. Rev.* **C94** (2016) 045805, [1511.09136].

[306] G.-y. Huang, T. Ohlsson and S. Zhou, *Observational Constraints on Secret Neutrino Interactions from Big Bang Nucleosynthesis*, *Phys. Rev.* **D97** (2018) 075009, [1712.04792].

[307] A. Crivellin, M. Hoferichter and M. Procura, *Accurate evaluation of hadronic uncertainties in spin-independent WIMP-nucleon scattering: Disentangling two- and three-flavor effects*, *Phys. Rev.* **D89** (2014) 054021, [1312.4951].

[308] P. Junnarkar and A. Walker-Loud, *Scalar strange content of the nucleon from lattice QCD*, *Phys. Rev.* **D87** (2013) 114510, [1301.1114].

[309] M. Hoferichter, J. Ruiz de Elvira, B. Kubis and U.-G. Meißner, *High-Precision Determination of the Pion-Nucleon σ Term from Roy-Steiner Equations*, *Phys. Rev. Lett.* **115** (2015) 092301, [1506.04142].

[310] J. Ellis, N. Nagata and K. A. Olive, *Uncertainties in WIMP Dark Matter Scattering Revisited*, *Eur. Phys. J.* **C78** (2018) 569, [1805.09795].

[311] Y. Farzan, M. Lindner, W. Rodejohann and X.-J. Xu, *Probing neutrino coupling to a light scalar with coherent neutrino scattering*, 1802.05171.

[312] J. Liao and D. Marfatia, *COHERENT constraints on nonstandard neutrino interactions*, *Phys. Lett.* **B775** (2017) 54–57, [1708.04255].

[313] I. Katsioulas, *NEWS-G, Light dark matter search with a Spherical Proportional Counter, First results and Future prospects*, in *53rd Rencontres de Moriond on Electroweak Interactions and Unified Theories (Moriond EW 2018) La Thuile, Italy, March 10-17*, 2018.

[314] C. A. J. O'Hare, *Dark matter astrophysical uncertainties and the neutrino floor*, *Phys. Rev.* **D94** (2016) 063527, [1604.03858].

[315] P. Ballett, M. Hostert and S. Pascoli, *Neutrino Masses from a Dark Neutrino Sector below the Electroweak Scale*, 1903.07590.